YAP1 drives ependymoma-like tumour formation in mice and post mitotic functions of LATS2 in the brain

Noreen Eder

University College London
and
The Francis Crick Institute
PhD Supervisor: Sila Ultanir & Bram Snijders

A thesis submitted for the degree of
Doctor of Philosophy
University College London
March 2020

Declaration

I Noreen Eder confirm that the work presented in this thesis is my own. Where information has been derived from other sources, I confirm that this has been indicated in the thesis.

Abstract

In a subset of paediatric ependymomas YAP1 (Yes-associated protein 1) gene fusions have been identified recently. In this study we show that YAP1 is expressed in the ventricular zone of the developing mouse brain. Depletion of two negative regulators of YAP1, Large tumour suppressor 1 and 2 (LATS1/2) kinases, in these cells using conditional NEX/NeuroD6-Cre knockout mice leads to the development of brain tumours. Nuclear YAP1 drives tumourigenesis by maintaining a nestin positive neural stem cell-like progenitor pool. These tumours display molecular, histological and ultrastructural similarities to human ependymoma. Additional depletion of YAP1 and its paralog TAZ (Transcriptional coactivator with PDZ-binding motif) in the Lats1/2 knockout NEX-Cre lineage rescues the phenotype, showing the dependence on YAP/TAZ. Furthermore, expression of active nuclear YAP1 (nlsYAP5SA) in the NEX-Cre linage is sufficient for high tumour burden in mice at the expense of proper hippocampal development. Transcriptomic and proteomic analysis of those murine tumours exhibit further similarities to YAP1-fusion supratentorial ependymoma. Moreover, we demonstrate an upregulation of the transcriptional cofactor HOPX in our mouse models. Finally, we show that HOPX is present in human YAP1-fusion ependymoma and absent in the RELA-fusion ependymoma in patient samples. In conclusion, our results demonstrate that uninhibited YAP/TAZ activity in neuronal precursor cells can lead to ependymoma-like tumours in mice.

Impact statement

With this PhD thesis we aim to shed more light on the understudied YAP1-fusion ependymoma subtype which is predominantly found in young children.

Ependymoma is the third most common pediatric brain tumour, however the data on the genetic and molecular mechanistic leading to its development is still spars. Furthermore, it is a are very heterogeneous cancer type from a clinical, molecular and morphological perspective and research into those separating aspects is still young. In addition, due to more recent discovery and the lower incidence rate of the YAP1-fusion subtype, the access of quality samples is more difficult. As well as it unfortunately gets excluded from multiple high throughput screens due to the lack of samples and consequent statistical robustness.

As a result of this work we believe we can provide the research community with two novel mouse models to study this rare cancer subtype. In this study we can show clear parallels to the human YAP1-fusion ependymoma on a morphological and molecular level. It identifies deregulation of YAP1 in neuronal progenitor cells as a key oncogene in ependymoma development. By combining transcriptomic and proteomics we were able to identify highly deregulated mRNA and proteins. This also led to the identification of a potential diagnostic marker HOPX, which showed high levels of expression in all tested patients with YAP1 but not RELA-fusion ependymomas. A larger cohort study is necessary to validate the subtype-specificity of this marker. Nonetheless it supports the nlsYAP5SA and LATS1/2 cKO mice as useful model systems for ependymoma research.

In conjunction with the other models our mouse models each can aid understanding the YAP1-fusion ependymoma and untangling its complexity, resulting in more targeted therapies for patients with this tumour subtype.

Acknowledgement

I would like to thank Sila and Bram for giving me the opportunity to work on this project. Especially, in letting me follow my curiosity as the work developed and took an unexpected direction. I am also very thankful for my past and present lab colleagues in both labs who have supported me in many different ways. Suzanne has been there from the beginning, introducing me to a variety of techniques in the lab and has been a help throughout the project in particular with the uncountable amount of genotyping she did for me. I am very grateful for Amy and Kali for helping me getting settled not only in the lab, but also exploring some hidden corners inside and outside of London and keep supporting me even after having both left the lab. Colin who I have done my very first Mass spectrometry run with and Helen, who continued on training me, sharing her sheer endless expertise and keeping me on top of the newest developments. Steve, who`s brain I could pick on basically any chemical reaction in the Mass spectrometry protocols. Luuk, Flavia, Margaux, Marisol, Simeon, Andre and our newest addition Almaz have given some great feedback and advice, making the lab a stimulating place to work which never got boring.

Special thanks to all my collaborators and scientific platforms within the Crick who have added invaluable expertise to this project. Federico, who has played a key role in identifying the tumour type. Stuart always happy to answer all my statistics related question. Bobbi and all BRF staff who have looked after my little ones all those years, whom without I would not have been able to complete this project.

A massive thanks to all my friends the “old” and the new. My friends from school and uni, even if not always happy with me having moved abroad again, being still so supportive and making it feel like having just met up yesterday. All my housemates, making the places we lived at, a place I could call home. My fellow agents ;). A special thanks to Amit, Lorena and Mohamed who have not only celebrated my highest highs, but were there in my darkest low.

Last but not least I want to thank my family who have given me the never ending support. Not only have you also patiently listened to me talking about the newest developments and struggles of my project, but you even asked for more.

Thanks to all of you (more than I can mention on this page), without you I could not have done it and in a way you all contributed to this work. So for my following thesis I refuse to write in the singular form of the first person, as you never walk alone.

Table of contents

Table of figures

List of tables

Abbreviations

aa	Amino acids
AGC	Protein kinases A, G, and C
AMPK	AMP-activated protein kinase
ATP	Adenosine triphosphate
BLBP	Brain-lipid-binding protein
CA1	Cornus ammonis 1 = Region I of hippocampus proper
CA3	Cornus ammonis 3 = Region III of hippocampus proper
cKO	Conditional knockout
CNS	Central nervous system
CTGF	Connective tissue growth factor
CTIP2	COUP-TF-interacting protein 2
DEGs	Differentially expressed genes
DG	Dentate gyrus
DIV	Days in vitro
DTT	Dithiothreitol
E#	Embryonic day
ECM	Extracellular matrix
EMA	Epithelial membrane antigen
EMT	Epithelial-to-mesenchymal transition
EPN	ependymoma
FC	Fold change
FDR	False discovery rate
FBS	Fetal bovine serum
GFAP	Glial fibrillary acidic protein
GFP	Green fluorescent protein
GO	Gene ontology
GPCR	G protein-coupled receptor
GSEA	Gene enrichment analysis
H&E	Haematoxylin and eosin staining
IHC	Immunohistochemestry
IF	Immunofluorecence

KD	Kinase dead
KEGG	Kyoto encyclopedia of genes and genomes
LATS	Large tumour suppressor
LC-MS/MS	Liquid chromatography-tandem Mass spectrometry
MAMLD1	Mastermind like domain containing 1
MEM	Minimum essential medium
micro-CT	Mirco-computed tomography
MOB	Mps one binder
MST	Mammalian Ste20-like serine/threonine kinase
MUC1	Mucin1
NBS	Neurobasal medium
NDR	Nuclear Dbf2-related
NEX	Neuronal helix-loop-helix protein
NF2	Neurofibromatosis type 2
NF-kB	Nulcear factor-kB
nls	Nuclear localisation sequence
NPC	Neural precursor cell
ns	Not significant
P#	Postnatal day
PCA	Principal component analysis
PCR	Poly chain reaction
PDL	Poly-D-lysine
PFA	Paraformaldehyde
PIF	PDK1-interacting fragment
RELA	RELA Proto-Oncogene, NF-KB Subunit
RGC	Radial glial cells
RIN	RNA integrity number
RNA	Ribonucleic acid
RT	Room temperature
SBF-SEM	Serial blockface scanning electron microscopy
SEM	Standard error of the mean
shRNA	Short/small hairpin RNA
SOX2	SRY-box 2
SVZ	Subventricular zone

TAZ	Transcriptional coactivator with PDZ-binding motif
TEAD	Transcription enhanced associated domain
TEM	Transmission electron microscopy
TMT	Tandem mass tag
UBA	Ubiquitin-associated domain
V-SVZ	Ventricular-subventricular zone
VZ	Ventricular zone
WHO	World health organisation
WT	Wild type
YAP1	Yes-associated protein 1

Chapter 1. Introduction

1.1 The Hippo pathway

The Hippo signalling pathway is well conserved through evolution (Chen et al 2020) and plays an important role in tissue homeostasis, organ size control and regulating tissue-specific stem cells across species (Davis & Tapon 2019) (Ma et al 2019). The canonical Hippo pathway consists of MST1/2 (mammalian Ste20-like serine/threonine kinase, Hippo in flies) which phosphorylates LATS1/2 (Large Tumour Suppressor, Warts in flies) at its C-terminal hydrophobic motif activating it. MOB (Mps-One Binder, Mob in flies), which itself is a phosphorylation substrate of MST1/2, acts as co-activator of LATS1/2 kinases (Figure 1.1). In addition, the conserved scaffold protein Salvador is required for LATS1/2 activity in cells. Activated LATS1/2 kinase phosphorylates the transcription coactivator YAP (Yes-associated protein, Yorkie in flies) and TAZ (WW domain–containing transcription regulator protein 1) on HxRxxS motifs (Hao et al 2008). YAP and TAZ lack DNA-binding domains.

When the Hippo pathway is on, YAP/TAZ get phosphorylated, bind to 14-3-3 and are no longer able to translocate into the nucleus resulting in the inhibition of their target genes transcription (Hergovich 2012) (Ma et al 2019). In the cytoplasm sequestered YAP/TAZ get ubitquitinated and proteasomal degraded. When the Hippo pathway is inactivated, dephosphorylated YAP/TAZ are translocating into the nucleus. They bind primarily to transcription factor TEAD1-4 (Transcription enhanced associated domain, Scaloped in flies) which induces expressions of genes such as CTGF (connective tissue growth factor) which is important in YAP1-mediated cell growth (Zhao et al 2008) (Pocaterra et al 2020). The regulation of the Hippo signalling network is rather dynamic. YAP and TAZ are constantly phosphorylated and dephosphorylated leading to a dynamic shuttling between the cytoplasm and the nucleus (Manning et al 2018).

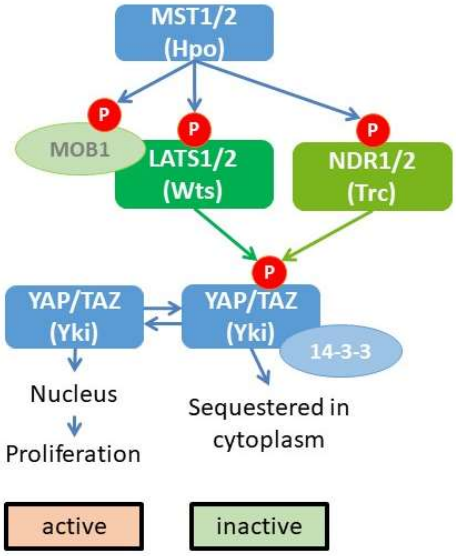

Figure 1.1. The canonical Hippo pathway extended.

In the canonical pathway MST1/2 phosphorylates LATS1/2 at the hydrophobic motif (LATS1 T1079, LATS2 T1041). Additionally, MST1/2 can also phosphorylate NDR1/2 (NDR1 T444, NDR2 T442). MOB, phosphorylated by MST1/2, binds to LATS1/2 increasing its activity. Activated LATS1/2 or NDR1/2 directly interacts with YAP/TAZ leading to their phosphorylation, which induces 14-3-3 binding and cytoplasmic retention. Therefore, YAP/TAZ are not able to translocate in the nucleus to trigger target gene expression.

Besides the core components of the pathway, there are additional kinases which are closely connected to the Hippo core cassette. NDR1/2 (Nuclear Dbf2-related kinase, Trc in flies), which is in the AGC (protein kinases A, G, and C) serine/threonine kinase family as is LATS1/2, has been identified to be able to directly phosphorylate YAP/TAZ (Zhang et al 2015) (Hergovich 2016). Depletion of NDR1/2-depleted intestinal tissue showed increased YAP1 activity demonstrated by elevated nuclear location and increased YAP1 target gene expression (Zhang et al 2015). It was further found that much like LATS1/2 also NDR1/2 can be phosphorylated on their hydrophobic motifs by MST1/2 kinases. It is suggested that LATS1/2 might be the major YAP1 regulators as it was noted that double knockout of *Lats1/2* in HEK293 cells decreases YAP1 phosphorylation substantially (Meng et al 2016) (Hergovich 2016). Also MAP4K kinase family members have been identified to play in the Hippo pathway signalling. They have been found to activate LATS1/2 through phosphorylation and consequently inhibit YAP/TAZ (Zheng et al 2015).

1.1.1 Upstream signals

Intrinsic as well as extrinsic signals are incorporated in the tight regulation of the Hippo pathway and thus affect the activity of YAP/TAZ. Such upstream signals include for example mechanical cues, cell polarity, soluble factors and stress signalling (Totaro et al 2018) (Ma et al 2019).

Mechanical forces have been recognised to play an important role in modulating this signalling pathway. Cell-cell contact, cell shape, cell stretching, cell tension and extracellular matrix (ECM) have been shown to affect the phosphorylation status and thus the localisation of YAP/TAZ (Zhao et al 2007) (Nishioka et al 2009). For example, in high cell density, LATS kinase is activated, able to phosphorylate and consequently inhibit YAP1 (Nishioka et al 2009) (Gumbiner & Kim 2014). Contact inhibition is an important factor in multicellular organisms to ensure controlled organ growth and tissue homeostasis. Similarly, cell polarity and cell adhesion components are involved in the regulation of the Hippo pathway. The activity of the LATS kinase can be controlled by those factors through for example NF2 (Neurofibromatosis type 2) by recruiting LATS to the cellular membrane and so promoting its phosphorylation and activation by the MST-SAV complex (Yin et al 2013). Further, some soluble factors like hormones and growth factors have shown to affect the activity of YAP/TAZ through G protein-coupled receptors (GPCRs). As an example the hormone lysophosphatic acid is able to inhibit LATS through GPCR (Yu et al 2012). Additionally, multiple cellular stresses have been linked with the regulation of the Hippo pathway. Lack of glucose has been observed to induce the inhibition of YAP/TAZ through the metabolic sensor AMP-activated protein kinase (AMPK) (DeRan et al 2014).

In a multicellular organism the proper regulation of tissue development and homeostasis is crucial. Consequently, it is not surprising that many factors contribute to the complex regulation of the Hippo pathway on many levels.

1.1.2 LATS1/2 Kinases in the brain

LATS1/2 are members of the Nuclear Dbf2-related (NDR) family, which has been classified as a subgroup of the serine/threonine AGC (PKA/ PKG/ PKC containing) class of protein kinases based on the sequence of the catalytic domain (Pearce et al

2010). LATS1/2 are able to auto-phosphorylate at the activation loop which positively regulates their activity. LATS1 and LATS2 are exhibit high sequence similarity in particular the kinase domain (85%) and share comparable modes of post-translational modifications (Figure 1.2) (Furth & Aylon 2017). The kinases have both redundant as well as distinct functions from each other. Complete depletion of *Lats2* was found to be embryonic lethal (McPherson et al 2004b), while *Lats1* knockout mice are viable (St John et al 1999).

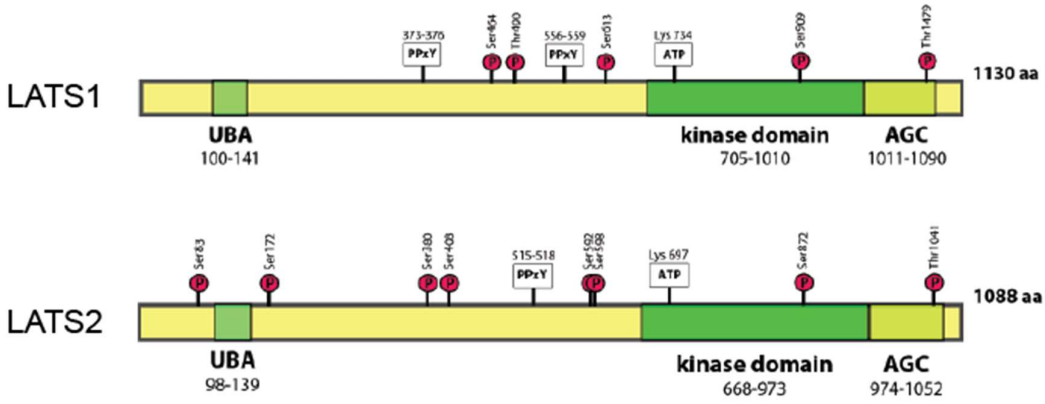

Figure 1.2. Comparison of LATS1 and LATS2.

Comparison of LATS1 and LATS2. Human LATS1 and LATS2 are very similar, in length, allocation of domains and phosphorylation sites. They show an overall 50% homology in sequence, their kinase domain being 84% homologues (Uniprot align). Phosphorylation sites associated with a function are shown. Ser909/872 and Thr1479/1041 are essential for the activity of LATS1/2. ATP binding site and PPxY motifs (interaction site with WW domains in for example YAP) are shown. aa = amino acids, AGC = AGC domain, ATP = adenosine triphosphate, LATS = Large Tumour Suppressor, UBA = ubiquitin-associated domain.

The Hippo pathway regulates the overall brain size via Yki in drosophila by as acting as a control mechanism for the proliferative potential of neuroblasts thus affecting the number of neurons (Poon et al 2016). However, the non-canonical role of LATS1/2 in mammalian brain development and function is not known.

Development and functioning of the brain depends on correct wiring of the neural circuitry (Supèr et al 1998). In order to have a functional nervous system, specialized cells, called neurons need to differentiate and form input receiving dendrites and output sending axons. In the hippocampus and cortex of the mammalian brain, pyramidal neurons make up the majority of neurons. Their dendrites have excitatory

postsynaptic sites called dendritic spines. Proper development of dendrites and dendritic spines is essential for the neuronal circuit wiring. Failure to either form or maintain these synaptic structures can be associated with neurodevelopmental and neurodegenerative diseases. Despite their importance, molecular mechanisms regulating these processes are not well-understood.

Depletion of both hippo and warts in Drosophila sensory neurons results in deficiency in maintaining dendritic arborisation, importantly this effect was independent of yorkie function (Emoto et al 2006). The role of Hippo kinase signalling in developing mammalian neurons and the molecular mechanisms downstream of LATS1/2 in mammalian neurons are not known. However, LATS2 mRNA is highly expressed in the CA3 region of the mouse hippocampus, while LATS1 was not detected in the murine brain using a single probe in Allen Brain Atlas suggesting a specialised function.

One of our goals is to test if the descripted function of Warts in Drosophila is conserved in mammalians via LATS1/2.

1.2 Hippo pathway in cancer

Dysregulation of the Hippo signalling network has been found in many human tumours, such as colorectal cancer and glioma (Ma et al 2019). Its tumourigenesis properties has also been shown *in vivo*. As an example, conditional knockout of *Mst1/2* or *Lats1/2* in the liver results in deregulation of progenitor cell proliferation and tumour development in mice (Lu et al 2010). Dysregulation of YAP increasing cell proliferation has been shown in multiple tissues (Yu et al 2015). Uncontrollable proliferation is one important factor in tumourigenesis. Under normal circumstances the Hippo pathway has been described to be important for contact imbibition, and suppressing proliferation in dense cell populations (Zhao et al 2007). A property which can be found lost in a variety of cancers. It has been further shown that deregulation of Hippo signalling can aid cell survival. YAP1 downstream targets such as Survivin and growth factors may lead to an insensitivity to apoptosis (Bai et al 2012) (Zanconato et al 2015). Furthermore, to increase migration and invasion cancer cells utilise EMT (epithelial-to-mesenchymal transition). YAP/TAZ have been shown to be active stimulator of EMT and multiple EMT-inducing signals are

supressing the Hippo pathway (Kim et al 2019). Importantly, active YAP/TAZ can induce cancer stem cell properties in multiple tumours (Panciera et al 2016). Cancer stem cells are believed to play a key role in tumour initiation and recurrence besides being able to unlimited self-renewal.

Recently, more efforts were put towards studying the relationship between the Hippo signalling network and the immune system. Multiple studies paint a complex picture of both enhancing and inhibitory tumour immune response. As an example the knockdown of LATS1/2 was shown to improve anti-tumour immune response (Moroishi et al 2016). On the other hand, *Lats1/2* knockout and active YAP1 in mouse liver have shown to result in a tumour-promoting microenvironment due to recruitment of type II macrophages (Guo et al 2017).

1.2.1 YAP1 in cancer

Increased levels of YAP1 have been linked with a poor prognosis and decrease survival for patients (Yan et al 2020). Multiple human tumours have been found to display apparent YAP/TAZ expression, also linking it to promoted tumour growth and drug resistance (Zanconato et al 2016). As an example, subtypes of Medulloblastoma demonstrate elevated YAP1 expression, which is also found increased in the corresponding mouse model (Fernandez-L et al 2009). Other tumours with reported YAP/TAZ activation include glioma, breast cancer, colorectal cancer, melanoma and many more (Zanconato et al 2016) (Han 2019). Studies have shown that inhibition of YAP1 can have promising effects in model systems (Zanconato et al 2016).

The shuttling of YAP/TAZ between the nucleus and the cytoplasm is a tightly regulated process. Nuclear localisation increases proliferation and promotes stem cell like characteristics (Ahmed et al 2017). Consequently, deregulated nuclear YAP/TAZ can trigger stem cell proliferation. Furthermore, it has been demonstrated that YAP/TAZ play a role in differentiation and maturation of cells (Zhao et al 2011). Both proteins can be disrupted in cancer in multiple ways.

The niches generated by tumours is different to normal tissue and it is known that the extracellular matrix can directly regulate YAP1/TAZ via Rho GTPase activity (Dupont et al 2011). Other signalling pathways often shown affected in cancer such

as Wnt signalling have been linked with the Hippo pathway and consequently impact the regulation of YAP/TAZ (Moroishi et al 2015). Furthermore, the loss of contact inhibition in cells overexpressing YAP/TAZ can be one reason for sustained proliferation in cancer (Piccolo et al 2014). It has been shown that YAP/TAZ can supress TNF-α mediated cell death giving tumour cells a survival benefit (Dong et al 2007). The ability of YAP/TAZ to maintain stem cell characteristic and inhibit differentiation or even loss of differentiation are traits further driving tumour growth and aid the development of metastasis (Piccolo et al 2014).

1.3 Brain tumours

The brain is a complex and highly organised organ with a fast array of different cell types and specialised microenvironments, making brain tumours a very heterogeneous group of diseases. The unique biology and the anatomy of the brain makes it challenging for both studying and treating those cancers (McFaline-Figueroa & Lee 2018) (Aldape et al 2019).

Gliomas are the most often found type of primary brain tumour in adults (Lapointe et al 2018). An increased understanding of genetic alterations and molecular features combined with the histological analysis have aided an updated 2016 WHO classification of CNS (Central nervous system) tumours (Wesseling & Capper 2018) (Lapointe et al 2018).

The improved molecular characterisation and subtyping of patients shows the complexity of those tumours, but simultaneously aids patient stratification and targeted treatment (Pollack et al 2019).

In children the most common type of solid tumour and accounting for the most cancer-related deaths are brain tumours (Jones et al 2019) (Malbari & Lindsay 2020). In general, pediatric brain tumours are known to be fundamentally different from adult CNS tumours (Jones et al 2019).

1.3.1 Ependymoma

Ependymomas are rare neuroepithelial tumours of the central nervous system (CNS) which occur in all age groups, but exhibit decreasing incidence rate with increasing

age (Ostrom et al 2016). It is the third most common pediatric brain tumour accounting for 5-10% of all primary tumours in children and adolescents. Symptoms include headaches, problems in coordination and balance, seizures and slowed mental development in children. The main treatment is surgery and sometimes radiotherapy depending on size, grade and position of the ependymoma (Thorp & Gandola 2019). They are largely resistant to chemotherapy, predominantly through the lack of molecular targets. Subsequently, this cancer type remains incurable in roughly 40% of cases (Parker et al 2014).

According to the "2016 WHO Classification of Tumors of the Central Nervous System" ependymal tumours can be divided into five major types; Subependymomas, Myxopapillary ependymomas, Ependymomas (which can be subdivided into further groups), Anaplastic ependymomas and Ependymoma RELA fusion-positive has recently been accepted as a genetically defined subtype (Louis et al 2016). However, a clear grading and reproducible classification of ependymomas is not yet achieved by existing WHO criteria due to the overlapping molecular features between so far defined subgroups. For example, microscopic characteristics of anaplastic ependymomas, which are linked with bad prognosis due to their increased growth rate, are not easily distinguishable from classical ependymomas (Benson et al 2016). Beside histological grade, patient age and the site of the tumour are important prognostic factors. Ependymomas can be found in three different locations: supratentorial, posterior fossa and those located in the spine (Yao et al 2011) (Pajtler et al 2015). These factors have led to a classification of ependymoma into nine molecular subgroups defined by genetic and epigenetic features (Pajtler et al 2015).

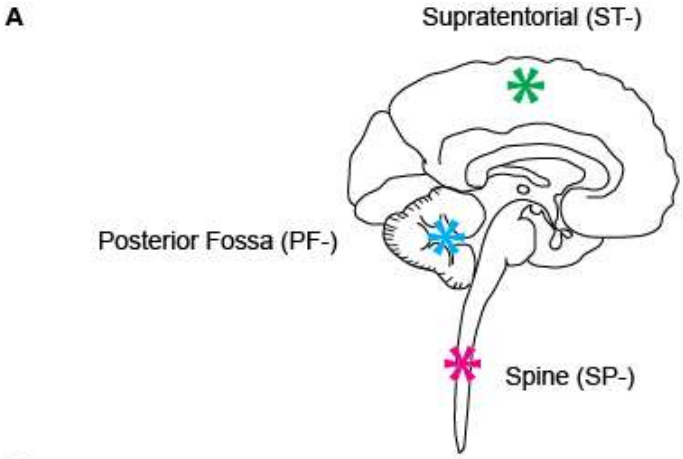

B

Location	Supratentorial (ST-)			Posterior Fossa (PF-)			Spine (SP-)		
Molecular Subtype	SE	EPN-YAP1	EPN-RELA	SE	EPN-A	EPN-B	SE	MPE	EPN
Oncogenic Driver	?	*YAP1*-fusion	*RELA*-fusion	?	?	?	?	?	*NF2*
Age Distribution [years]	4 18 60	4 18 60	4 18 60	4 18 60	4 18 60	4 18 60	4 18 60	4 18 60	4 18 60

Figure 1.3. Ependymal tumour subtypes.

A. A schematic representation of the three locations ependymoma can be found and basis for division into nine subpopulations. **B**. Simplified overview of molecular subtypes of ependymoma according to their location, oncogenic drivers and age distribution (Pajtler et al 2015). EPN = ependymoma, MPE = myxopapillary EPN, PF = posterior fossa, SE = subependymoma, SP = spine, ST = supratentorial,

Of the three locations ependymoma has been reported each divides into three further subpopulations according to molecular and clinical characteristics (Figure 1.3). For most of them the oncogenic driver remains unknown. One spinal (SP-EPN) was shown with most frequent loss of the 22q locus which includes NF2, being suspected as a potential driver. Two other subgroups, both supratentorial, are characterised by a fusion gene involving either RELA (ST-EPN-RELA) or YAP1 (ST-EPN-YAP1).

70% of supratentorial ependymoma can be found with a RELA-fusion, most commonly with C11orf95 (Parker et al 2014). Expression of C11orf95-RELA leads to nuclear translocation and activation of abnormal NF-kB (nuclear factor-kB) signalling. Increased NF-kB activity has been linked to the generation of a pro-tumourigenic microenvironment, but also promoting tumour initiation and

development through other factors (Xia et al 2014). In YAP1-fusion ependymoma, the identified fusion partners are most often MAMLD1 (Mastermind Like Domain Containing 1) or an uncharacterised protein, FAM118B. This subtype is almost exclusively found in infants with an average age of 1 year. In such YAP1-MAMLD1 tumours, an increase nuclear expression of YAP1 is reported independent of S127 phosphorylation (Pajtler et al 2019).

Ependymoma heterogeneity, which expresses in the variation of patient age, tumour localisation and histological grade in addition to limited number of samples to study make it challenging to investigate this cancer type. Also a lack of model systems makes it difficult to identify and define molecular mechanism underlying development and progression of ependymomas in order to improve prognostic and treatment for patients.

1.3.2 The role of the Hippo pathway in ependymoma

Three of the nine molecular characterised subtypes have been associated with an oncogenic driver, while for the remaining six the drivers remain to be identified (Pajtler et al 2015). Out of those three, two are directly linked with the Hippo pathway. A subtype of spinal tumours (SP-EPN) has been found to with an abnormal chromosome 22, leading to the loss of the NF2 gene (Buccoliero et al 2010). This gene translates into the protein merlin, which has implications in the cytoskeleton and cell adhesion (Li et al 2014). Furthermore, NF2 is upstream of the Hippo pathway and has been found as a major factor of its activation. Thus loss of merlin results in accumulation of YAP1 in the nucleus and consequently triggering for example proliferation (Boin et al 2014) (Li et al 2014).

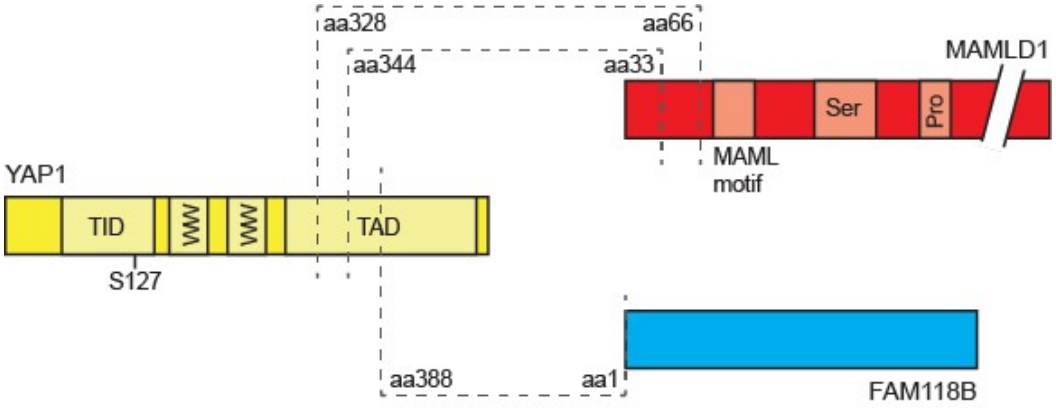

Figure 1.4. Examples of YAP1 fusion types on protein level.

Described YAP1 fusion types with MAMLD1 or FAM118B found in ependymoma subtype ST-EPN-YAP1. Dashed lines indicate fusion sites. TID = TEA domain-containing factor-interaction domain for TEAD, WW = protein-protein interaction domain, TAD = transcriptional activation domain for TEAD, MAML = mastermind-like domain, Ser = serine-rich region, Pro = proline-rich region. (Pajtler et al 2019)

The second identified ependymoma subtype linked to the Hippo pathway is the YAP1 fusion supratentorial ependymoma (ST-EPN-YAP1). The most common fusions reported are YAP1-MAMLD1 and YAP1-FAM118B and those have not been reported in any other tumour type (Pajtler et al 2019). It has been suggested that MAMLD1 mediates nuclear localisation of the fusion protein and so YAP1 is able to function as an oncogenic driver (Pajtler et al 2019).

1.3.3 Radial glia and ependymal cells

Radial Glial cells (RGC) are reported to give rise to ependymal cells and are suggested as ependymoma stem cells. Detecting the cell of origin for a type of cancer can be crucial in identifying following oncogenic events and developing targeted therapies.

During development cells from the ectoderm differentiate into multipotent neuronal stem cells which can generate neurons as well as glial cells (Bertrand et al 2002). Those neuroepethelial cells can give rise to radial glial cells, a more fate-restricted progenitor. Radial glial cells keep several neuroepithelial features such as apical-basal polarity and expression of Nestin (Gotz & Huttner 2005). However, they gain some astroglial characteristics for example GFAP (Glial fibrillary acidic protein),

Vimentin and BLBP (Brain-lipid-binding protein) expression. Radial glial cells can give rise to astrocytes, oligodendrocytes, neurons and ependymal cells.
BrdU experiments showed that RGCs are identified to the ependymal cells linage at the age of around E14-E16 in mice (Spassky et al 2005). However, ependymal cell differentiation is initiated after birth and is accomplished by 20 days of age in mice. Ependymal cells are ciliated epithelium lining the ventricular lumen of the CNS. They are important components of the adult V-SVZ (Ventricular-subventricular zone) nice, impacting the correct cytoarchitecture as well as the regulation of self-renewal and differentiation decisions of NSCs (Kyrousi et al 2017). Besides acting as a barrier they are also vital for transporting small molecules between the cerebrospinal fluid and the brain (Bigio 2010). When mature these cells have a decreased proliferative activity and limited repair capability.

1.3.4 Mouse model of ependymoma

Mouse models of diseases are very important and useful in understanding the pathogenesis and the complex interactions within a living system. Cancer specific model systems enable studying particular tumour subtypes and aid the development of targeted treatments. In the effort of a better understanding of ependymoma and improving the therapeutic interventions, patient derived xenograft models have been developed (Mclendon et al 1996) (Guan et al 2011) (Milde et al 2011) (Barszczyk et al 2014). This type of model system has a higher reliability when it comes to reproducing the heterogeneity of the human disease and reflecting therapeutic responses (Hermans & Hulleman 2020). However, some available xenograft models have been established without molecular characterisation which can hinder the classification into the newer defined molecular subgroups (Hermans & Hulleman 2020).
Besides the xenografts, some mouse models mimicking the genetic alterations in the cells of origin have shown valuable for investigating the tumour development (Johnson et al 2010) (Ozawa et al 2018) (Pajtler et al 2019). As an example, cerebral embryonic neural stem cells have been isolated from Ink4a/Arf-depleted mice, a genetic aberration observed in human ependymoma patients (Taylor et al 2005) and were transformed by an Ephb2-expressing virus (Johnson et al 2010). The resulting

mEP^{Ephb2re} mouse model has been used in high-throughput screens identifying 5-fluoroucil as an effective treatment (Atkinson et al 2011). A hypothesis that has been taken forward to clinical trials and showing the antitumour activity of 5-fluoroucil in human ependymoma patients (Wright et al 2015). Another mouse model was developed by transducing nestin expressing mouse stem cells with a C11orf95-RELA fusion protein (Ozawa et al 2018). Striking similarities to human ependymoma could be found in both of those models (Johnson et al 2010) (Ozawa et al 2018). Rosettes or pseudo-rosettes are often described in human ependymoma patients were present in the mEP^{Ephb2} model (Milde et al 2011), but were not found in other mouse models (Johnson et al 2010) (Pajtler et al 2019).

Chapter 2. Materials & Methods

2.1 Human tissue

2.1.1 Patient samples

Tissue of six ependymoma patient samples were provided by Dr Felipe Andreiuolo (Institute of Neuropathology, University of Bonn Medical Center, Bonn, Germany) with known subtype (MAMLD1-YAP1 or C11orf95-RELA fusion, 3 each). Written consent was given by the patient (one adult RELA tumour) or by legal representatives (five children, three YAP and two RELA ependymoma). All tumours at diagnosis without any previous treatments such as chemotherapy nor radiotherapy.

2.1.2 Immunohistochemistry

Immunohistochemistry stainings were done by the Experimental Histopathology Platform at the Francis Crick Institute. For immunohistochemistry (IHC) tissue analysis of YAP1, HOPX, ANXA1 and RELA (NF-kB p65) expression, the patient tissues were deparaffinised and subject to Heat-Mediated Antigen Retrieval (pH6 Citric Buffer, microwave 23 min). The slides were incubated with YAP1 (1:400, Cell Signalling #14074), HOPX (1:250, Proteintech #11419-1-AP), ANXA1 (1:350, Proteintech, #21990-1-AP), NF-kB p65 (1:800, Cell Signalling #8242) in signal stain diluent overnight at 4°C and 45 min in secondary antibody. Diaminobenzidine was utilised as the chromogen and the sections were counterstained with haematoxylin. Images were acquired with an Olympus VS120 Slide Scanner and a Leica DM2500 LED.

2.2 Primary neuronal cultures

2.2.1 Hippocampal cell cultures

Pregnant Long Evans rats are ordered from Jackson. E18.5 rat embryos were removed from the uterus and the brains were taken. The hippocampi were dissected

out, pooled from multiple animals and washed three times with Hank's balanced salt solution (HBSS). An incubation with 0.25% trypsin for 20 minutes at 37°C was followed by four times washing with HBSS. Cells were dissociated by carefully re-suspending 20 times and counted using a haemocytometer. Glass coverslips, were coated over night with 0.1 M borate buffer containing 60 µg/ml poly-D-lysine (PDL) and 2.5 µg/ml laminin at room temperature. 150,000 cells were plated on each coverslip with plating media containing 10% FBS (Fetal bovine serum), 0.5% dextrose, sodium pyruvate, 2 mM glutamine and penicillin/streptomycin in minimum essential medium (MEM). After 3-4 hours plating media was replaced for maintenance media containing B27, 0.5 mM glutamine, 12.5 µM glutamate, penicillin/streptomycin and ciprofloxacin in neurobasal medium (NBM). Primary neuronal cultures were kept at 37°C and 5% CO_2. Every 3-4 days, 20-30% of the maintenance media was refreshed. The majority of primary neuronal cultures was prepared by Suzanne Claxton.

Neurons were transfected with 1 µl Lipofectamine 2000 (Thermo Scientific) and 1 µg DNA at DIV4 (Days in vitro) for 15 minutes at 37°C. Prior to transfection, half of the maintenance media was taken off and supplemented with the same amount of fresh maintenance media. This was used to replace the media after the transfection.

2.2.2 Fixation and staining

Coverslips with cultured and treated primary hippocampal neurons were fixed at DIV 18 with 4% paraformaldehyde (PFA), 4% sucrose for 10 minutes at room temperature. Subsequently they were washed three times with PBS. Coverslips were blocked and permeabilised for 1 hour with 0.1% TritonX in 10% normal goat serum at room temperature (RT). In the same buffer, the following primary antibodies were incubated o/n at 4°C: CTIP2 (1:2000, Abcam #ab18465), GFP (1:2000, Aves Lab), HA (1:1000, Covance). After three 5-10-minute washes with PBS, 1:500 secondary antibodies in blocking solution were incubated for 2 hours at RT. Coverslips were again washed three times, of which the second contained 1:2000 DAPI stain (Thermo Scientific). Coverslips and were mounted with Fluoromount-G (Southern Biotech) on glass slides.

2.2.3 Imaging and analysis

Dendritic arbours of GFP (Green fluorescent protein) and HA expressing dissociated primary neurons were imaged. Pyramidal neurons were identified by typical morphological hallmarks like the presence of an axon and a branched dendritic arbour. Hippocampal CA3 neurons were specifically selected by negative CTIP2 staining. Images were acquired with a Leica MPSP5 Upright Confocal microscope (20x/0.5 air, 455 nm voxel, 1.5 µm z-step size). Dendrites were manually reconstructed using Neurolucida 360 (MBF Bioscience) and analysed with Neurolucida Explorer (MBF Bioscience). Z-stacks of secondary dendrites were acquired at DIV18 with the same microscope and a Leica HyD photodetector (100x/1.46 oil, 75 nm voxel, 0.29 µm z-step size). Images were processed with Leica Application Suite and Fiji. Spine density and maturation was manually measured and classified.

2.3 Animals

2.3.1 Mouse lines

Maintenance and handling of animals were performed under regulations of the Animal (Scientific procedures) Act 1986 of the United Kingdom and approved by institutional ethical reviews. The experiments were conducted in accordance to the project licence P5E6B5A4B (previously: 70/7771). Mice were group housed and maintained on a 12 hr light/dark cycle, with food and water provided *ad libitum*. None of the experimental mice were immune compromised. Both male and female mice were used and randomly allocated to experimental groups according to genotypes. LATS1/2 cKO (conditional knockout) and nlsYAP5SA mice were closely monitored and weighed regularly. The majority of LATS1/2 cKO mice were collected at < 3 weeks of age. In accordance to the project license, a subset of LATS1/2 cKO animals were aged up to 2 months of age, provided they did not exceed 10% weight loss criteria (about 50% were collected before reaching 1 month of age to prevent reaching this end point) and nlsYAP5SA mice were aged only up to 2 weeks due to higher severity.

NEX-Cre (*Neurod6*$^{tm1(cre)Kan}$, MGI:2668659) was a generous gift from Dr. Klaus Nave. *Lats1*$^{f/f}$ *Lats2*$^{f/f}$ (Lats1$^{tm1.1Jfm}$ MGI:5568586 and Lats2$^{tm1.1Jfm}$ MGI:5568589) mouse containing the ROSA$^{mT/mG}$ (Gt(ROSA)26Sor$^{tm4(ACTB-tdTomato,-EGFP)}$) allele were kindly provided by Dr. R. Johnston (University of Texas MD Anderson Cancer Center, USA). Ai14 (Gt(ROSA)26Sor$^{tm14(CAG-tdtomato)Hze}$; Stock Number:007908) was purchased from Jackson Laboratories. YAP1$^{f/f}$ (Yap1$^{tm1c(KOMP)Mbp}$, MGI:5603606), TAZ$^{f/f}$ (Wwtr1$^{tm1c(EUCOMM)Wtsi}$, MGI:5603602) mice were from Barry Thompson's laboratory and nlsYAP5SA mice were described previously (Cotton et al 2017). Lats mice are on a mixed background (C57BL/6J, CD-1 and 129vEV). All other lines are on a C57BL/6J background.

2.3.2 Genotyping

Ear, toe or tail toe biopsies were lysed with lysis buffer containing 25 mM NaOH and 200 µM EDTA for 30 minutes at 95°C, and neutralised with 1 M Tris-HCl pH 7.5. PCR reactions were set up containing 0.2 µM of each primer, 2 µl lysate, 0.2 mM dNTP mix, 1x Kapa Hifi buffer and 2.5 U Kapa Hifi Taq polymerase. In case of LATS2 PCR`s 4 µl Betaine was added. The following PCR program was used: 1. 94°C for 4 minutes, 2. 94°C for 45 seconds, 3. 58°C for 30 seconds, 4. 72°C for 45 seconds, 5. 72°C for 7 minutes, 6. hold at 4°C. Steps 2-4 are repeated 32 times. Only the NEX PCRs was slightly adapted to 55°C annealing temperature and an extension time of 30 seconds. After collection of experimental animals, a second PCR was performed with new material to confirm the genotype.
Most genotyping was done by Suzanne Claxton.

Table 2.1. Primers for genotyping

Primer	Sequence 5` → 3`	Expected bands
Lats1 forward	TCC CTT GAT TTG TTG CTG CT	Mutant = ~350 bp
Lats1 revers	GGC CAT TAC ACA GAA TGA ATG A	Wild type = ~ 206 bp
Lats2 forward	GGC GCA TGC CTT TAA TCC T	Mutant = ~350 bp
Lats2 reverse	CAC ATT CCC CTC CAC TGA	Wild type = ~ 249 bp
Yap1 forward	GCT TCC TGT AGT CAT GTG GTT GT	Depleted = ~457 bp
Yap1 reverse	TGT TGT CAT ATG CCA TTG TGT AA	Floxed = ~154 bp
Yap1 delta forward	CAC AGA GAT CCT CCT GTC TCA G	Wild type = ~138 bp

Taz forward	AGC AAA GTA AGG GCA CTG TAT G	Depleted = ~249 bp
Taz reverse	GCT CCC AAA CCA CAT CAC AG	Floxed = ~295 bp
Taz delta reverse	TCT ACT CTT GGC TCT TAG CTG G	Wild type = ~161 bp
LacZ forward (nlsYAP5SA)	GAC GTC TCG TTG CTG CAT AA	Band = ~ 400 bp
LacZ reverse (nlsYAP5SA)	CAG CAG CAG ACC ATT TTC AA	
Nex forward	GAG TCC TGG AAT CAG TCT TTT TC	Mutant = ~500 bp
Nex reverse	AGA ATG TGG AGT AGG GTG AC	Wild type = ~700 bp
Cre forward	CCG CAT AAC CAG TGA AAC AG	
Ai14 wt forward	AAG GGA GCT GCA GTG GAG TA	Wilt type = ~297 bp
Ai14 wt reverse	CCG AAA ATC TGT GGG AAG TC	
Ai14 mt forward	CTG TTC CTG TAC GGC ATG G	Mutant = ~196 bp
Ai14 mt reverse	GGC ATT AAA GCA GCG TAT CC	

2.3.3 Harvesting brains

For Western blot lysates and proteomics, fresh brains were taken promptly from mice after cervical dislocation and decapitation. When desired, brain regions were dissected and tissue was flash frozen in liquid N_2.

For brain tissue section staining, P0-P10 mice were decapitated and the brain fixed in 4% ice-cold PFA in PBS for 2 days at 4°C. Older mice were put under surgical anaesthesia with 80-100 mg/kg ketamine (Vetalar) + 10 mg/kg xylazine (Rompun) injected intraperitoneal. Once deeply anaesthetised animals were transcardial perfused first with PBS (~0.5 ml per g body weight) to clear from blood, followed with 4% PFA (~1-1.5 ml per g body weight). Brains were dissected out and post-fixed in 4% PFA overnight at 4 °C. Brains were then kept in PBS with Sodium Azide at 4°C until further processing.

2.4 Processing harvested tissue

2.4.1 Western blots

Flash frozen mouse brains were homogenized by sonication in sample buffer containing 0.2 M DTT (Dithiothreitol). Lysates were centrifuged at 13,000 g for 15

minutes and supernatants denatured at 95°C for 10 minutes. Equal amount of protein from the brain lysates were ran on a NuPAGE 4-12% Bis-Tris polyacrylamide gels (Invitrogen) and then transferred to a PVDF membrane (Millipore). After blocking in 5% non-fat milk in TBST for 1 hour, the membrane was incubated with the primary antibodies in blocking solution overnight at 4°C. The following antibodies were used; CTGF (1:1,000, Abcam #ab6992); CYR61 (1:1,000, Abcam #ab24448); GAPDH (1:5,000, Abcam #ab8245); GFAP (1:1,000, Sigma-Aldrich #G6171); HOPX (1:1,000, ProteinTech #11419-1-AP); LATS1 (1:1,000, Cell Signalling #3477), LATS1/2 (1:2,000, Bethyl Laboratories #A300-479A), LATS2 (1:1,000, Abcam #ab174499; 1:400, Atlas #HPA039191), TAZ (1:1,000, Abcam #ab84927); Tubulin (1:50,000), Vimentin (1:5,000, Abcam #ab92547) and YAP1 (1:2,000, Cell Signalling #14074). Subsequently, the membrane was incubated with the horseradish peroxidase-conjugated (HRP) secondary antibody for 1 hour - HRP conjugated mouse (1:10,000; Jackson #715-035-151) and HRP conjugated rabbit (1: 10,000; Jackson #711-035-152). Finally, the membrane was developed with ECL system (Pierce) and visualised by a chemiluminescence detection system (Amersham WB System). Western blot analysis was performed using ImageJ software (version 1.52r).

2.4.2 Immunofluorescence staining

For immunofluorescence coronal or sagittal sections were prepared from the PFA fixed brains with a Leica VT1000S vibrating blade microtome at 50 µm. The sections were blocked with 10% serum and 0.2% Triton-X in PBS for 1 hour at RT and incubated with primary antibody in blocking solution overnight at 4°C (Exception, in case of tumour measurements a subset of brain sections were incubated with primary antibody against Vimentin for 2 hrs at RT and then proceeded as described). Used antibodies include AMOTL2 (1:100, GeneTex #CTX120712), ANKRD1 (1:100, Proteintech #11427-1-AP), ANXA1 (1:100, Proteintech, #21990-1-AP), AXL (1:100, R&D Systems #AF854), C3 (1:100, Abcam #ab11862), Cre (1:500, Covance #PRB-106P), CTIP2 (1:500, Abcam #ab18465), Cytokeratin (1:100, Abcam #ab9377), GFAP (mouse 1:500, Sigma #G6171 and chicken 1:1000, Abcam #ab134436), HOPX (1:100, Proteintech #11419-1-AP), Ki67 (1:100/1:300, BD #550609), MUC1

(1:500, Abcam #ab45167), Nestin (1:100, Millipore #MAB353), NeuN (1:100, Millipore #MAB377), SOX2 (1:100, Abcam #ab79351) and YAP1 (rabbit 1:100, CST #14074 (D8H1X) and mouse 1:100, Santa Cruz Biotechnology #sc-101199). Sections were incubated with the appropriate Alexa fluor 488-, 546- or 647-conjugated secondary antibodies (1:500; Thermo Fisher) for 2 hr at room temperature. Nuclei were stained using DAPI. Sections were mounted on slides with Fluoromount. Images were acquired with Olympus IX83 P22F (camera: Hamamatsu ORCA-Flash4.0; software: OLYMPUS cellSens Dimension 1.13 (Build 13479)) or Leica MPSP5 Upright Confocal as indicated in the figure legends.

2.4.3 Immunohistochemistry and histology

Murine brains subject to histological analysis were dehydrated and embedded in paraffin after completion of 4% PFA fixation. The tissues were sectioned (4 µm) and sections were prepared for H&E (Haematoxylin and eosin staining) or IHC. Unless stated otherwise the heat induced antigen retrieval (citrate buffer pH = 6, 23 min microwave) has been applied and primaries were incubated for 1 hr at RT. The following antibodies were used for IHC; ANXA1 (1:300, Proteintech, #21990-1-AP), CK18 (1:3000, ThermoFisher #PA5-14263; Tris-EDTA pH9), GFAP (1:750, DAKO #z0334), HOPX (1:250, Proteintech #11419-1-AP), Ki67 (1:350, Abcam #ab16667), MUC1 (1:500, Abcam #ab15481), Nestin (1:600, BD Biosciences #611659), RELA/ NF-kB p65 (1:800, Cell Signalling #8242), NeuN (1:600, Chemicon #MAB377), Vimentin (1:600, Abcam #ab92547), YAP1 (1:400, CST #14074; in signal stain (from CST) overnight at 4°C). Paraffin embedding, sectioning and IHC stainings were done by the Experimental Histopathology Platform at the Francis Crick Institute.
Slices were imaged using the Olympus VS120 Slide Scanner and/or the Leica DM2500 LED.

2.5 Electron microscopy

For serial blockface scanning electron microscopy (SBF SEM) and transmission electron microscopy (TEM), mouse brains were perfused fixed in 2% PFA, 2.5% GA in 0.1 M PB pH 7.4 and post-fixed for at least 4-5 hours in 2% PFA in 0.1 M PB pH

7.4 at 4°C. The brains were then sectioned using a Leica VT1000 S vibrating blade microtome (Leica). 50 and 100µm sections were collected and stored in 0.1M PB. The 50 µm sections were then stained with DAPI and imaged as previously to identify the locations of the tumours. The consecutive 100µm sections were then transferred to polypropylene 24-well plates (Caplugs Evergreen, Buffalo, USA) and processed using a Pelco BioWave Pro+ microwave (Ted Pella Inc, Redding, USA) and following a protocol adapted from the National Centre for Microscopy and Imaging Research protocol (Latest version available: https://ncmir.ucsd.edu/sbem-protocol). Each step was performed in the Biowave, except for the PB and water wash steps, which consisted of two washes on the bench followed by two washes in the Biowave without vacuum at 250W for 40s. All the chemical incubations were performed in the Biowave for 14 min under vacuum in 2 min steps alternating with/without 100W power. The SteadyTemp plate was set to 21ºC unless otherwise stated. In brief, the samples were fixed again in 2.5% glutaraldehyde (TAAB) / 4% formaldehyde in 0.1M PB. The cells were then stained with 2% osmium tetroxide (TAAB) / 1.5% potassium ferricyanide (Sigma), incubated in 1% thiocarbohydrazide (Sigma) with SteadyTemp plate set to 40ºC, and further stained with 2% osmium tetroxide in ddH2O. The cells were then incubated in 1% aqueous uranyl acetate (Agar Scientific, Stansted, UK) with SteadyTemp plate set to 40ºC, and then washed in dH2O with SteadyTemp set to 40ºC. Samples were then stained with Walton's lead aspartate with SteadyTemp set to 50ºC, and dehydrated in a graded ethanol series (20%, 50%, 70%, 90%, and 100%, twice each), followed by 3 dry acetone washes at 250W for 40 s without vacuum. Exchange into Durcupan ACM® resin (Sigma) was performed in 25%, 50% and 75% resin in acetone, followed by 4 pure Durcupan steps, at 250 W for 3 min, with vacuum cycling (on/off at 30sec intervals), before embedding at 60ºC for 48h. Blocks were then mounted for micro-computed tomography (micro-CT) on a cylindrical specimen holder with Devcon S-210 epoxy glue. The mounting was done with the longitudinal axis of the brain section oriented vertically. Tomographic imaging was conducted in an Xradia Versa 510 (Carl Zeiss Ltd, Cambridge, UK). A low resolution scan was captured at xkV/xW, with x projections and a pixel size of x. The region of interest was identified using 3DXMViewer software (Zeiss) and co-ordinates located for positioning in the Xradia Versa 510. A high resolution scan was captured at xkV/xW, with x projections and a pixel size of x. The data were exported as tiff, to be visualised in 3D in ClearVolume, a plug-in of the FIJI framework (Royer

et al 2015). The samples were then trimmed to a small trapezoid, excised from the resin block, and attached to a SBF SEM specimen holder using conductive epoxy resin (Circuitworks CW2400). Prior to commencement of a SBF SEM imaging run, the samples were coated with a 2 nm layer of platinum to further enhance conductivity.

SBF SEM data was collected using a 3View2XP (Gatan Inc., Pleasanton, CA) attached to a Sigma VP SEM (Carl Zeiss Ltd). Inverted backscattered electron images were acquired through the entire extent of the region of interest. For each 50nm slice, a low resolution overview image (horizontal frame width 800 µm for 02 / 384 µm for 03; pixel size of 78 nm for 02 / 48 nm for 03; using a 2 µs dwell time) and several high resolution images of the different regions of interest (horizontal frame width 170 µm for 02 / 183 µm for 03; pixel size of 8.3 nm for 02 / 11.4 nm for 03, using a 2 µs dwell time) were acquired. The SEM was operated in variable pressure mode at 5Pa. The 30µm aperture was used, at an accelerating voltage of 2.5 kV for 03, 2 kV for 02. 130 (for 02) and 400 (for 03) slices were necessary to get enough 3D information for an entire tumour. As data was collected in variable pressure mode, only minor adjustments in image alignment were needed. All the images were converted as tiff in Digital Micrograph (Gatan Inc.), and the tiff stacks were automatically aligned using TrakEM2, a plug-in of the FIJI framework (Cardona et al 2012).

After SBF SEM, the samples were serial sectioned using a UC7 ultramicrotome (Leica Microsystems, Vienna, Austria) and 70nm sections were picked up on Formvar-coated 2mm slot copper grids (Gilder Grids Ltd., Grantham, UK). The first sections were viewed using a 120 kV Tecnai G2 Spirit transmission electron microscope (FEI Company, Eindhoven, Netherlands) and images were captured using an Orius CCD camera (Gatan Inc.). Sample processing and imaging after brain collection were carried out with the Electronmicroscopy Facility at the Francis Crick Institute in close collaboration with Marie-Charlotte Dolmart.

2.6 RNA Sequencing and Mass Spectrometry

2.6.1 Tissue collection

For RNA Sequencing and Mass spectrometry control and nlsYAP5SA littermates from 2 matings were collected at the age of P11 (five animals per genotype). Additionally, three age matched C57BL/6 animals where collected. The pups euthanize by cervical dislocation, decapitated and the brain dissected out of the skull. Olfactory bulbs and cerebellum were split off and the hemispheres were separated. While the right hemisphere and the cerebellum were cut into smaller pieces and put into RNAlater (Qiagen), the left hemisphere was snap frozen in liquid nitrogen.
For Western blotting control and nlsYAP5SA mice were collected at the age of P11 (three animals per genotype). The pups euthanize by cervical dislocation, decapitated and the brain dissected out of the skull. As before the olfactory bulbs and cerebellum were split off and the hemispheres were separated, flash freezing the right hemisphere in liquid nitrogen.

2.6.2 RNA extraction and sequencing

Total RNA of tissue stabilised in RNAlater was extracted using the RNeasy Mini Kit (Qiagen) according to manufactures protocol. The samples were quantified via GloMax (Promega) and RNA quality evaluated using an RNA ScreenTape on the Agilent TapeStation. All RNA samples had RIN (RNA integrity number) scores above 7 except from one C57BL/6 cerebellum sample at 6.5. The libraries were prepared with the KAPA mRNA HyperPrep kit (Roche), normalising samples to 500 ng RNA input and prepared these into Illumina compatible libraries according to the kit manufacturer's instructions. The 26 libraries were normalised and pooled for sequencing. Sequencing was carried out on the Illumina HiSeq 4000, where the pool was mirrored across 2.5 lanes- yielding an average of 27 million reads per sample (+/- 2 million reads). Sample quality control, library preparation and sequencing were carried out with the Advanced Sequencing Facility at the Francis Crick Institute.

2.6.3 RNA Sequencing data analysis

Raw fastq files were adapter trimmed using CutAdapt 1.5 (Dobin et al 2012) and these trimmed reads were mapped to GRCm38 release 86 with associated ensemble transcript definitions using STAR 2.5.2a (Dobin et al 2012) wrapped by the R package RSEM 1.3.0 (Li & Dewey 2011) which was used to calculate estimated read counts per gene. Where necessary, bam files were merged using samtools 1.8 (Li et al 2009). Estimated counts were normalised and differentially expressed genes were called between genotype group using the R package DESeq2 1.12.3 (Love et al 2014). Genes with an adjusted p-value less than or equal to 0.05 were said to be differentially expressed. Heatmaps were generated using the R package pheatmap 1.0.8 https://CRAN.R-project.org/package=pheatmapall analyses were performed using R 3.3.1 (R Core Team "R: A Language and Environment for Statistical Computing" https://www.R-project.org/). This analysis was performed in close collaboration with Stuart Horswell, part of the Bioinformatics and Biostatistics Platform at the Francis Crick Institute.

Gene enrichment analysis of complete pre ranked gene list was done using GSEA 4.0.1 (Subramanian et al 2005) set to classic enrichment statistics utilising the c2.cp.kegg.v7.0.symbols.gmt gene matrix containing 186 gene sets.
Significantly differentially expressed gene list was uploaded to DAVID 6.8 (Huang et al 2008) (Huang et al 2009) with 44.8% (887) found annotated in KEGG Pathway.
To investigate the resemblance of nlsYAP5SA mouse model to human ependymoma subtypes, previously reported microarray data on differentially expressed genes between human ST-EPN-YAP1 and ST-EPN-RELA subtypes was utilized, which were also present and differentially expressed in YAP1-MAMLD1 induced and C11orf95-RELA induced mouse models of ependymoma (Pajtler et al 2015) (Pajtler et al 2019). The summarized synthesis of these subtype-associated, differentially expressed genes listed in Supplementary Data 6 from Pajtler *et al* (Pajtler et al 2019) was compared with our complete gene list as well as our significantly differentially expressed gene list. Log2 fold change of our data set was plotted and the identified of specification was taken from the other dataset using R 3.5.1.

2.6.4 Sample preparation and LC-MS/MS

Liquid chromatography - tandem Mass spectrometry (LC - MS/MS) was used to analyse differences in protein expression in P11 nlsYAP5SA compared to control animals (n=5 each). The left hemisphere of each animal was taken and lysed in lysis buffer containing 8M Urea, 50mM HEPES pH8.2, 10mM Glycerol 2-phosphate, 50mM sodium fluoride, 5mM sodium pyrophosphate, 1mM EDTA, 1mM sodium vanadate, 1mM DTT, 1x Protease Inhibitor Cocktail (Roche), 1x Phosphateae inhibitor Cocktail, 1 uM okadaic acid and incubated for 30 minutes on ice. Protein concentration was determined with BCA protein assay according to manufacture instructions. 100 ug per samples was reduced with DTT, alkylated with IAA, quenched with DTT and digested with rLysC (Lysyl Endopeptidase, Mass Spectrometry Grade (Lys-C), 21-05063, Lot#CAR2347) and Trypsin (Pierce™ Trypsin Protease, MS Grade, 90058, Lot#TK276718). After acidification with TFA the samples were desalted on C18 MacroSpin columns (Nest Group) followed by freeze drying them in liquid nitrogen prior to drying them on the speed vac. Subsequently the samples were labelled with a TMT (Tandem mass tag) 10plex hit (ThermoFisher, 90110, Lot#TJ268160) according to manufacturer protocol. TMT labelling efficiency was confirmed (>99%) and mixing check was performed prior to quenching the labelling reaction. The samples were combined, partially dried and then cleaned on a C18 SepPak and aliquoted. Subsequently one tenth of the sample was resolubilised and fractionated into 8 fractions utilising the Pierce High pH Reversed-Phase Peptide Fractionation Kit (Thermo Fisher #84868). All samples were dried and resolubilised in 0.1%TFA prior to LC-MS/MS analysis. Peptides were separated on a 50 cm, 75um I.D. Pepmap column over a 180 min gradient and eluted directly into the mass spectrometer (Orbitrap Fusion Lumos ETD) with HCD MS2 fragmentation and in a second injection (7ul each) analysed in MS3. Xcalibur software was used to control the data acquisition. The instrument was run in data dependent acquisition mode with the most abundant peptides selected for MS/MS by HCD fragmentation.

2.6.5 Proteomics data processing

MaxQuant v1.6.6 was used to process the raw data acquired with a reporter ion quantification method. Adjusted reporter ion isotopic distributions according to the TMT Lot number. Protein database searching was done by Andromeda search engine using the Uniprot KB database of *mus musculus* sequences. The protein group table was uploaded into Perseus 1.4.0.2 for subsequent statistical analysis and data visualisation. A two sided t-test with threshold set to FDR (False discovery rate) = 0.05 and s0 = 0.1 was used to display significance.

To investigate association of proteins to particular cell types the data was merged with existing datasets from Sharma *et al* (Sharma et al 2015). From this publication, Supplementary Data 15 was used to identify protein association to isolated cell types and Supplementary Data 8 was used to include data from cultured cell types. The data sets were partially merged (by matching gene name, integrating the log2 fold expression columns per cell type of the other dataset into ours) and association to particular isolated CNS cell type was defined by expression value being a minimum of 3 in one of the four isolated cell types (astrocytes, microglia, neurons and oligodendrocytes) and with a value of at least double in one compared to any of the other cell types.

2.6.6 Merging transcriptome and proteome data

The total RNA and protein lists were merged by gene name and plotted using the stat and Welch difference values respectively. Annotation was done in Perseus 1.4.0.2 using annotation sets KEGG (Kyoto encyclopedia of genes and genomes), Gene Ontology Cellular Compartment, Molecular Function and Biological Process. 2D annotation of the proteome and transcriptome was done using Benjamini-Hochberg FDR as truncation and a threshold value of 0.02.

2.7 Further analysis

2.7.1 Tumour measurements

Three animals of LATS1/2 cKO, Mutant YAP$^{f/+}$ (*Nex*$^{Cre/+}$ *Lats1*$^{f/f}$ *Lats2*$^{f/f}$ *Yap1*$^{f/+}$ *Taz*$^{+/+}$), Mutant YAP$^{f/f}$ (*Nex*$^{Cre/+}$ *Lats1*$^{f/f}$ *Lats2*$^{f/f}$ *Yap1*$^{f/f}$ *Taz*$^{+/+}$) and Rescue (*Nex*$^{Cre/+}$ *Lats1*$^{f/f}$ *Lats2*$^{f/f}$ *Yap1*$^{f/f}$ *Taz*$^{f/+}$) were subject to detailed tumour size analysis. The brains were sectioned coronal using the vibratome with 50 µm depth. Every second section was stained with DAPI and a tumour marker (Vimentin, YAP1 or GFAP) to aid tumour identification. All sections were evaluated and imaged using the Olympus IX83. The area of each identified tumours was measured in all sections using FIJI and volume was calculated by section thickness and taking gap sections into account. Kruskal-Wallis test was performed to evaluate if the tumour size is significantly different from any group to another ($p = 0.0009$). Post hoc the Dunn`s multiple comparisons test was performed to identify which groups are significant from each other.

Additionally, the effect of change of genotype on estimates volume was determined by encoding genotype as an ordered factor (Mutant$^{f/f}$ < Mutant$^{f/+}$ < LATS1/2 cKO) and fitting a linear mixed effects model with animal as the random effect using the function glmmPQL from the MASS package with the call “glmmPQL(vol ~ geno, random = ~1|animal, family=”gaussian”)” diagnostic plots from lm(vol ~ geno/animal) indicate that normality of residuals and heteroscedasticity were reasonable assumptions but the mixed effects function was used for hypothesis testing to account for “proper” nesting of animals within genotypes. The quadratic term for genotype was non-significant ($p = 0.8764$). The linear mixed effect model was performed by Stuart Horswell.

2.7.2 Statistical analysis

Statistical analysis was performed using GraphPad Prism 7 software, R3.3.1 or R 3.5.1 using statistical tests as indicated in the text. Statistical significance was visualised as: ns = not significant ($p > 0.05$), * = $p < 0.05$, ** = $p < 0.01$, *** = $p < 0.001$, **** = $p < 0.0001$.

Chapter 3. Function of LATS2 in post-mitotic neurons and the developing brain

3.1 Post-mitotic function of LATS2

It has been reported that depletion of both hippo and warts in drosophila sensory neurons results in deficiency in maintaining dendritic arborisation. Importantly, this effect was demonstrated to be independent of Yorkie function (Emoto et al 2006). However, the role of hippo kinase signalling in the developing mammalian neurons is not known.

3.1.1 LATS2 does not show a significant effect on dendrite development

LATS2 mRNA has been shown to be highly expressed in the CA3 region of the murine hippocampus, while LATS1 was not detected in the mouse brain using a single probe in Allen Brain Atlas which could suggest a specialised function.
Therefore, focusing on LATS2, to investigate its function in neuronal development we prepared dissociated primary hippocampal cultures from E18.5 Long-Evans rats allowing easier accessibility and manipulation of the cells of interest. Constitutively active LATS2 (LATS2pif-WT; containing the PIF (PDK1-interacting fragment) modification at the C-terminus) or dominant negative (LATS2pif-KD; kinase dead with point mutation D809A and PIF modification) containing plasmid (kind gift of Alexander Hergovich) were co-transfected with a GFP-expressing plasmid to reveal dendrite and spine morphology. The primary neurons were transfected at four days *in vitro* (DIV4) and fixed 14 days later at DIV18. In order to focus the efforts on CA3 pyramidal neurons, we stained the cells for CTIP2, a maker present in CA1 (Cornus ammonis 1) and DG (Dentate gyrus), and only neurons exhibiting absence of staining were chosen for imaging and downstream analysis. Having looked at total dendritic length, branching points and number of intersections, we did not find a significant effect on dendritic complexity at DIV18, between the two constructs nor to the empty vector control (Figure 3.1).

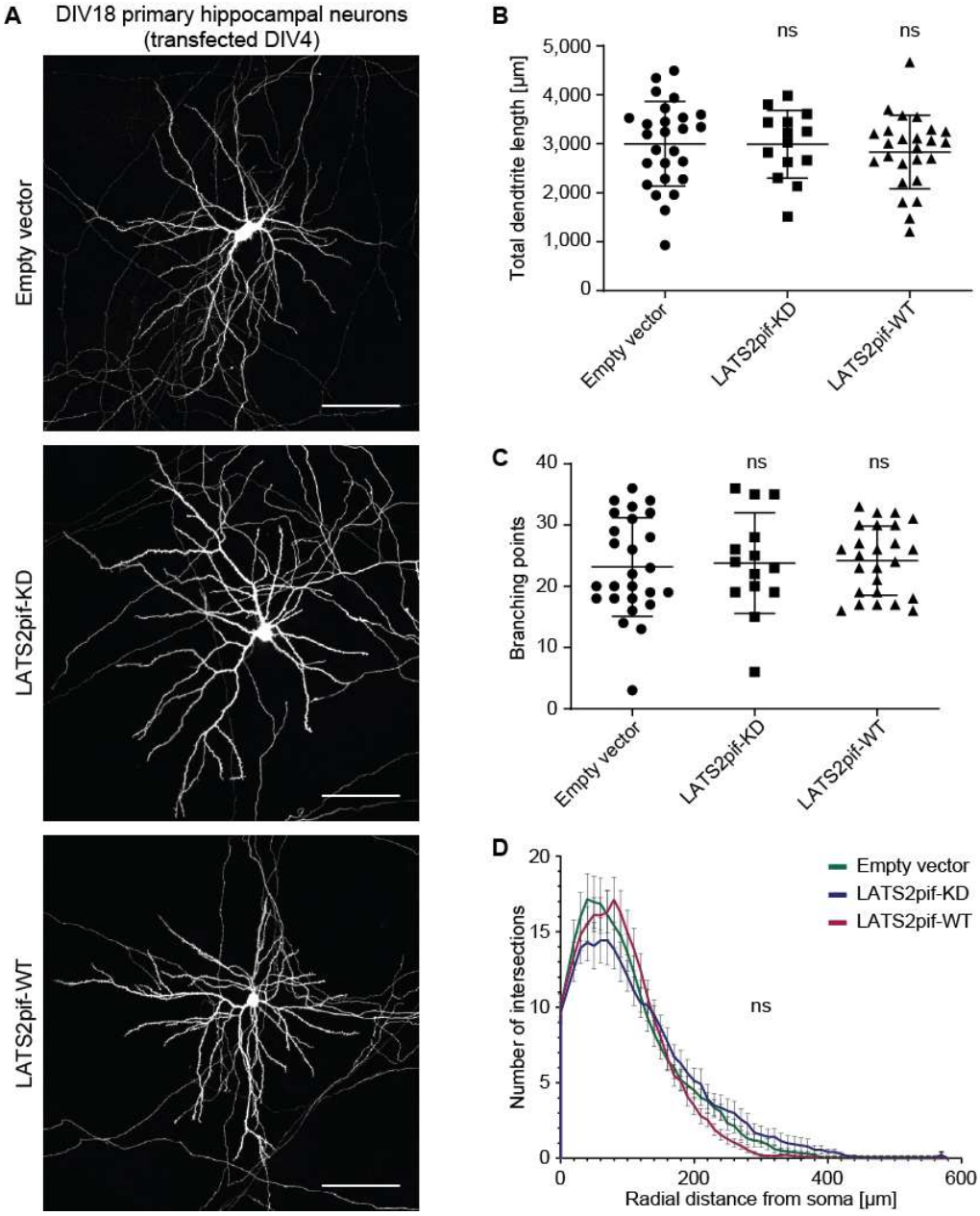

Figure 3.1. Dendritic growth and arborisation of primary hippocampal CA3 neurons is not affected by different LATS2 constructs.

A. Representative images of GFP labelled DIV18 rat primary hippocampal cultured neurons transfected at DIV4. Scale bar = 100 µm. No significant difference was observed in total dendritic length (**B**) nor in number of branching points (**C**). Unpaired t-test; N = 2 transfections, n = 26 empty vector, 14 LATS2pif-KD, 25 LATS2pif-WT (number of neurons); ns = not significant; error bars show SEM. **D**. No significant difference was found in the dendritic arborisation in the primary hippocampal transfected cultures. Two stage linear step-up procedure of Benjamini, Krieger and Yekutieli; N = 2 transfections, n = 26 empty vector, 14 LATS2pif-KD, 25 LATS2pif-WT (number of neurons); ns = not significant. Error bars = SEM.

3.1.2 Potential function of LATS2 in spine density and maturation

Since the dendritic arbore did not show any significant differences, we evaluated dendritic spine density and morphology. In primary cultures, neurons develop dendritic spines after approximately two weeks *in vitro*. To sustain a higher degree of reproducibility, only secondary dendrites of GFP-labelled and CTIP2-negative neurons were imaged and analysed.

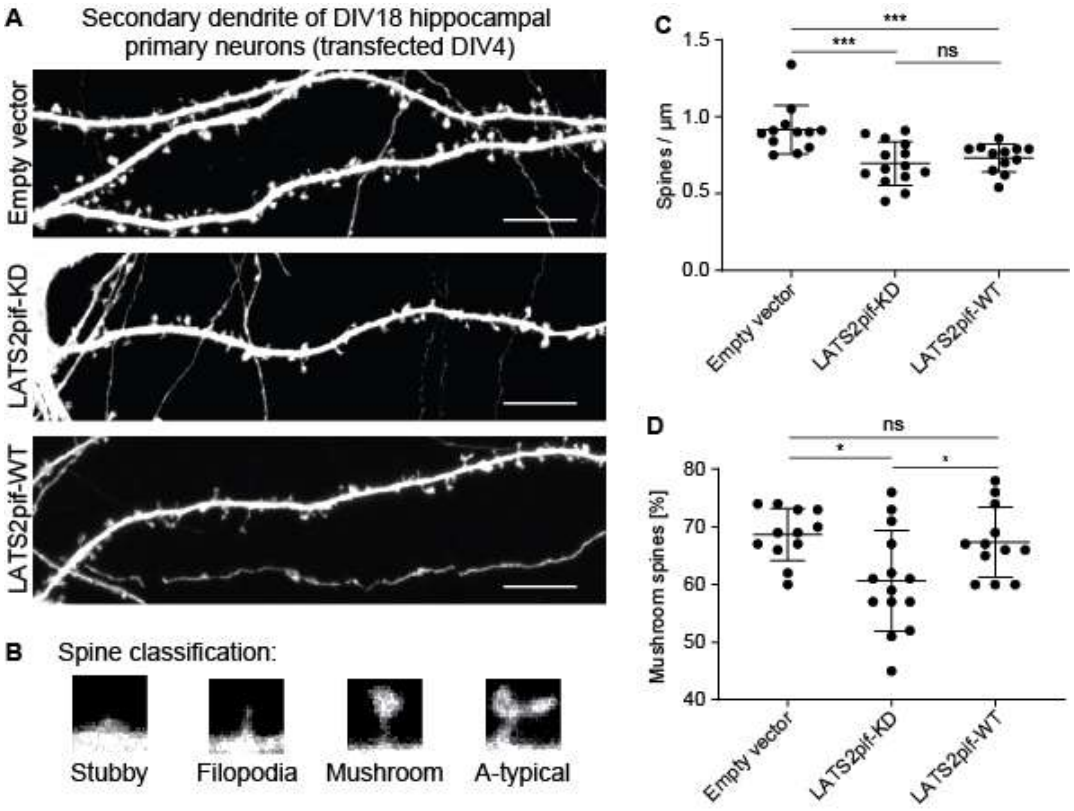

Figure 3.2. Dendritic spine formation appears affected by LATS2.

A. Representative images of GFP labelled secondary dendrites of DIV18 rat primary hippocampal cultured neurons transfected at DIV4. Scale bar = 10 µm. **B**. Representative spines of the four types classified. **C**. A significant reduction in spine density seen for LATS2pif-KD ($p = 0.0007$) and LATS2pif-WT ($p = 0.0007$) when compared to the empty vector control (non-parametric unpaired Mann Whitney test). Error bars show SEM. **D**. Spine classification revealed a significant reduction in mushroom spines when LATS2pif-KD is compared to Empty vector control ($p = 0.0145$) and to LATS2pif-WT ($p = 0.0448$) using the non-parametric unpaired Mann Whitney test. Error bars show SEM.

ns = not significant, n = 12 dendrites (2 neurons) Empty vector, 14 dendrites (9 neurons) LATS2pif-KD, 12 dendrites (7 neurons) LATS2pif-WT (maximum 2 dendrites per neuron);

Preliminary results showed spines might be affects as dendritic spine density appear to be reduced in both constitutively active and dominant negative treated neurons when compared to the empty vector control (Figure 3.2.C). Furthermore, spines were also manually classified into filopodia, stubby-, mushroom- and a-typical spines (Figure 3.2.B). We found that the neurons transfected with LATS2pif-KD have a significantly lower number of mature mushroom spines and increased amount of immature filopodia when compared to the other two constructs (Figure 3.2.D). We did not see a significant difference for the LATS2pif-WT transfected neurons compared to the empty vector controls.

In conclusion, LATS2 does not appear to have an effect on the development of the dendritic arborisation, but might be important for spine formation and maturation in developing CA3 neurons. However, maintenance of those structures could not be studied with those cultures.

3.2 Conditional knockout of LATS kinases and family members

To investigate the remaining question if LATS1/2 could be important for the maintenance of the dendritic structure a mouse model approach was chosen. It has been shown that complete knockout of *Lats2* results in embryonic lethality (McPherson et al 2004a) while Lats1 knockout is vital, but leads to an increased incidence rate of soft-tissue sarcoma and ovarian tumour development without major phenotypes (St John et al 1999). This indicates an essential role of LATS2 in development and a possible compensatory mechanism between the two homologs. Further, it has been shown that conditional knockout of LATS1/2 in the mouse liver increases proliferation and represses maturation of hepatocytes leading to pre-natal lethality (Yi et al 2016). Whether or not LATS1/2 play a role in neuronal differentiation of maintenance in mammals is not known.

3.2.1 Double but not single conditional knockout of LATS1 and LATS2 leads to severe phenotype in mice

Firstly, we investigated whether the murine brain is expressing LATS1/2. Therefore, brains of wild type mice at different ages were collected and for the post-natal age of 20 days (P20) the brain was dissected into different regions (cortex, hippocampus, striatum, midbrain and cerebellum). With Western blot and an antibody recognising both LATS1 and LATS2, we could determine that those proteins are present in the brain at all tested ages and brain regions (Figure 3.3). Furthermore, primary hippocampal cultured neurons from rats were lysed at DIV18 and showed expression of LATS1/2. As a result, we anticipated that neurons in the developing mouse would express LATS1/2.

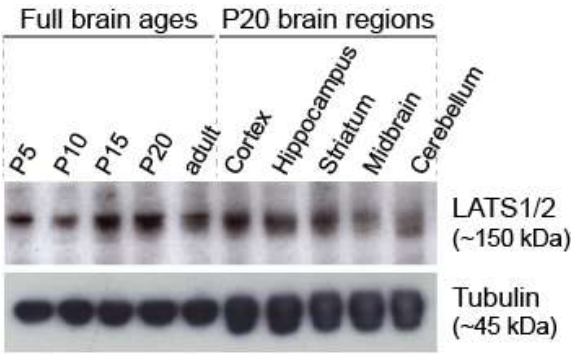

Figure 3.3. LATS1/2 is expressed in the murine brain.

Western blot of wild type mouse brains at 5, 10, 15 and 20 days post-natal and adult mouse brain. Furthermore, dissected brain regions (cortex, hippocampus, striatum, midbrain and cerebellum) of a P20 wild type mouse showed LATS1/2 expression. Tubulin was used as loading control.

In order to tackle the question if LATS1/2 are important for neuronal development, we generated conditional knockout of *Lats1* and *Lats2* in the brain. The NEX-Cre ($Neurod6^{tm(cre)Kan}$) conditional mouse line was chosen (Wu et al 2005). NEX (Neuronal helix-loop-helix protein) expression starts at embryonic age 11.5 and continues to be expressed in pyramidal neurons throughout adulthood. This model is used to study excitatory neurons in the cortex and the hippocampus. NEX is not reported to be expressed in glia. NEX-Cre expressing mice were crossed with a Rosa26-tdTomato (Ai14) mouse reporter line (Madisen et al 2010). The previously described locations of Cre activation could be confirmed with the reporter and in combination with CRE staining (Figure 3.4, Figure 3.5). It is of note, that Ai14 is a membrane tagged reporter, therefore axon tracks are clearly marked as well.

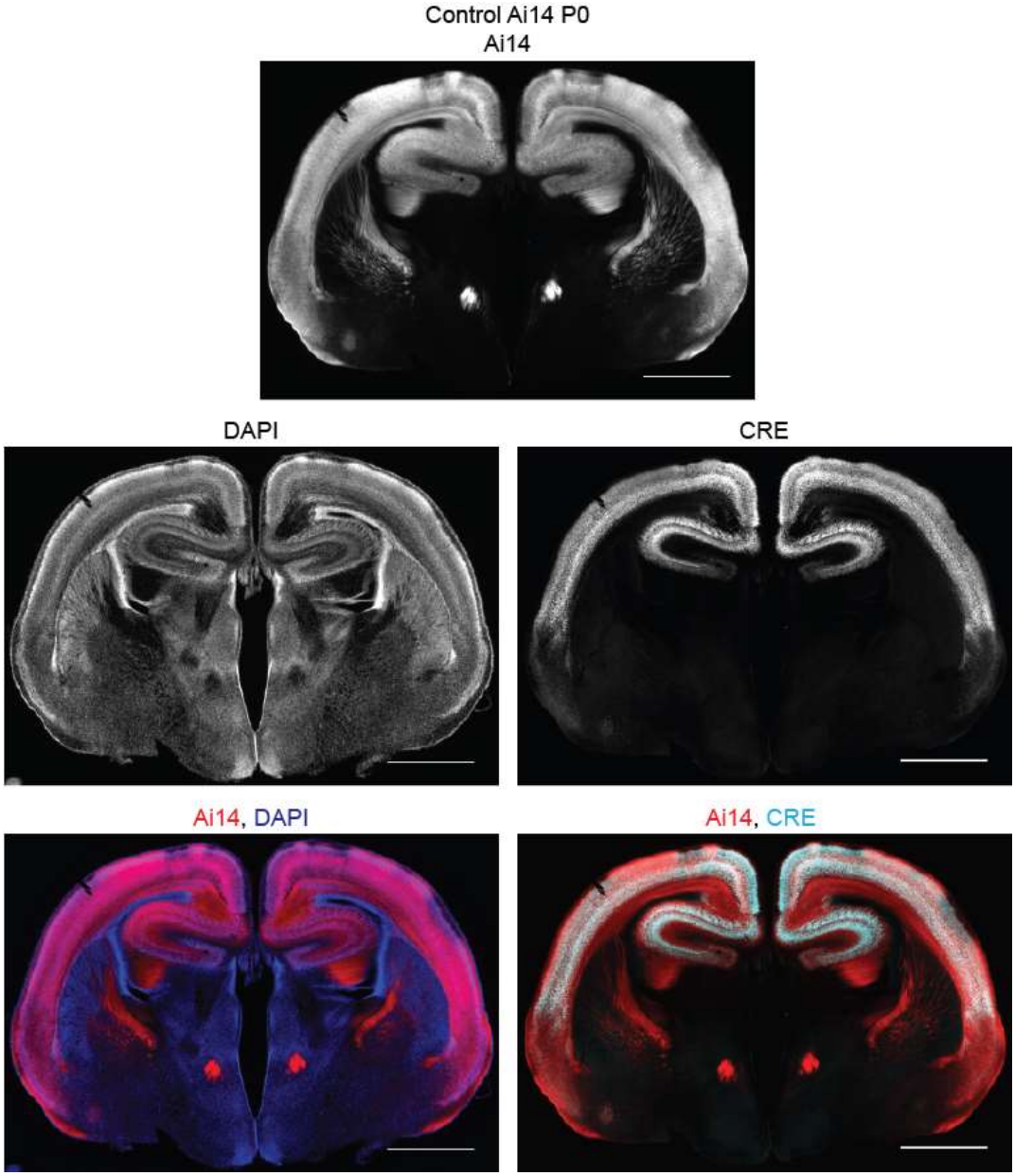

Figure 3.4. Cre mediated recombination in P0 NEX-Cre mouse brain confirmed by Ai14 reporter.

Coronal vibratome section of P20 *Nex*$^{Cre/+}$ *Ai14* brain. Expression of CRE and reporter detected in cerebral cortex and hippocampus. Also axon tracks of targeted NEX expressing neurons are visible due to the membrane tagged reporter. Scale bars = 1 mm.

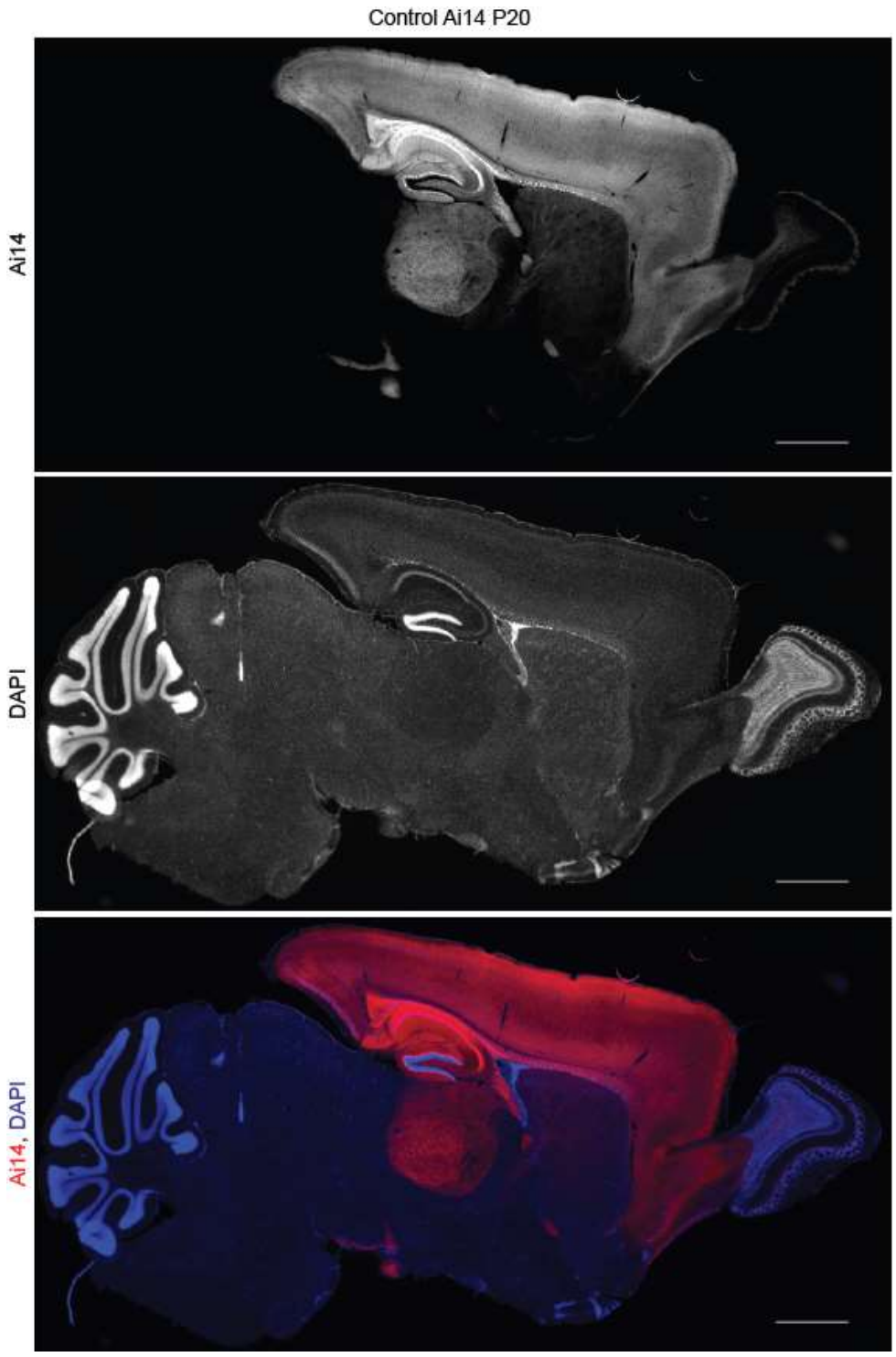

Figure 3.5. Cre mediated recombination in P20 NEX-Cre mouse brain confirmed by Ai14 reporter.

Sagittal vibratome section of P20 *Nex*$^{Cre/+}$ *Ai14* brain. Expression of reporter detected in cerebral cortex and hippocampus. Also axon tracks of targeted NEX expressing neurons are visible due to the membrane tagged reporter. Scale bars = 1 mm.

To study the brain specific role of LATS1/2 *in vivo* NEX-Cre animals were crossed with *Lats1*$^{f/f}$ *Lats2*$^{f/f}$ mice (Yi et al 2016) to generate experimental brain specific conditional knockout animals (Figure 3.6.A). A phenotypical difference between double conditional knockouts and other genotypes became apparent as early as two weeks of age. Double mutants, but not single mutants, presented with reduced size and weight and often showed balance issues. Other abnormal behaviours we could observe include spinning, head tilt and flicking, increasingly agitated, slow shaky walk and hunched posture (Figure 3.6.B). Not all symptoms presented in each animal and signs also manifested in a range of levels from very subtle to severe. Likewise, the exact age of noticeable symptomatic onset varied between individual animals.

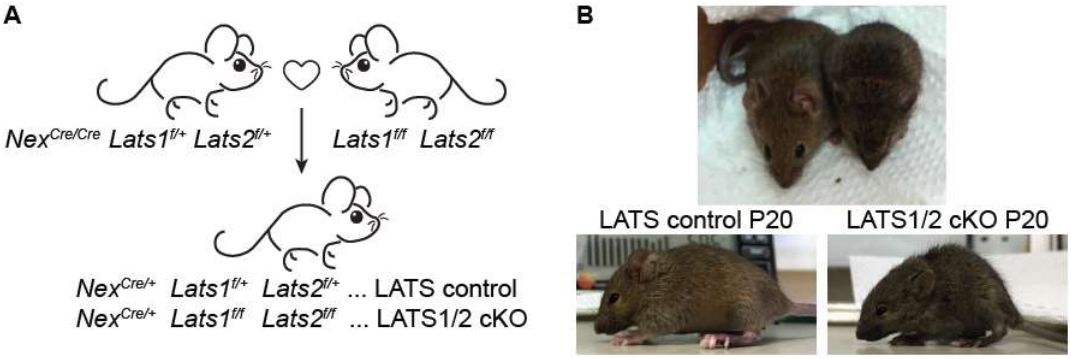

Figure 3.6. Conditional knockout of LATS1/2 under control of NEX-Cre leads to phenotypic difference.

A. Breeding scheme to generate LATS1/2 conditional knockout mice (LATS1/2 cKO) and control littermates (LATS control). **B**. Representative double knockout animals present with reduced size, weight and hunched posture compared to littermate at the age of P20.

At the age of P19-P21, a significant difference in body weight was measured between LATS controls (*Nex*$^{Cre/+}$ *Lats1*$^{f/+}$ *Lats2*$^{f/+}$) and LATS1/2 cKO (*Nex*$^{Cre/+}$ *Lats1*$^{f/f}$ *Lats2*$^{f/f}$) animals (Figure 3.7.A). On average a LATS1/2 cKO mouse weighs 6.5 g, which is approximately 40% less than the average LATS control mouse with 10.1 g at three weeks postnatal age. All animals dissected have been checked for food in their digestive system and a subset have been observed eating, leading to the conclusion that they are still able to obtain food. We did not see differences between gender, both male and female were equally affected. Single cKO animals for neither LATS1 (*Nex*$^{Cre/+}$ *Lats1*$^{f/f}$ *Lats2*$^{+/+}$) nor LATS2 (*Nex*$^{Cre/+}$ *Lats1*$^{+/+}$ *Lats2*$^{f/f}$) showed any statistical significant difference in bodyweight when compared to the LATS control

animals at P19-21. Furthermore, single cKO animals did not display any of the phenotypical features that could be observed in double cKO animals. Looking at the weight progression, we found LATS control and LATS1/2 cKO animals to be significantly different in weight from the age of P14-15 onwards (Figure 3.7.B).

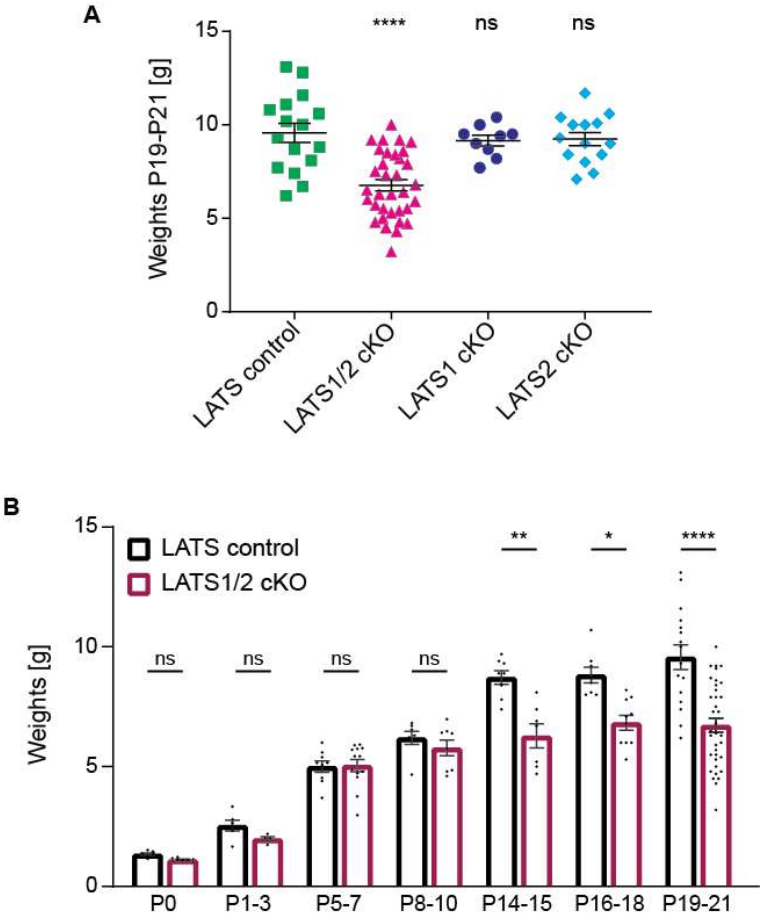

Figure 3.7. Significant lower weight recorded in double cKO of LATS1/2 under control of NEX-Cre from P14-15 onwards.

A. LATS control (*Nex*$^{Cre/+}$ *Lats1*$^{f/+}$ *Lats2*$^{f/+}$), LATS1/2 cKO (*Nex*$^{Cre/+}$ *Lats1*$^{f/f}$ *Lats2*$^{f/f}$), LATS1 cKO (*Nex*$^{Cre/+}$ *Lats1*$^{f/f}$ *Lats2*$^{+/+}$) and LATS2 cKO (*Nex*$^{Cre/+}$ *Lats1*$^{+/+}$ *Lats2*$^{f/f}$) animals were weighted at the age of P19-P21. A significant difference between the LATS control and the conditional double knockout animals (padj = 0.0001, Dunnett`s multiple comparisons test), but not the single knockout was revealed. **B**. Weights of LATS control and LATS1/2 cKO animals were taken at multiple ages. Significant difference between those two genotypes was found at P14-15 (p = 0.0031, Sidak`s multiple comparisons test), P16-P18 (p = 0.0113, Sidak`s multiple comparisons test) and at P19-P21 (p<0.0001, Sidak`s multiple comparisons test). Each dot represents one individual weighted animal per age group and genotype. ns = not significant. Error bars show SEM.

We determined the level of knockdown in P20 LATS1/2 cKO and LATS control animal brains by Western blot as none of the LATS antibodies tested in brain slices showed specific staining. To avoid masking of knockdown as much as possible by including NEX-Cre unaffected brain regions, the hippocampus and the cortex of the mice were dissected and lysed separately. A significant reduction in LATS1 signal could be confirmed in the hippocampus ($p = 0.0436$, Student`s t-test) (Figure 3.8.B,D). The cortical lysates however showed no significant reduction ($p = 0.7017$, Student`s t-test). On the other hand, we found LATS2 levels were significantly reduced in the cortex ($p = 0.0008$, Student`s t-test) (Figure 3.8.A,C), but the lower levels in the hippocampus were not statistically significant ($p = 0.0599$, Student`s t-test). As only a subset of cells was targeted by the NEX-Cre promoter, the remaining signal will be expressed by unaffected cells in the brain. This could be sufficient to mask a subtle reduction of protein in the targeted sub population of cells in the examined areas.

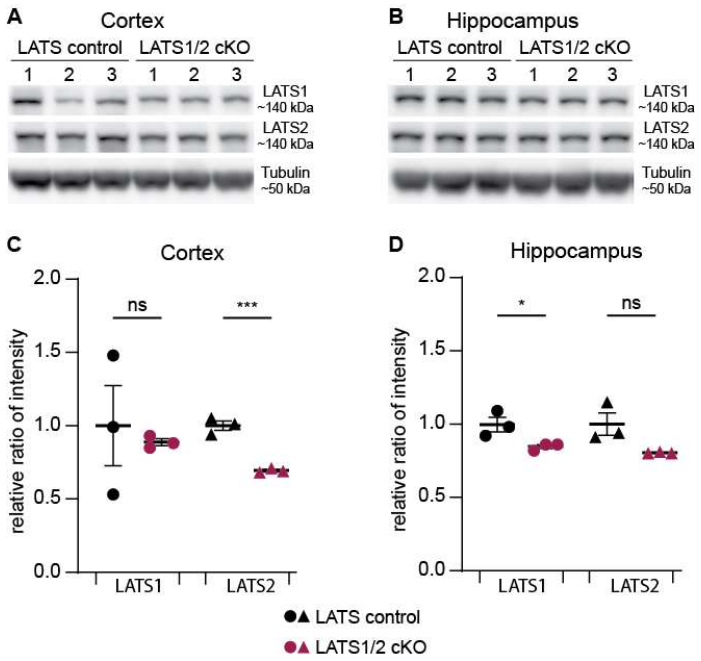

Figure 3.8. Knockdown of LATS1 and LATS2 in the brain shown by Western blot.

Cortex (**A**) and hippocampus (**B**) were dissected from LATS control and LATS1/2 cKO animals (n = 3 per genotype) and were subject to Western blot analysis. The blots were stained for LATS1 and LATS2, tubulin was used as loading control. **C-D**. Quantification shows reduction of signals in LATS1/2 cKO animals compared to control. Significance (Student`s t-test) in reduced signal found in hippocampus for LATS1 (**D**) to 85% and in cortex for LATS2 (**C**) to 69% compared to control. Error bars = SEM.

3.2.2 Deletion of LATS1/2 but not NDR1/2 kinases in the NEX-Cre lineage leads to the formation of cell clusters in the brain

Based on the phenotypical features of the mutant animals we suspected that the development of the murine brain has been affected due to the dual depletion of LATS1/2. Fixed brains of perfused P20 animals were taken and investigated further. Multiple cell clusters were found in all P20 LATS1/2 cKO (18/18) without exception (Figure 3.9.A), but none could be detected in LATS controls (0/6) nor in individual LATS1 cKO (0/3) or LATS2 cKO (0/3), which indicates redundancy between LATS1 and LATS2. All observed lesions were detected in association with the ependymal layer.

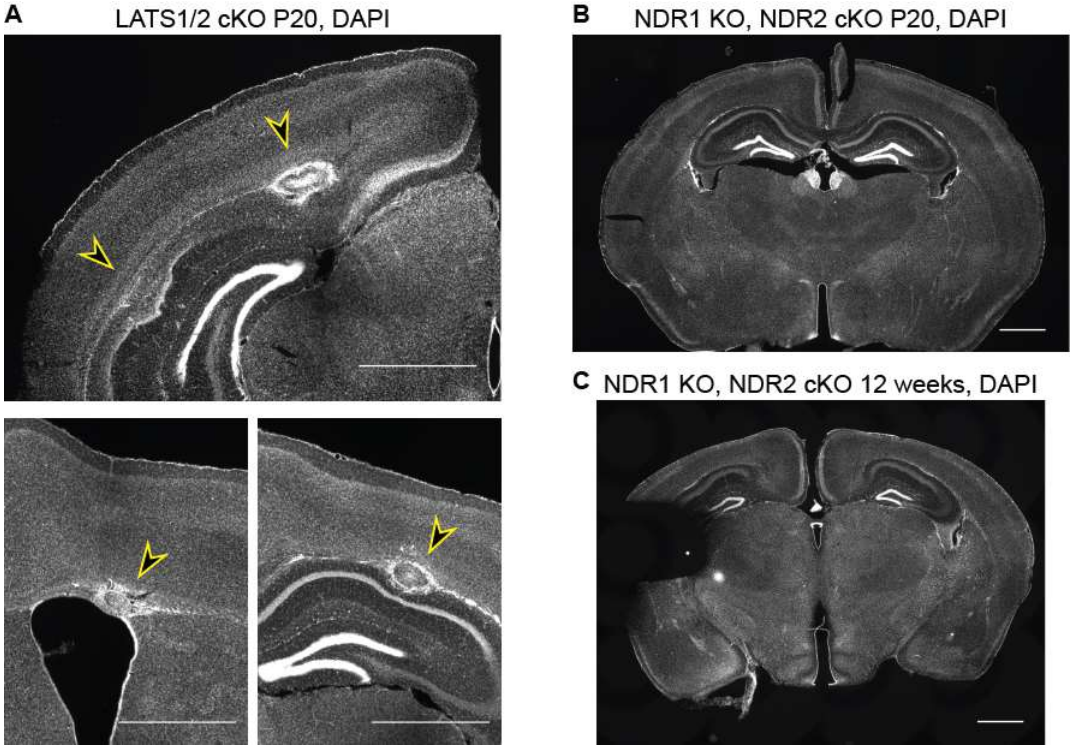

Figure 3.9. Conditional dual knockout of LATS1/2, but not NDR1/2, under NEX-Cre control results in cell cluster formation in the brain.

A. Multiple cell clusters (yellow arrowheads) could be found in each P20 LATS1/2 cKO brain (two different brains are shown; lower two panels are from the same brain at different coronal planes). Each cluster was associated with the ependymal layer. **B**. No cell cluster was detected in NDR1/2 knockout brains (*Ndr1*$^{KO/KO}$ *Nex*$^{Cre/+}$ *Ndr2*$^{f/f}$) at P20 or 12 weeks of age. At 12 weeks a thinning of the cortical layer was observed. Coronal vibratome sections, Scale bars = 1 mm.

Similar knockout crosses were set up for NDR1/2, a member of the same kinase family as LATS and part of the Hippo pathway to investigate redundancy between kinase family members. As also it has been suggested that LATS1/2 and NDR1/2 kinases have a phosphorylation motif is common and both have been reported capable of phosphorylating YAP1 (Hao et al 2008) (Zhang et al 2015).
Hereby, NDR1 was a complete knockout in all cells of the animal (Cornils et al 2010) and NDR2 (Zhang et al 2015) was under the control of the NEX-Cre driver (*Ndr1*$^{KO/KO}$ *Nex*$^{Cre/+}$ *Ndr2*$^{f/f}$). Those animals did not show any cell cluster formation in their brain at the age P20 nor at a later checked age of 12 weeks. A reduction of cortical thickness was observed in dual knockout compared to control animals at 12 weeks of age with GFAP-glia positive cell infiltration (data not shown).

3.2.3 Inducible knockout of LATS1/2 at a later stage does not result in a phenotype

It was of further interest if the cluster formation in LATS1/2 cKO animals is a developmental phenotype or can be induced at a later stage. For this purpose, we made use of the Tamoxifen inducible system, NEX-CreERT2 (Neurod6$^{tm2.1(cre/ERT2)Kan}$) (Agarwal et al 2012) (Figure 3.10.A). After drug administration, cells with active NEX promoter would activate Cre recombinase and lead to knockout in those cells. The animals were aged to 37 days ± 1 day and then injected with Tamoxifen twice a day for five days (Figure 3.10.B) (n = 5 LATS1/2-ERT2 cKO, 5 LATS-ERT2 control; from 3 litters; each genotype cohort included 3 males and 2 females). The mice were kept in at least pairs of one mutant and one control, were closely monitored and weight daily. The weights were normalised to first measurement for each animal to correct for initial weight difference and focus on the effects of the treatment (females were on average 3-4g lighter compared to their male littermates) (Figure 3.10.C). We did not see any phenotypical abnormally nor a significant difference in weight throughout the experiment. We collected the brains 30 days after the first injection. Upon sectioning of the brain, we could not detect a cell cluster in any LATS1/2-ERT2 cKO animal. The brain sections showed positive staining for CRE in the expected areas: cortex and hippocampus. To further investigate the recombination efficiency FISH could have been done.

A follow-up cohort of animals was aged for six months post initial injection, but again the double conditional knockout animals of the aged cohort developed normally with no weight difference nor phenotypical abnormal signs were noted. This suggested, that the cell cluster development observed in LATS1/2 cKO is triggered during development and not able to be induced later. Likewise, it is possible that the cells giving rise to the cluster do not express NEX in one month old animals anymore.

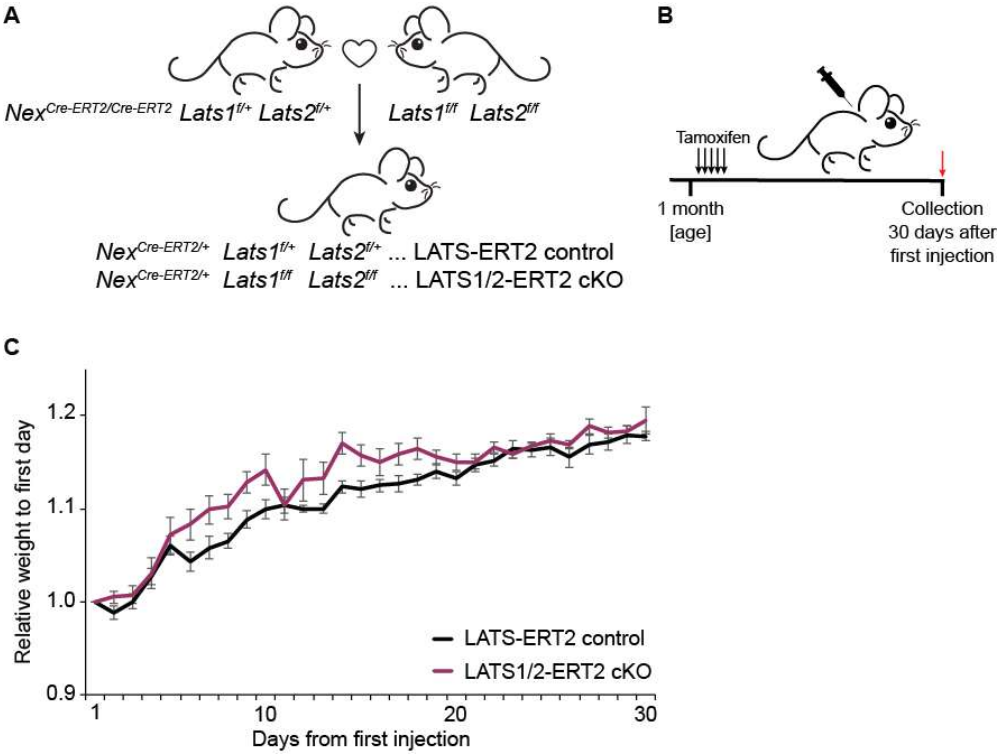

Figure 3.10. Tamoxifen injected LATS1/2-ERT2 cKO animals did not show significant difference to LATS-ERT2 control mice.

A. Breeding scheme to generate inducible LATS1/2 conditional knockout mice (LATS1/2-ERT2 cKO) and control littermates (LATS-ERT2 control). **B**. Treatment schematic of tamoxifen induction. At roughly one month of age (37 ± 1 days), the animals were administered two inter peritoneal injections of 100 µl tamoxifen (10 mg/ml) per day (injections at least 6 hours apart from each other) for five days. The animals were sacrificed 30 days after the first injection. **C**. The mice were weight daily from the first injection onwards. Weights of each animal were normalised to the weight of their first day. N = 5 LATS1/2-ERT cKO, 5 LATS-ERT2 control; each group included 3 males and 2 females. Error bars = SEM.

In this subchapter we showed that LATS2 does not affect the development of the dendritic arbour in cultured neurons, but potentially plays a role in dendritic spine development and maturation. When aiming to investigate the maintenance role of LATS kinases in post-mitotic neurons in the brain, we found the animals severely affected. However, those phenotypical differences to control littermates go hand in hand with the formation of cell clusters in dual knockout brains. Those lesions appear to be primary reason for the differences between LATS1/2 cKO and LATS control animals, as later induction of the knockout in NEX-Cre expressing cells did not result cell cluster nor in comparable obvious phenotypical changes.

Chapter 4. Characterisation of LATS1/2 knockout induced dysplasia in the brain

4.1 Location and expression profile of the cell clusters found in LATS1/2 cKO brains

In order to determine the location of origin of cells giving rise to those clusters the location of smaller tumours in earlier developmental stages were studied. Lesions in animals as young as P5 were detected (Table 4.1). Between P5-P21 we have detected tumours in 93 % of animals (one animal at P7 did not present with a visible cell cluster in any inspected brain section). We observed a considerable variation in size and exact location of the dysplasia from different mice, which might occur due to the mixed background of the animals. Otherwise, this could also indicate that additional mutations may be causing the development of these tumours, stochastic nature of additional mutagenesis leading to clonal tumours at different developmental stages (Loeb & Loeb 2000) (Gerstung et al 2020).

Table 4.1. Cluster occurrence: number of animals sectioned per age group and number of observed clusters in percentage.

Age range	P0-P2	P5-P7	P8-P10	P19-P21
Sectioned brains	3	3	3	18
Tumours detected	0%	67%	100%	100%

In all cases, we observed that the cell clusters were adjacent to the ependymal layer. In some cases, we found a cluster growing out of ependymal layer of the lateral ventricle. It is to be noted that in some cases an additional cell cluster could be detected anterior to the cerebellum within the same mouse (Figure 4.1).

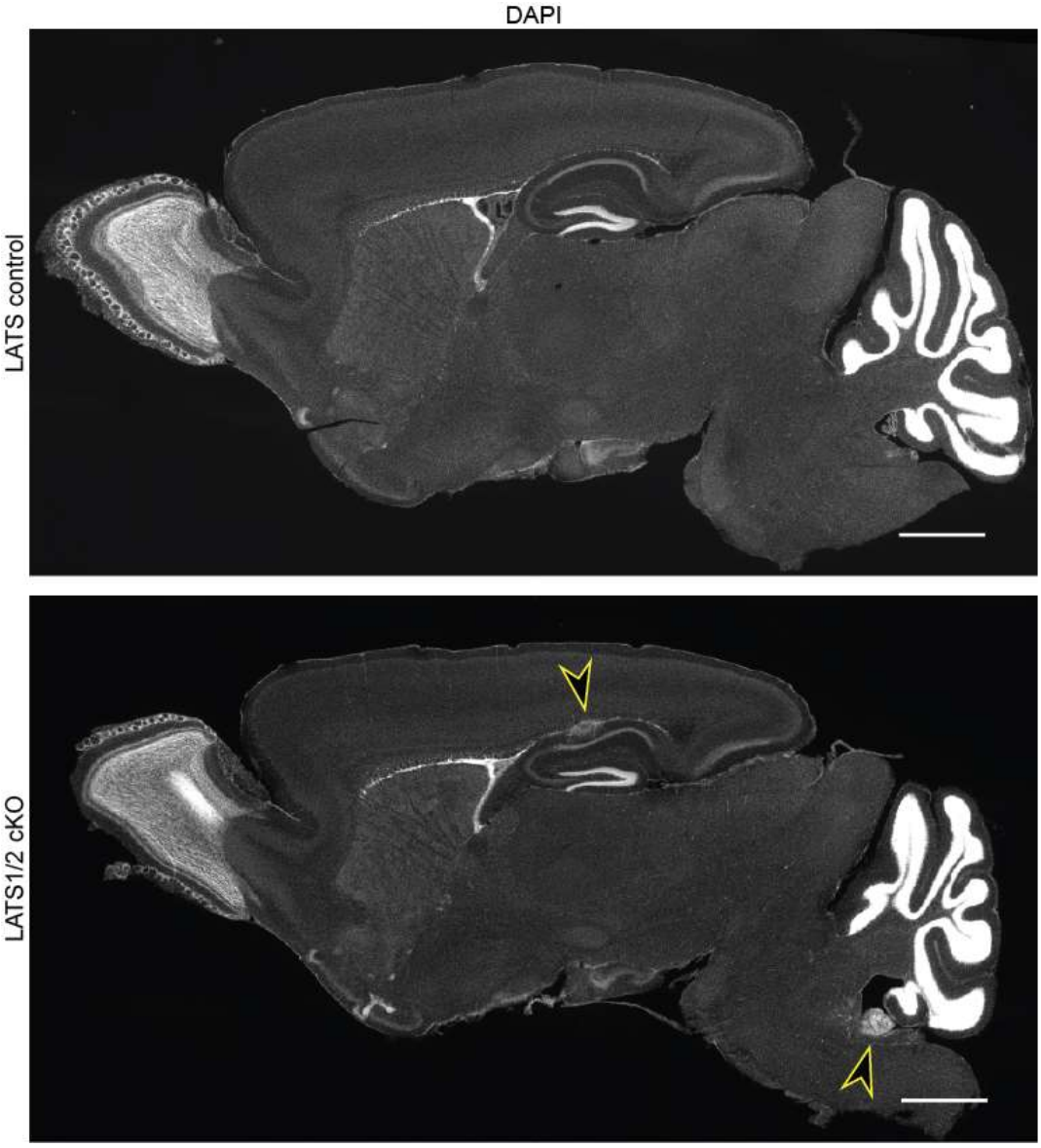

Figure 4.1. Some LATS1/2 cKO present with an additional cell cluster anterior to the cerebellum.

Sagittal vibratome section of LATS control and LATS1/2 cKO mouse brains. In addition to the dysplasia adjacent to the ependymal layer, in a subset of LATS1/2 cKO animals also a cluster located at the cerebellum could be found, yellow arrow heads pointing at cell clusters. Scale bars = 1 mm.

To investigate if the cell clusters indeed originate from cells subject to the LATS1/2 conditional knockout, animals were crossed with the ROSA$^{mT/mG}$ (Gt(ROSA)26Sor$^{tm4(ACTB-tdTomato,-EGFP)}$) mouse line with a two-colour fluorescence Cre-reporter allele (Muzumdar et al 2007). All cells express membrane-localised tdTomato (mT). Upon Cre recombinase expression the red fluorescence is replaced by membrane-localised EGFP (mG) in those cells and all their descendants. LATS1/2 cKO brains positive for the mTmG allele were collected at P20 and analysed for reporter expression within the cell cluster. It was found that a part of the identified tumours lacked completely any signal and neither reporter was expressed, the other part of clusters showed a clear mG signal indicating Cre recombinase activation and consequent knockout of LATS1/2 (Figure 4.2**Error! Reference source not found.**.A).

Surprisingly, one animal can present with both cases. Lack of reporter mG signal was more frequent then presence of the signal. Clusters anterior to the cerebellum could also be observed positive for mG (Figure 4.2**Error! Reference source not found.**.B). These observations indicate that the cell clusters indeed are originating from cells targeted by the Cre recombinase. The complete absence of mG signal could indicate, that the cells have been altered, potentially mutated, and subsequently mG reporter allele was not expressed due to unknown mechanisms.

It has not yet been directly reported that ependymal cells or their precursors express NEX at least transiently and therefore would be subject to the conditional knockout in this mouse model. NEX was previously shown to be expressed in post mitotic excitatory neuronal cells. However, it has been reported that a small but significant number of cells (4.3%) in the sub ventricular zone (SVZ) stain positive for the mitotic marker P-H3 (Wu et al 2005) (Goebbels et al 2006). This indicates a small number of cell targeted by NEX-Cre could be mitotic at a snapshot of time.

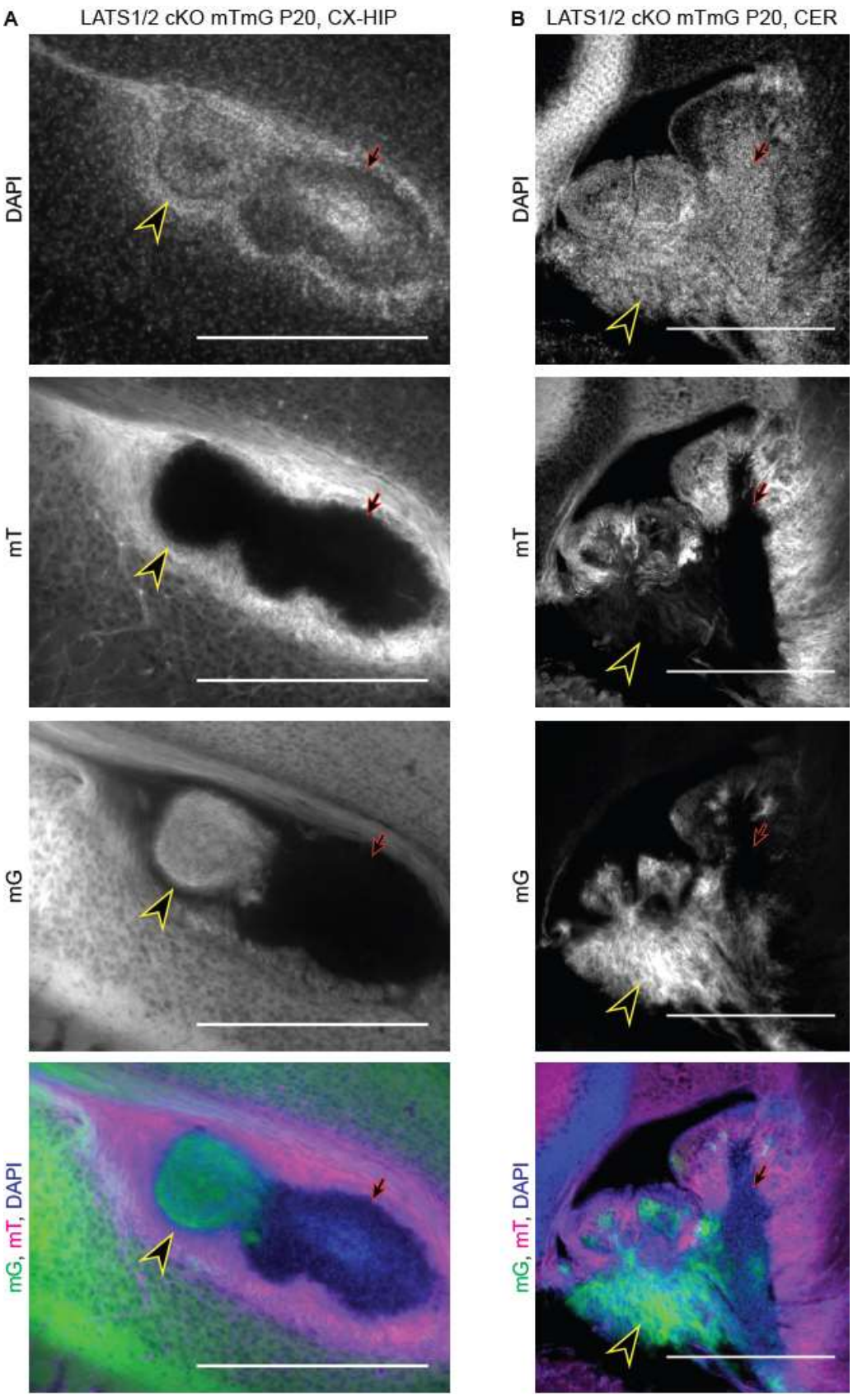
A
LATS1/2 cKO mTmG P20, CX-HIP
B
LATS1/2 cKO mTmG P20, CER
DAPI
mT
mG
mG, mT, DAPI

Figure 4.2. Reporter (mTmG) signal in cell clusters.

Representative vibratome sections of LATS1/2 cKO animals with crossed in reporter allele show expression of mG signal (Cre recombinase has been activated) in a part of the cell clusters detected (yellow arrow head). In contrast, some lesions were found absent of any reporter signal even within the same brain (red arrow). **A**. Dyspepsia arising from ependymal layer. **B**. Cell cluster anterior to cerebellum. Scale bars = 500 μm.

4.1.1 Cell clusters in LATS1/2 cKO brains and ependymal layer are positive for YAP1

To further investigate the effects of LATS1/2 dual cKO the cellular location of the direct canonical Hippo pathway target YAP1 was evaluated. Phosphorylation of YAP1 by LATS1/2, results in its inhibition, cytoplasmic retention and degradation. Deficiency in YAP1 phospho-regulation due to absence of LATS1/2, leads to YAP1 subsequently being able to enter the nucleus and trigger target gene expression.

We observed that the overall protein level of YAP1 within the dysplasia compared to the surrounding tissue was increased (Figure 4.3). This further confirms that Cre has been activated and consequently *Lats1/2* being conditionally knocked out in those cells.

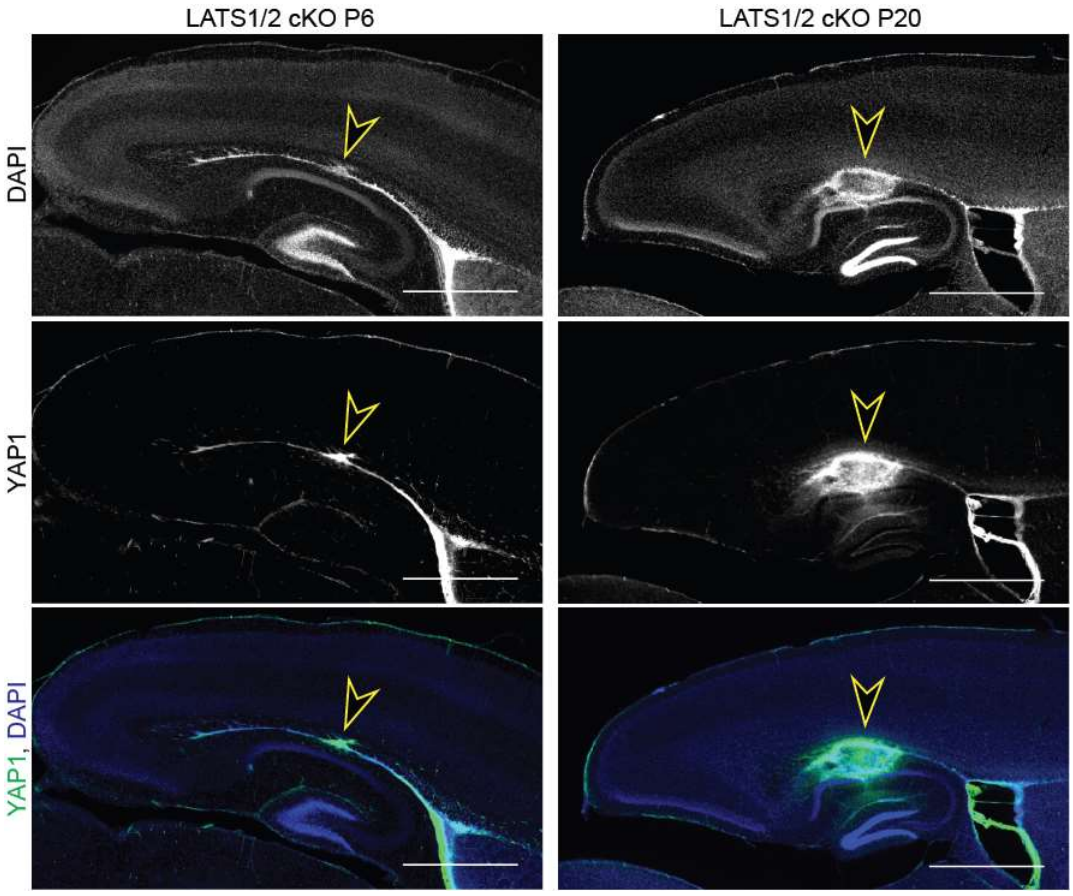

Figure 4.3. LATS1/2 conditional knockout under NEX-Cre control leads to YAP1 positive dysplasia.

Sagittal vibratome sections of LATS1/2 cKO brains at P6 and P20 exhibit strong YAP1 immunofluorescence staining in cell clusters (yellow arrow heads) arising from the ependymal layer. Scale bars = 1 mm

In addition, we found that the ependymal layer within the brains showed strong YAP1 staining, at the same expression level as the cell clusters in double cKO animals (Figure 4.3). LATS control animals at different ages in postnatal development were evaluated, all showing clear YAP1 positive ependymal layers (Figure 4.4). At P0 increase expression of YAP1 in the ventricular zone (VZ) was detected, becoming localised in the ependymal layer at P20 (Orr et al 2011).

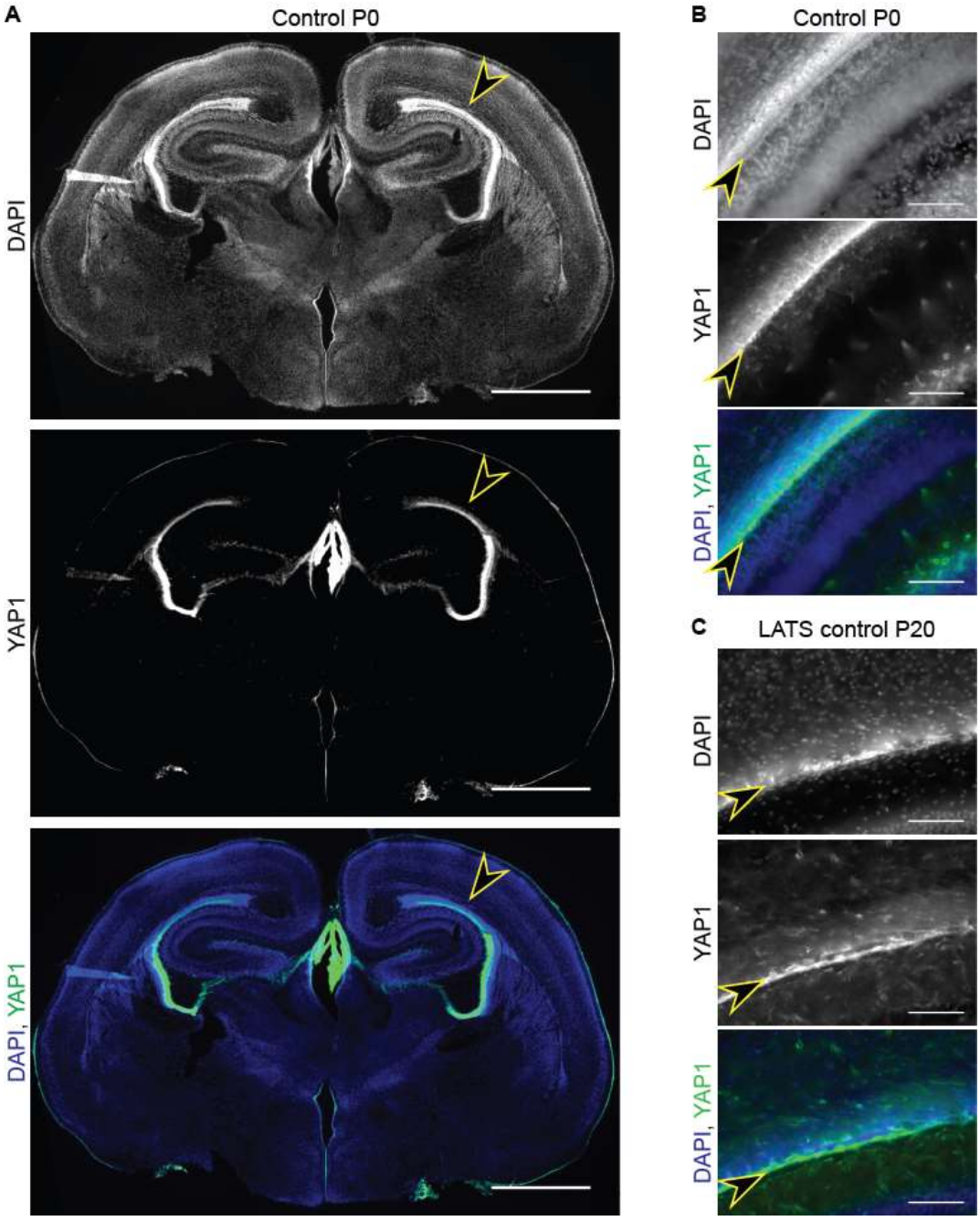

Figure 4.4. Ependymal layer stains positive for YAP1 at multiple postnatal ages.

A. Representative coronal section of a P0 Control mouse brain stained for YAP1. Strong positive YAP1 staining observed in the ependymal layer / ventricular zone (VZ) (yellow arrow head). Scale bars = 1 mm. **B-C**. Higher magnifications of ependymal layer / ventricular zone in Control brain vibratome sections at P0 (**B**) and P20 (**C**) with immunofluorescence positive signal for YAP1. Yellow arrow heads pointing at YAP1 positive ependymal layer. Scale bars = 100 µm.

To further address whether or not these cells expressing YAP1 normally in higher levels in the developing brain are targeted by the NEX-Cre driver leading to those cell clusters we did additional immunofluorescence stainings in LATS control animals. A proportion of YAP1 expressing cells in the VZ at P0 were found to be of radial glial origin and mitotically active shown by Nestin and Ki67 staining (Figure 4.5). It is known that NEX-Cre expressing neuronal precursor cells (NPCs) are generated in the VZ starting at E11.5. Also that the NEX/NeuroD6/Math2 linage gives rise to pyramidal neurons in the cortex and the hippocampus but does not contribute to astrocytes nor oligodendrocytes (Wu et al 2005) (Goebbels et al 2006). Utilising again control Ai14 mice (NEX-Cre expressing mice crossed with a Rosa26-tdTomato mouse reporter line (Madisen et al 2010)), animals at the age of P0 were inspected more closely. In addition to the neurons, we found a number of Ai14 positive cells in the ventricular zone (Figure 4.6). Moreover, a small fraction of cells could be seen still expressing CRE at P0 in the VZ whereas most only expressed TdTomato at this stage, indicating a transient expression of NEX in those cells. These observations are in agreement with previous reports showing NEX Cre in dividing NPCs (Wu et al 2005). TdTomato reporter (Ai14) positive cells also expressed YAP1, indicating that the NEX-Cre driver can be used to manipulate a sub-population of neural precursor cells.

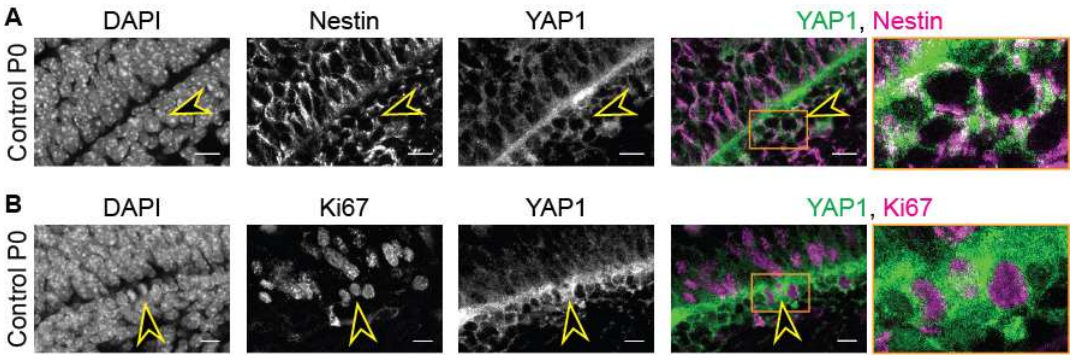

Figure 4.5. Co-expression of YAP1 with Nestin/Ki67 in VZ at P0.

Immunostaining of YAP1 together with either Nestin (**A**) or Ki67 (**B**) show co-localisation in the VZ of control mice at P0. (yellow arrow heads indicate co-localisation, overlap of stainings result in white). Scale bars = 10 µm.

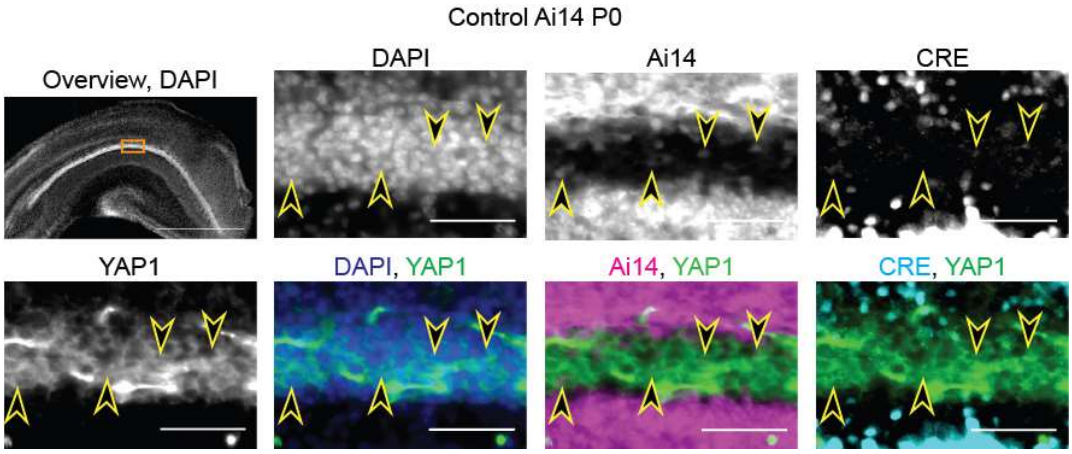

Figure 4.6. NEX-Cre is activated in cells in the VZ of P0 animals.

Higher magnification of a P0 VZ showing the presence of Ai14 positive cells expressing YAP1. A small proportion of still CRE expressing cells that also express YAP1 was observed. Yellow arrow heads point at cells expressing detectable levels of YAP1 (green), Ai14 (magenta) and CRE (cyan). Scale bars, overview = 1 mm, higher magnification = 50 µm.

4.1.2 Lesions found in LATS1/2 cKO mice show neuronal stem cell characteristics

To get a better understanding of the molecular make-up of the cell clusters a variety of markers were used. YAP1 positive tumours in early stages of development and also at P20 showed increased nestin expression (Figure 4.7.B; Figure 4.8.B), which could be found in both cells within the cluster with nuclear on those with cytoplasmic localised YAP1 (Figure 4.7). This indicates that tumour contains undifferentiated cells of radial glial origin. While GFAP positive cells were found highly enriched surrounding the dysplasia (Figure 4.8.A), in contrast to nestin positive cells.

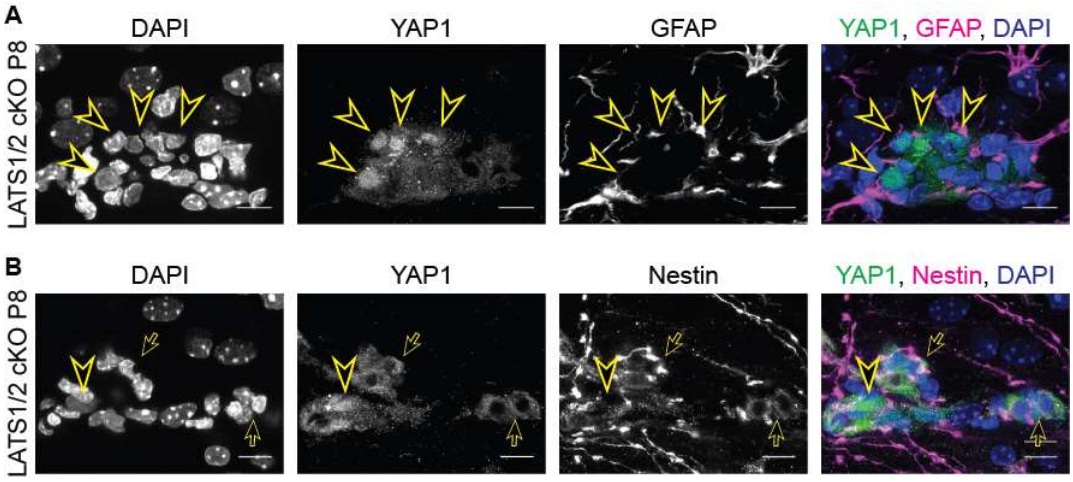

Figure 4.7. Early cell clusters show YAP1 nuclear and co expressing with Nestin but not GFAP.

Confocal images (max projection of 3 planes out of more taken) of immunofluorescence stainings in P8 LATS1/2 cKO brain, adjacent sections. YAP1 staining is increased in the dysplasia compared to surrounding. YAP1 is localised nuclear in some cells (yellow arrow heads). **A**. YAP1 expression does not overlay with GFAP positive cells. **B**. YAP1 and Nestin are co-expressed within the lesion (red arrows). Scale bars = 10 µm.

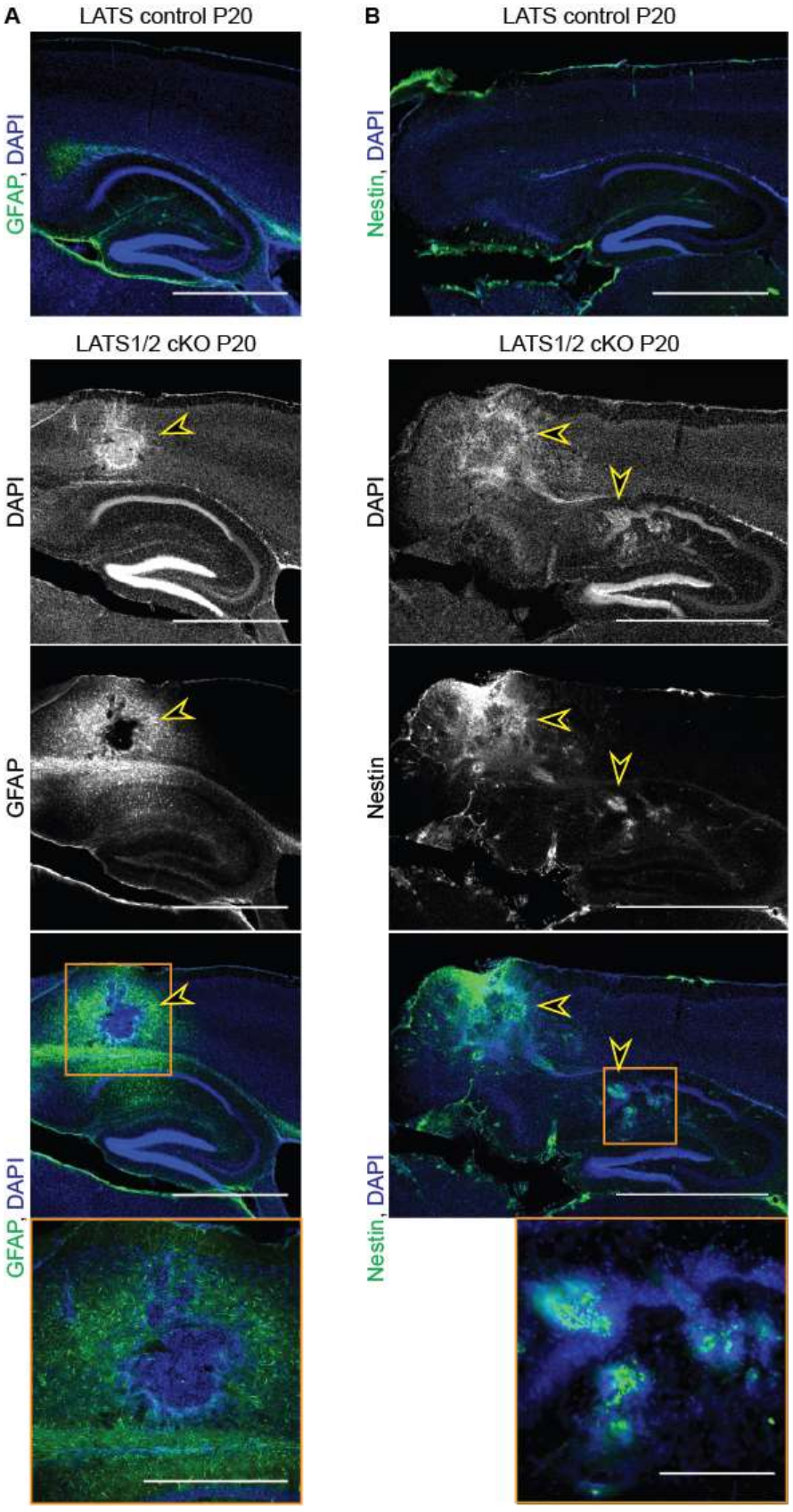
A
LATS control P20
GFAP, DAPI
B
LATS control P20
Nestin, DAPI
LATS1/2 cKO P20
DAPI
LATS1/2 cKO P20
DAPI
GFAP
Nestin
GFAP, DAPI
Nestin, DAPI

Figure 4.8. Nestin positive cell clusters surrounded by GFAP positive cells.

Sagittal vibratome sections of P20 LATS control and LATS1/2 cKO brains. Yellow arrow heads pointing at cell clusters. **A**. Number of GFAP positive cells highly increased in dual knockout brains surrounding the lesion, but remain absent of the cluster centre itself. **B**. Nestin immunofluorescence staining increased within the cell clusters. Scale bars, overviews = 1 mm, close ups = 500 µm.

Neuronal markers NeuN and Tuj1 and transient neural progenitor cell marker TBR2 were found negative and excluded from the dysplasia, which is indicative of a lack of differentiated neurons (**Error! Reference source not found.**). Further pointing towards, post mitotic neurons expressing NEX-Cre were not the origin of the cell cluster. Also, we found microglial cell marker Iba1 and oligodendrocyte marker Olig2 to be also absent from the dysplasia centre, but appeared to line the outskirts of the tumour (Figure 4.10). These cells did not show increased expression to cells detected in controls or neighbouring tissue. These results indicate that YAP1 is activated in LATS1/2 deleted ependymal cell or its precursor leading to a nestin and YAP1 positive tumour formation, surrounded by GFAP positive glia, likely recruited to this site.

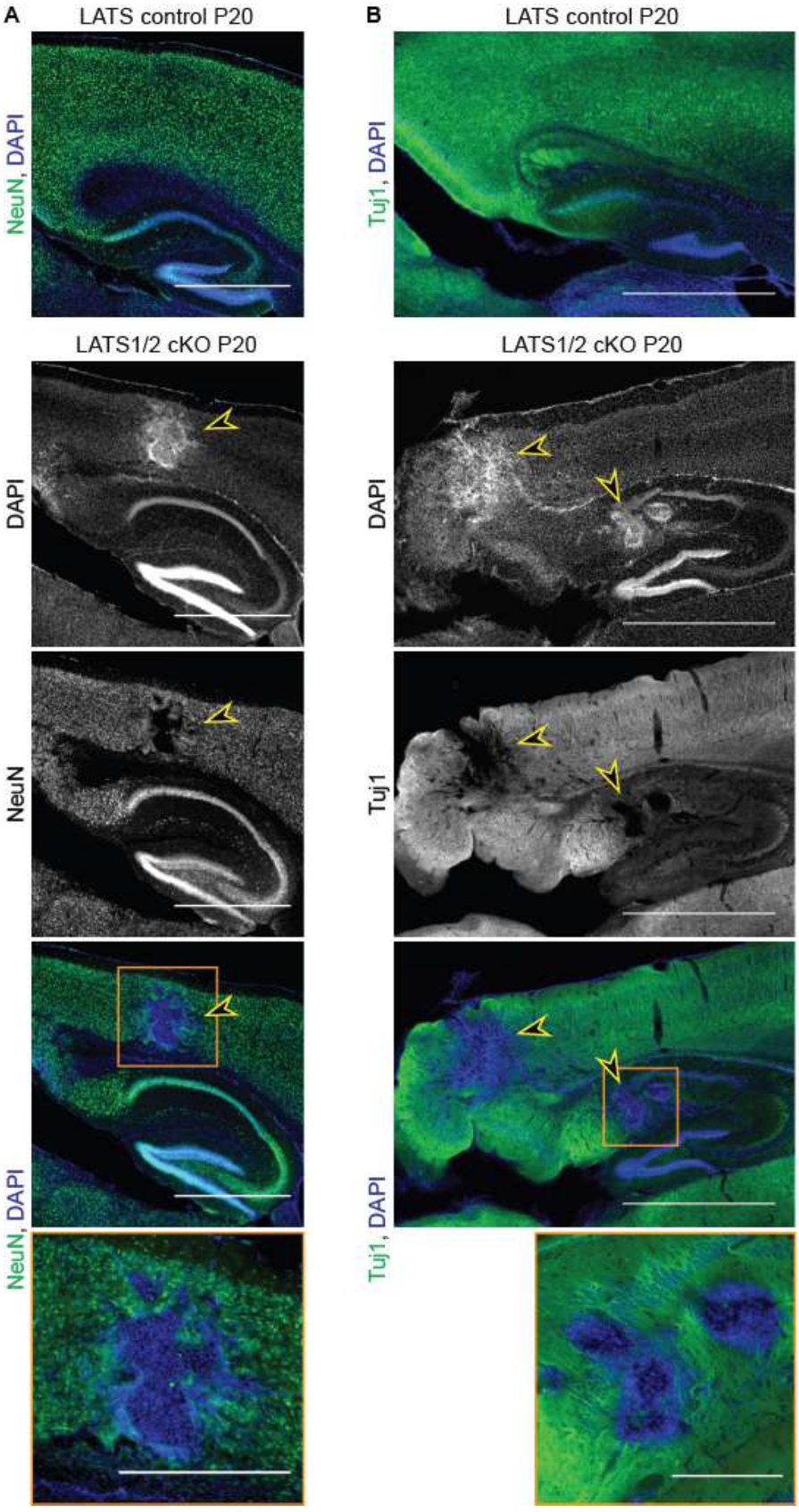
A
LATS control P20
NeuN, DAPI
LATS1/2 cKO P20
DAPI
NeuN
NeuN, DAPI
B
LATS control P20
Tuj1, DAPI
LATS1/2 cKO P20
DAPI
Tuj1
Tuj1, DAPI

Figure 4.9. Cell clusters absent for neuronal markers such as NeuN and Tuj1.

Sagittal vibratome sections of P20 LATS control and LATS1/2 cKO brains (different animals per staining). Yellow arrow heads pointing at cell clusters. Detected cell clusters appear absent of NeuN (**A**) and Tuj1 (**B**). Scale bars, overviews = 1 mm, close up NeuN = 500 µm, close up Tuj1 = 200 µm.

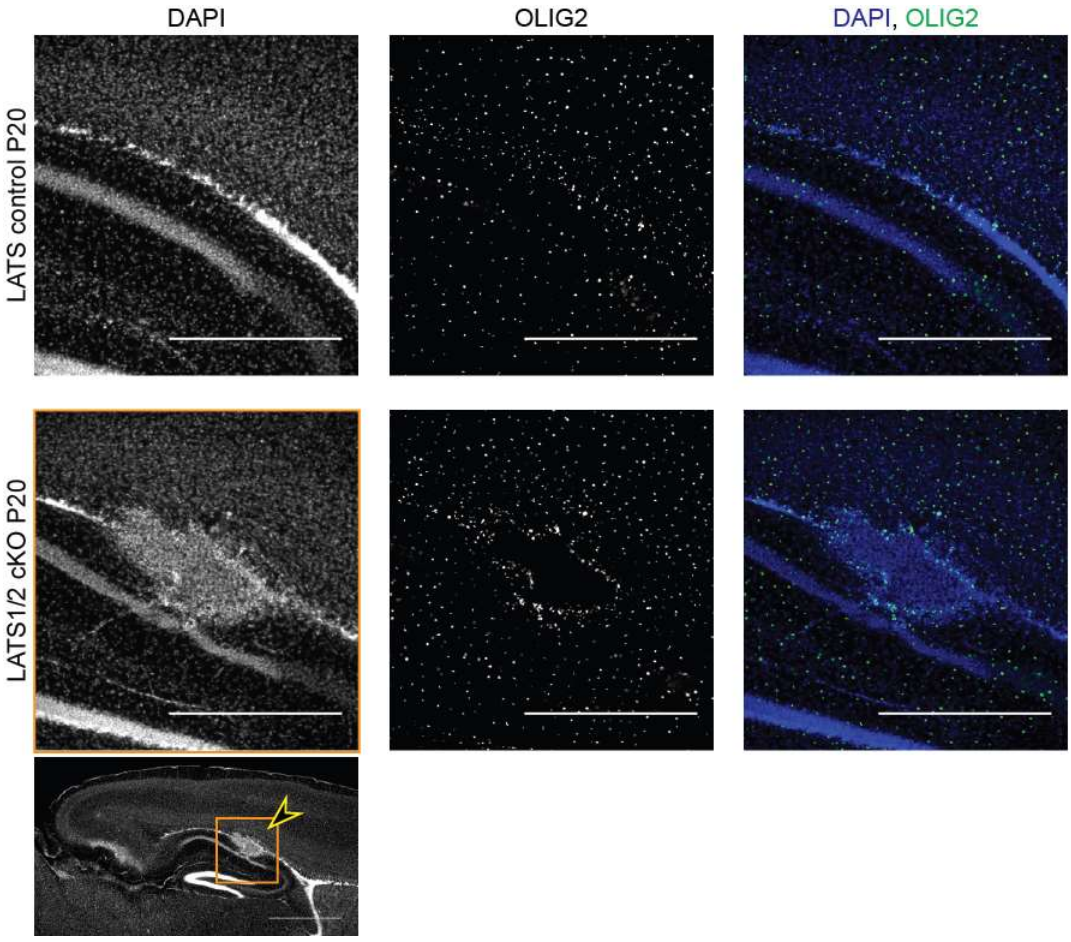

Figure 4.10. OLIG2 is not expressed within the lesion.

Sagittal vibratome sections of P20 LATS control and LATS1/2 cKO brains Yellow arrow head in dual knockout overview points at cell cluster. OLIG2 in not expressed in the detected dysplasia, but appears to line the outskirts. Scale bars = 500 µm, mutant overview = 1 mm.

Due to the observation of these lesions arising from the ependymal layer, a closer attention was put towards proteins found to be expressed in ependymal cells and also makers used in human ependymoma, a tumour arising from those cells (Vege et al 2000). Vimentin which is reported to be typically expressed in ependymal cells was found to be highly increased in the dysplasia (Figure 4.11) (Schnitzer et al 1981). Another ependymal marker MUC1 (Mucin1), also known as EMA (Epithelial membrane antigen), which is also used for ependymoma identification was also highly expressed in dysplasia (Figure 4.12.A) (Hasselblatt & Paulus 2003). Cell clusters in LATS1/2 cKO brains further exhibit high cytokeratin expression indicating presence of epithelial-like cells, another marker used for ependymoma classification (Figure 4.12.B) (Vege et al 2000). Further, SOX2 (SRY-box 2), a transcription factor essential to maintain embryonic stem cells, can be found enriched in dysplasia (Figure 4.11) (Basu-Roy et al 2015). Finally, a subset of cells within the cell mass expressed the proliferation marker Ki67, showing that the tumour contains actively dividing cells (Figure 4.12.C). Overall, immunostaining and characterization of the YAP1 positive dysplasia in *Lats1/2* knockout brains indicate that these cell clusters resemble tumour like features and are positive for markers found and commonly used in ependymoma.

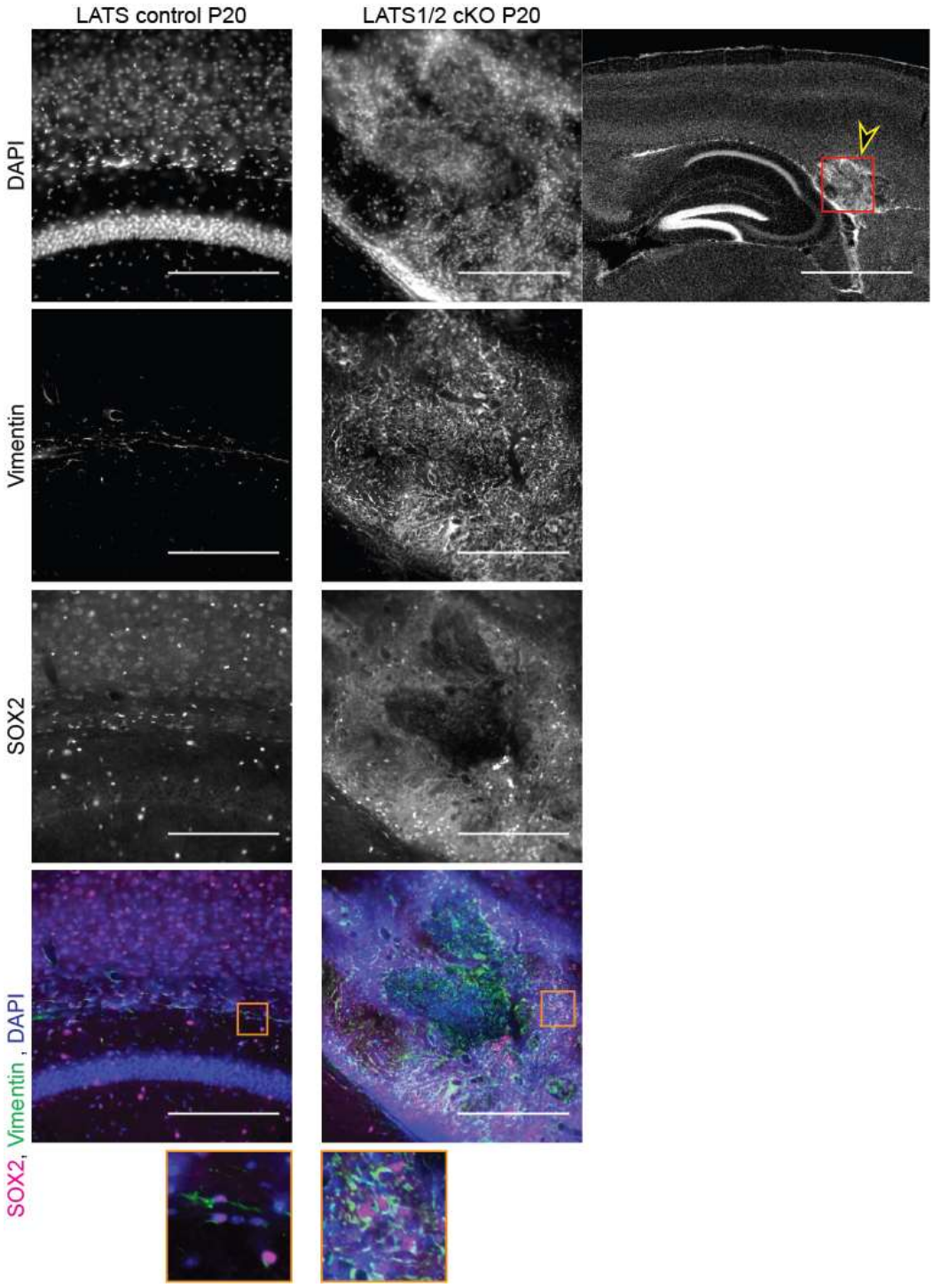

Figure 4.11. Increased expression of Vimentin and SOX2 in cell cluster.

Sagittal vibratome sections of P20 LATS control and LATS1/2 cKO brains. Yellow arrow head in dual knockout overview points at cell cluster. Vimentin is highly upregulated throughout the dysplasia compared to unaffected tissue. SOX2 positive cells are increased in lesion. Co-expression of both markers are observed in ependymal layer (LATS control zoom) and in the cell cluster (LATS1/2 cKO zoom). Scale bars = 200 µm, mutant overview = 1 mm.

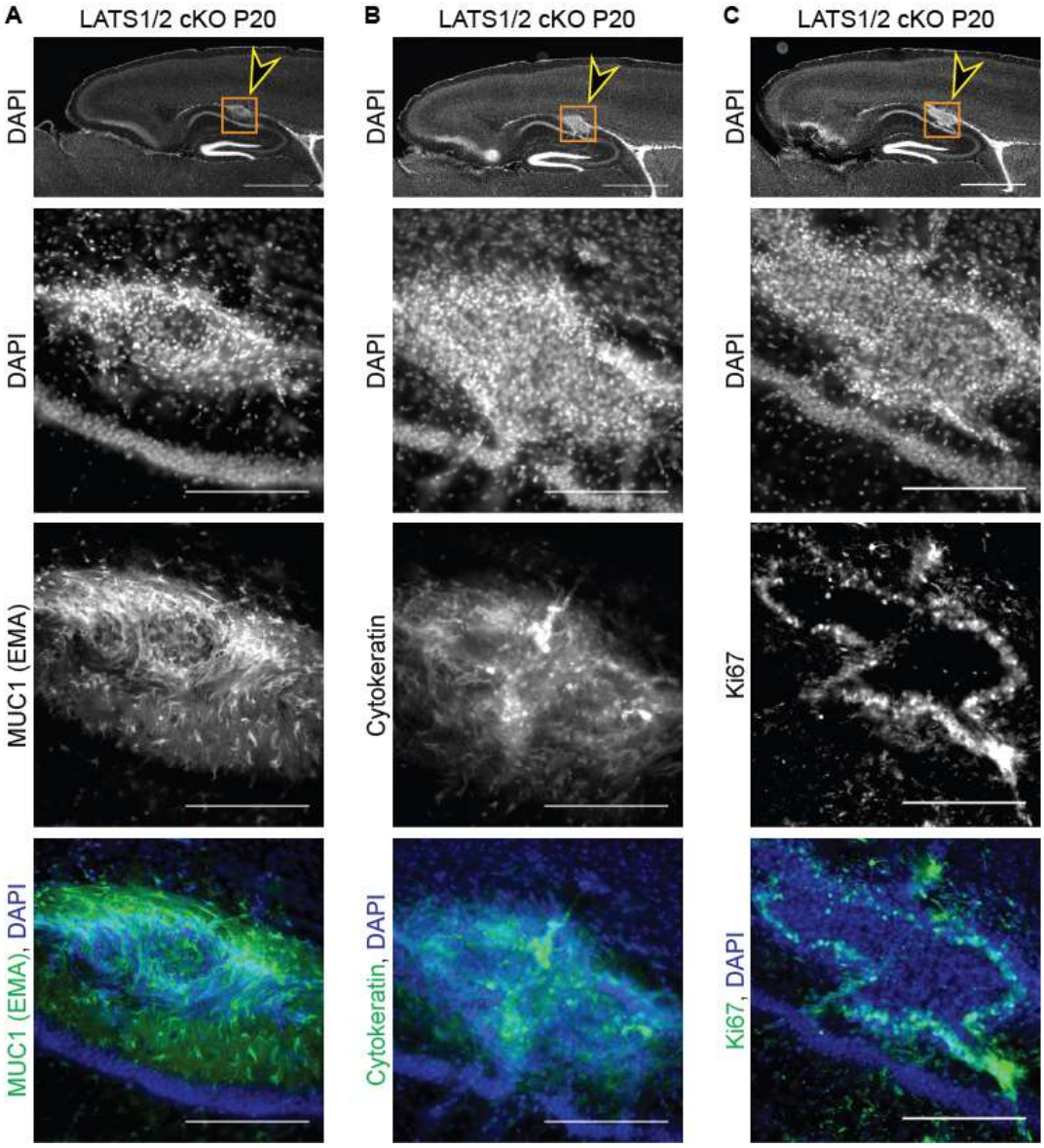

Figure 4.12. Cell cluster is positive for MUC1 and Cytokeratin and appears enriched in Ki67 expressing cells.

Representative vibratome sections of P20 LATS control and LATS1/2 cKO brains. Yellow arrow head in dual knockout overviews points at cell cluster. MUC1/EMA (**A**) and wide-spectra Cytokeratin (**B**) are highly increased throughout the lesion. A higher occurrence of Ki67 (**C**) positive cells is detected in the tumour in particular towards the boarder. Scale bars, overviews = 1 mm, stainings = 200 µm.

4.2 The central role of YAP1 in the tumour formation

It is generally accepted that YAP1 is one of the main substrate of LATS1/2 and the key functional output of the canonical Hippo pathway. While several lines if evidence support an oncogenic role for YAP1, the impact of upstream kinase regulation on its activity is not well understood.

4.2.1 Expression of active YAP1 in the NEX-Cre linage is sufficient for tumour development in the murine brain at the expense of hippocampal formation

To address whether elevated YAP1 activity is sufficient to cause tumour formation in the NEX-Cre expressing mouse model, an uncontrollable form of YAP1, nlsYAP5SA, which is preceded by a floxed STOP codon (Cotton et al 2017), was crossed in (Figure 4.13.A). Upon CRE mediated recombination these transgenic animals express murine phosphomutant YAP1 (S61A, S109A, S127A, S164A, S381A). This protein cannot be phosphorylated and consequently inhibited by kinases such as LATS1/2 (Zhao et al 2007). Moreover, this construct contains a nuclear localisation sequence (nls) which prompts the active protein to be translocated to the nucleus.
Crossing the transgenic NEX-Cre mouse line with nlsYAP5SA animals resulted in mice showing multiple subependymal tumours (Figure 4.13.C). YAP1 mutant animals displayed much earlier onset of phenotypical features compared to the LATS1/2 cKO mice and could not be kept past the age of P14. From a young age we found the mutant animals different from their littermates by size and evident features like balance issues, spinning, hunched posture or lethargy. At the age of P7 the measured weights of nlsYAP5SA mice were significantly lower compared to their unaffected littermates ($p = 0.0006$, Mann Whitney test) (Figure 4.13.B). Due to increasing severity of phenotype and clear weight loss, 28.6% of mutant animals had to be sacrificed prior to reaching P11. A separate litter was weight at P0 and with an average weight of 1.3 g we did not detect a difference in weight between genotypes. Intriguingly, it was found that mutant males were lighter than the female littermates with the same genotype, significantly from the age of P10 ($p = 0.005$, Mann Whitney test) (Figure 4.13.B). We did not see such a gender dependent difference in LATS1/2 cKO animals.

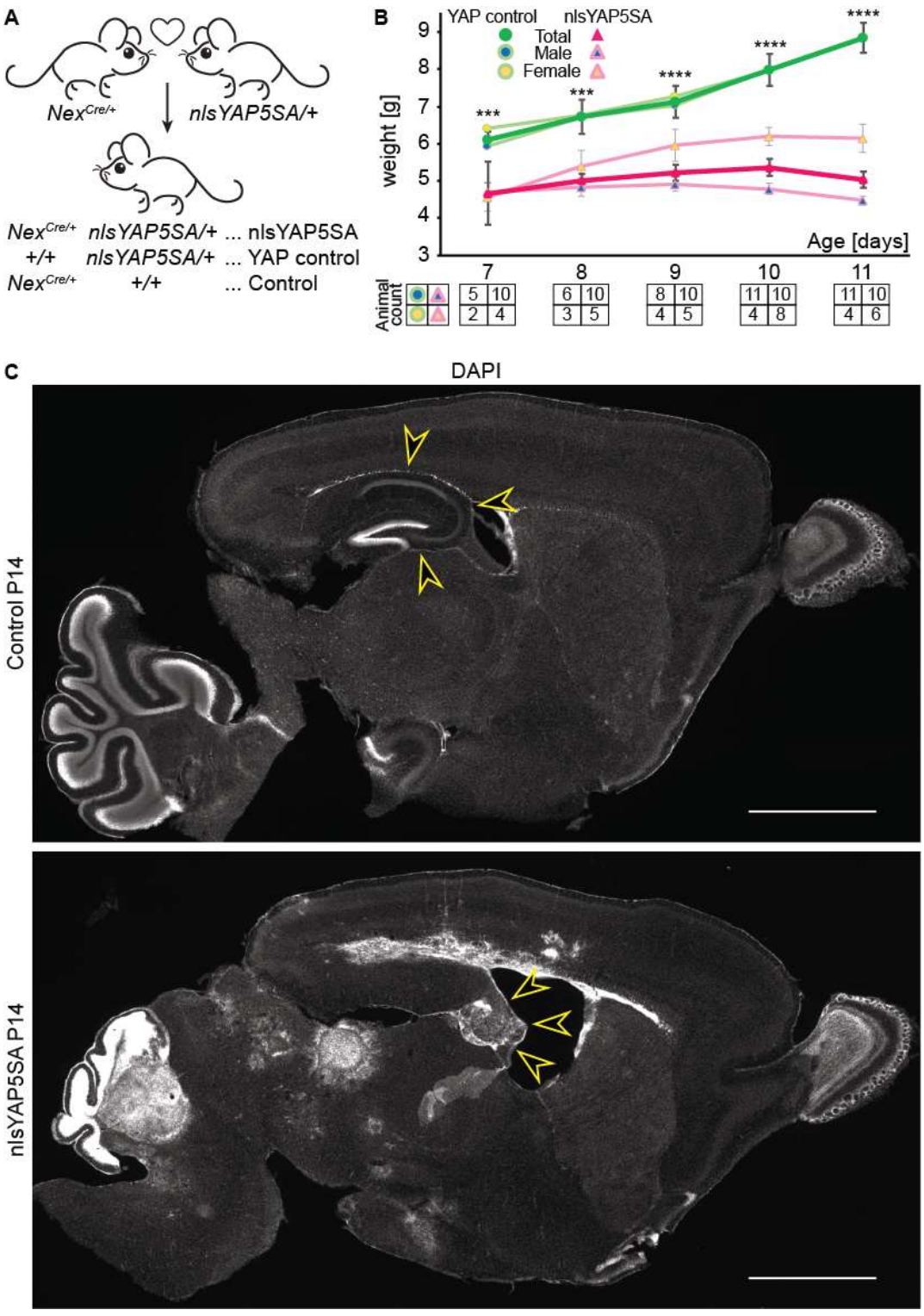

Figure 4.13. Hyperactive YAP1 form under the control of NEX-Cre expression is sufficient to cause tumour development at the expense of the hippocampal differentiation.

A. Breeding scheme to generate mice expressing nlsYAP5SA under the control of NEX-Cre and control animals. **B**. Measured average weights of YAP control (green) and nlsYAP5SA (pink) mice

from P7 to P11. Significant difference in weight found for all ages measured (P7 $p = 0.0006$; P8 $p = 0.0003$; P9-P11 $p < 0.0001$; Mann Whitney test). Gender specific average weights are plotted as well (male blue fill, female yellow fill). Numbers of weight animals per age, genotype and gender shown in the table below. Error bars show SEM. **C**. Sagittal whole brain vibratome sections of Control and nlsYAP5SA animals at P14 are shown. In nlsYAP5SA mice, numerous cell clusters are detected across the brain, the ependymal layer appears destructed and the hippocampus is not developed. Yellow arrow heads point at hippocampus location. Scale bars = 1 mm.

The effects of nlsYAP5SA expression on the brain and tumour formation was further investigated at earlier stages of development to get a better understanding of the progression and tumour origin location. As expected, we found YAP1 located in the nucleus throughout the cortex and the hippocampus of nlsYAP5SA mice (Figure 4.14). Its expression level exceeded the normal levels found in the ependymal layer. Furthermore, as demonstrated with the neuronal markers NeuN and CTIP2, those animals showed a loss of neurons and proper layering of the hippocampal formation (CA1, CA3 and DG) when compared to controls (Figure 4.15). Hippocampus formation appears altered in nlsYAP5SA compared to Control brains. However, we found the cortical structure less affected by the hyperactivity of YAP1.

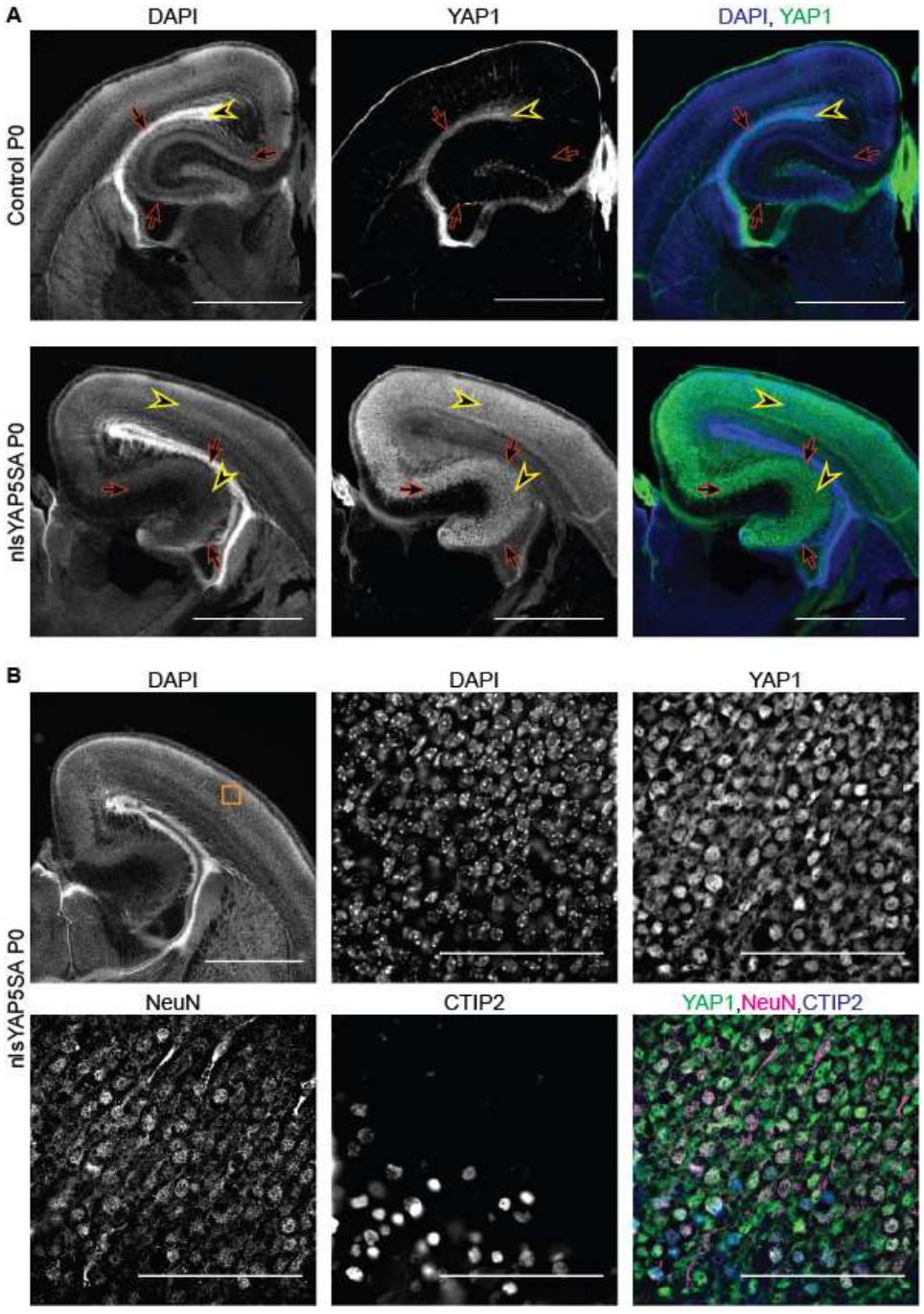

Figure 4.14. YAP1 is highly expressed in the cortex and hippocampus and is localised in the nucleus.

A. Representative coronal vibratome sections of Control and nlsYAP5SA animals at P0. Strong nuclear IF staining of YAP1 found in nlsYAP5SA cortex and hippocampal formation. Yellow arrow heads point at highest detected YAP1 IF signal, red arrows point out hippocampal formation. Scale bars = 1 mm. **B**. Representative vibratome section of nlsYAP5SA shows co-expression of nuclear YAP1 with neuronal markers NeuN and CTIP2 in the cortex. Scale bars, overview = 1 mm, close ups = 100 µm.

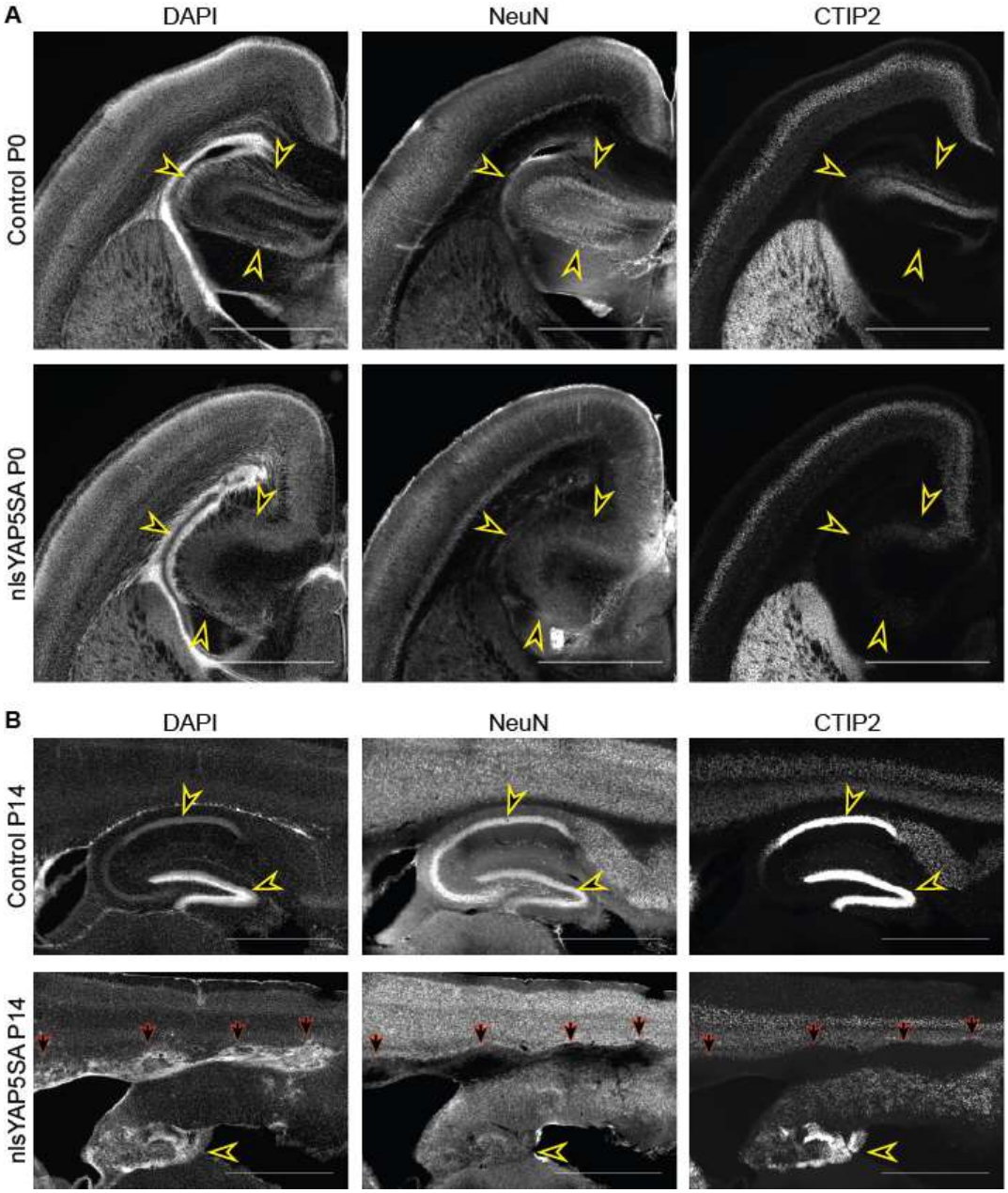

Figure 4.15. NEX-Cre nlsYAP5SA animals present with compromised hippocampus development.

A. Representative coronal vibratome sections of P0 Control and nlsYAP5SA brains stained for NeuN and CTIP2. Reduction of either marker in hippocampal formation in nlsYAP5SA when compared to Control. Cortex does not show striking difference in IF staining. Yellow arrow heads indicate hippocampus. Scale bars = 1 mm. **B**. Representative sagittal vibratome sections of P14 Control and nlsYAP5SA brains stained for NeuN and CTIP2. Layering of cortex appears preserved in nlsYAP5SA animals, whereas hippocampus formation is severely affected (yellow arrow heads). Cluster formation along the ependymal layer in nlsYAP5SA brains (red arrows). Scale bars = 1 mm.

We detected multiple tumours in P0 nlsYAP5SA brains, all adjacent or close proximity to the ependymal layer depending on brain section (Figure 4.16.A). We investigated the molecular profile of those tumours to confirm if the found profile in LATS1/2 cKO was replicated in this model (Figure 4.16.B). Again, the tumours did not express the neuronal marker NeuN. Also in accordance with the LATS1/2 cKO model, stem cell marker Nestin, proliferation marker Ki67 and ependymal marker MUC1 (EMA) were positive in the studied cell masses.

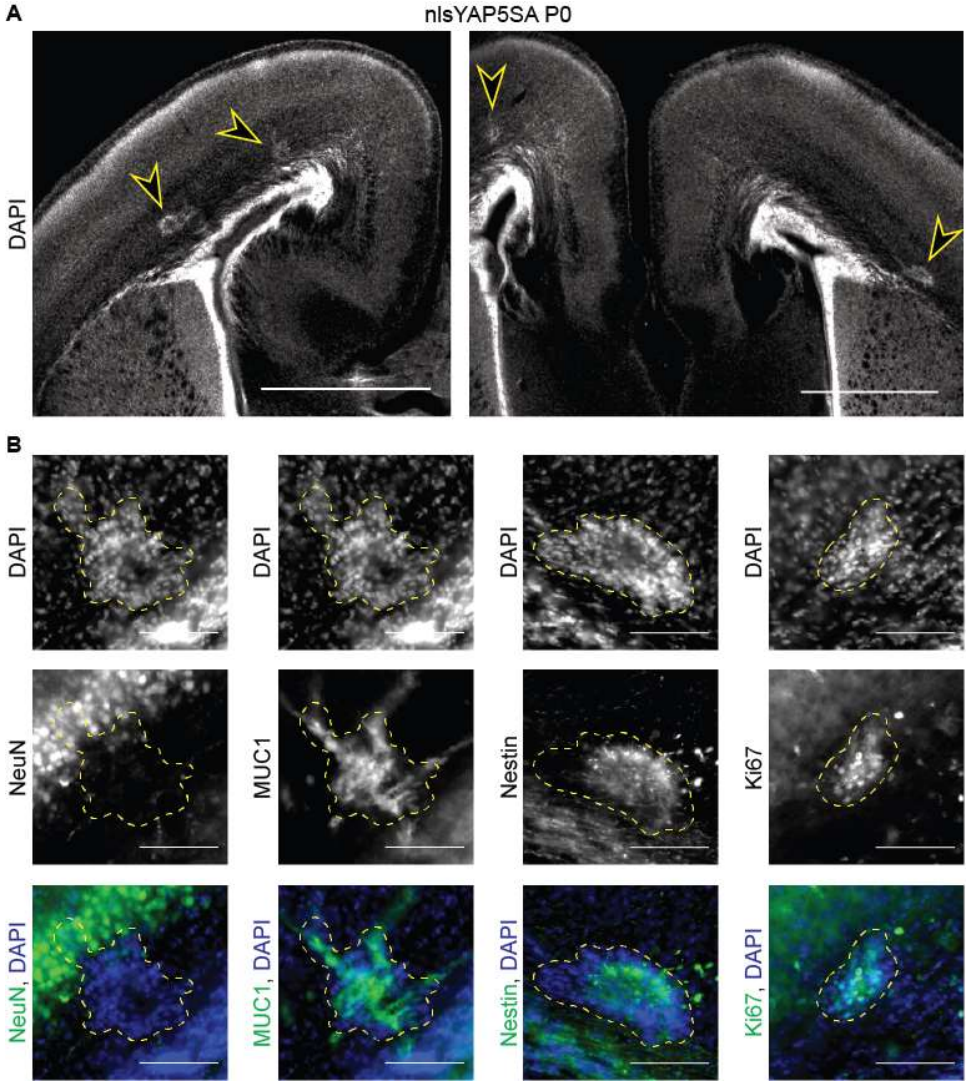

Figure 4.16. IF profile of nlsYAP5SA tumours recapitulate findings in LATS1/2 cKO model. **A**. Yellow arrow heads point at tumours found in the coronal sections of P0 nlsYAP5SA mice. Scale bars = 1 mm. **B**. IF stainings of vibratome sections of nlsYAP5SA brains. NeuN appears absent while MUC1, Nestin and Ki67 show intense staining in tumours (outlined by yellow dashed line). Scale bars = 100 µm.

4.2.2 YAP1 and TAZ are necessary for tumour formation in LATS1/2 cKO animals

From the previous results it could be concluded that YAP1 is sufficient to generate tumours. Nevertheless, it remained to be investigated if YAP1 is necessary and does play a crucial role in the tumour development in LATS1/2 cKO animals. The transcriptional co activators YAP1 and its close homolog TAZ are both effectors of the Hippo pathway. It has been reported that they have both overlapping and distinct functions within a cell. Therefore, *Lats1*$^{f/f}$ *Lats2*$^{f/f}$ mice (Yi et al 2016) were crossed with Yap1$^{f/f}$ Taz$^{f/+}$ mice (Elbediwy et al 2016) and Nex$^{Cre/Cre}$ animals (Wu et al 2005) to determine whether tumourigenesis depends on YAP1 as well as TAZ1 (Figure 4.17).

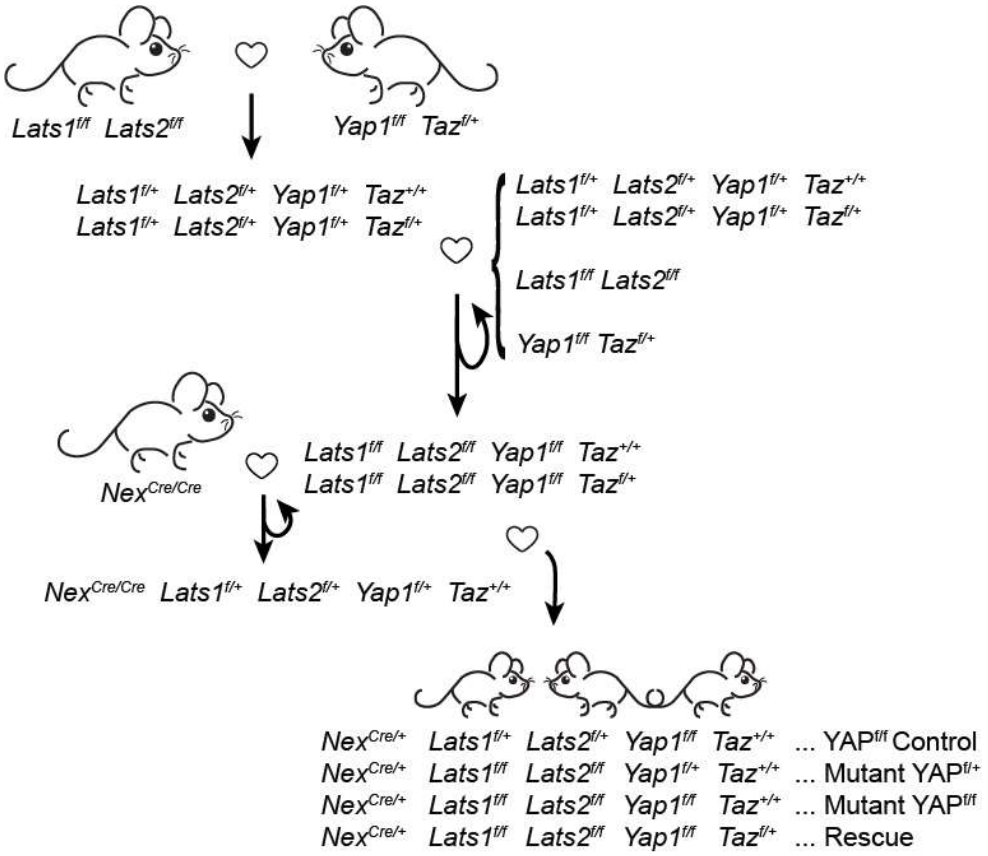

Figure 4.17. Breeding scheme to generate rescue animals.

Lats1$^{f/f}$ *Lats2*$^{f/f}$ mice were crossed with *Yap1*$^{f/f}$ *Taz*$^{f/+}$ and re-breed to generate *Lats1*$^{f/f}$ *Lats2*$^{f/f}$ *Yap1*$^{f/f}$ *Taz*$^{f/+}$. Those subsequently were crossed with *Nex*$^{Cre/Cre}$ animals in two generations to result in *Nex*$^{Cre/Cre}$ *Lats1*$^{f/+}$ *Lats2*$^{f/+}$ *Yap1*$^{f/+}$ *Taz*$^{+/+}$ mice. Those were crossed with *Lats1*$^{f/f}$ *Lats2*$^{f/f}$ *Yap1*$^{f/f}$ *Taz*$^{f/+}$ to generate experimental offspring.

In this rescue experiment it was found that LATS1/2 cKO animals with one or both copies of YAP1 depleted still generated tumours at the age of P20 (Figure 4.18.A). Only depletion of an additional copy of TAZ resulted in the rescue of the phenotype. We did not find tumours at the age of P20. This supports that both YAP1 and TAZ are activated in the tumour mediating its formation.

Taking three P20 animals per genotype (LATS1/2 cKO, Mutant $YAP^{f/+}$, Mutant $YAP^{f/f}$), the number and the volume of the tumours per brain were assessed (Figure 4.18.B). When both alleles of YAP1 were depleted, a significant reduction in average tumour size compared to the LATS1/2 cKO animals could be shown ($p < 0.001$, Dunn`s multiple comparison test). The reduction of tumour size within the brains where only one allele of YAP1 is depleted appeared overall reduced but did not show statistical significance. Albeit, integrating a random effect model to account for the multiple tumours being detected per animal, a significant evidence for an additive dosage effect could be found (Figure 4.18.B). In more detail, each YAP1 wild type allele depleted corresponds to a decrease in estimated tumour volume of approximately 0.03 mm^3 ($p = 0.0068$). Even though the average tumour size reduced, the total brain count between LATS cKO and Mutant $YAP^{f/+}$ remained almost the same and only the depletion of both YAP1 alleles resulted in a lower total number of tumours (Figure 4.18.C).

We obtained one single animal with all four alleles (*Lats1, Lats2, Yap1, Taz*) double floxed. This mouse did not show any difference to its littermates and as expected no tumour was found in the brain at P20. The cortex and the hippocampus did not show any obvious structural difference to the control animals. Also NeuN IF staining appeared normal (data not shown).

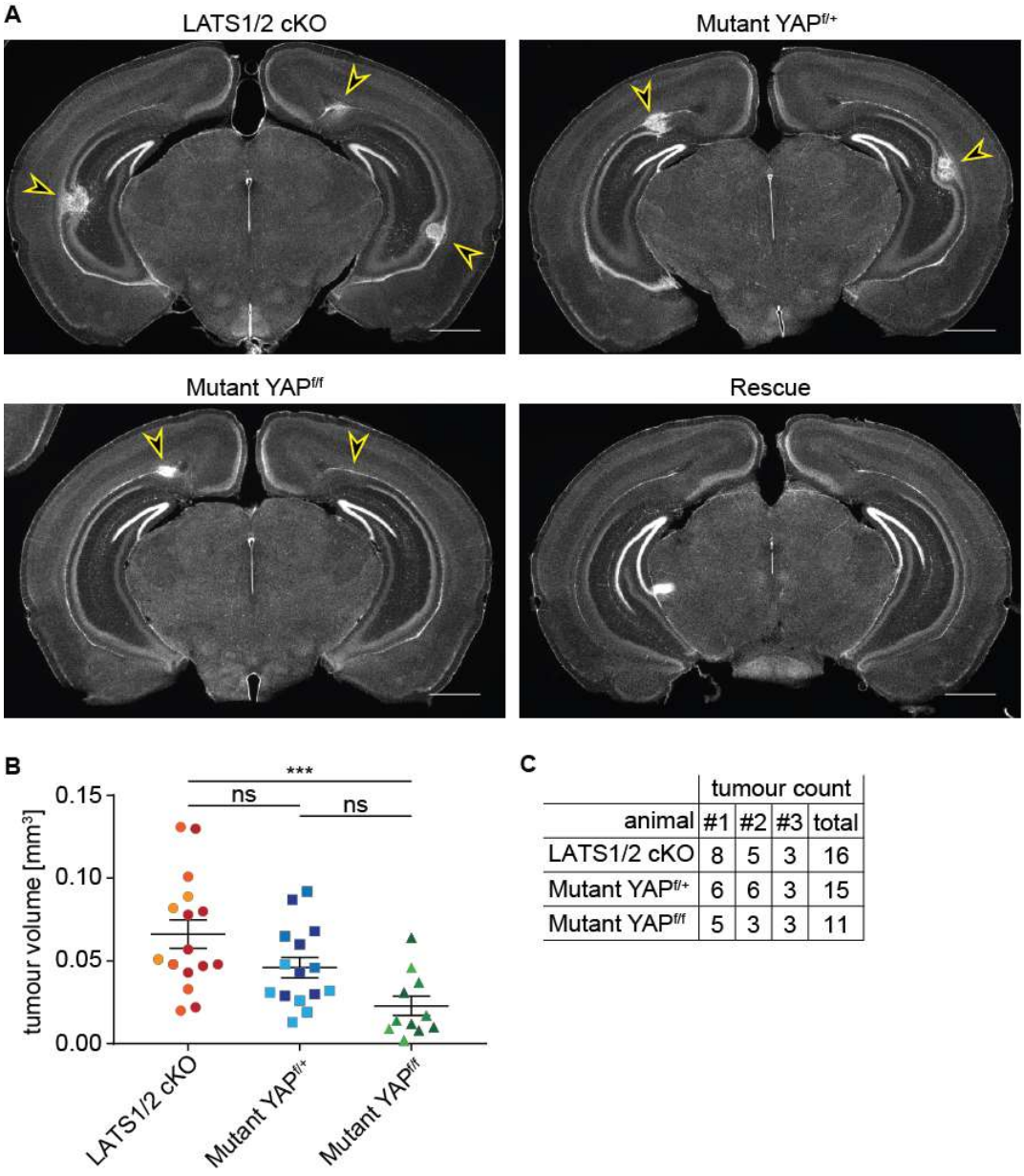

C

	tumour count			
animal	#1	#2	#3	total
LATS1/2 cKO	8	5	3	16
Mutant YAP$^{f/+}$	6	6	3	15
Mutant YAP$^{f/f}$	5	3	3	11

Figure 4.18. YAP1 and TAZ is necessary for tumour formation.

A. Representative coronal vibratome full brain sections of LATS1/2 cKO (*Nex$^{Cre/+}$ Lats1$^{f/f}$ Lats2$^{f/f}$*), Mutant YAP$^{f/+}$ (*Nex$^{Cre/+}$ Lats1$^{f/f}$ Lats2$^{f/f}$ Yap1$^{f/+}$ Taz$^{+/+}$*), Mutant YAP$^{f/f}$ (*Nex$^{Cre/+}$ Lats1$^{f/f}$ Lats2$^{f/f}$ Yap1$^{f/f}$ Taz$^{+/+}$*) and Rescue mice (*Nex$^{Cre/+}$ Lats1$^{f/f}$ Lats2$^{f/f}$ Yap1$^{f/f}$ Taz$^{f/+}$*) stained with DAPI. Yellow arrows point at detected tumours, which could be found in all animals except for Rescue mice. Scale bars = 1 mm. **B**. Tumour volume measurements found in LATS1/2 cKO, Mutant YAP$^{f/+}$, Mutant YAP$^{f/f}$ from n = 3 brains per genotype. Colour shade indicates tumours from the same animal. Comparing the tumours measured in LATS1/2 cKO to Mutant YAP$^{f/f}$ animals, a significant difference in volume between the genotypes could be found (padj = 0.0006 Dunn`s multiple comparison test). Average and error bars show SEM. **C**. Tumour count per animal.

Additionally, tumours generated in Mutant YAP$^{f/f}$ animals showed complete absence of YAP1 staining (Figure 4.19). Showing both the specificity of the antibody and supporting the hypothesis that the tumours are indeed generated by the NEX-Cre expressing cells.

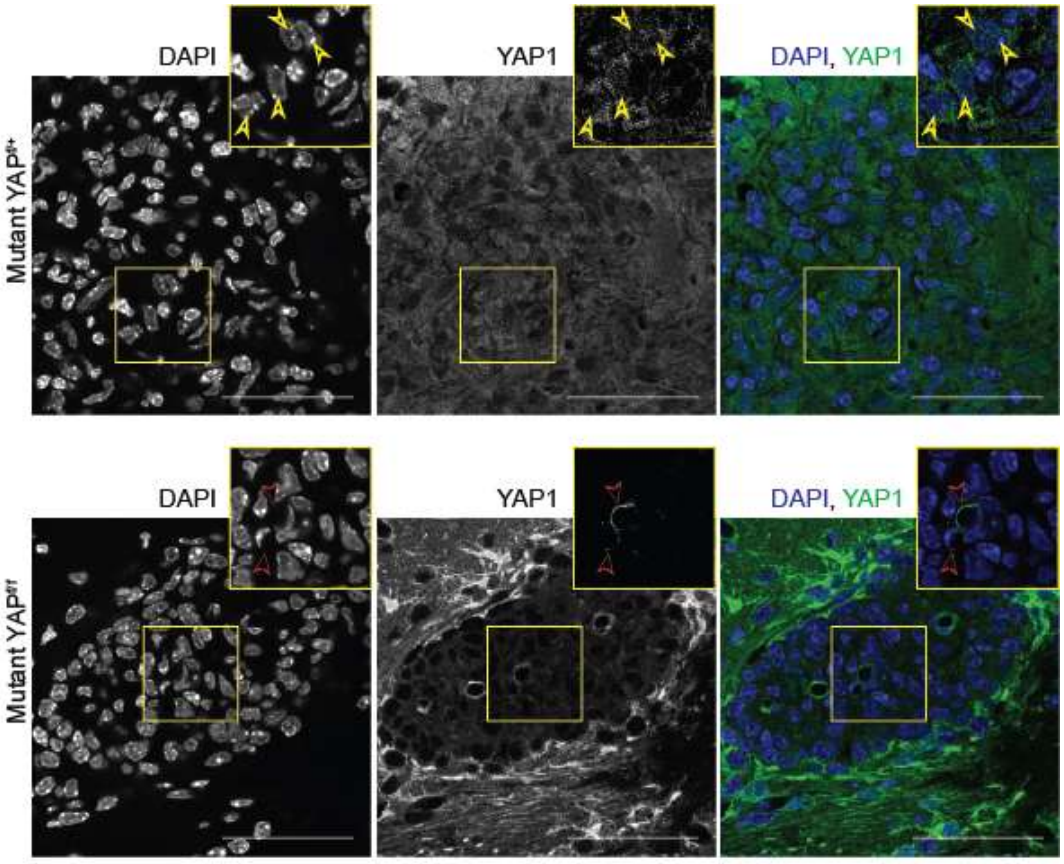

Figure 4.19. YAP1 antibody specificity in Immunofluorescence.

Confocal images of YAP1 IF staining shown in tumours of Mutant YAP$^{f/+}$ (top, *Nex*$^{Cre/+}$ *Lats1*$^{f/f}$ *Lats2*$^{f/f}$ *Yap1*$^{f/+}$ *Taz*$^{+/+}$) and Mutant YAP$^{f/f}$ (bottom, *Nex*$^{Cre/+}$ *Lats1*$^{f/f}$ *Lats2*$^{f/f}$ *Yap1*$^{f/f}$ *Taz*$^{+/+}$) mice. YAP1 staining is present in the tumour in Mutant YAP$^{f/+}$ and can be found located nuclear in a subset of cells (yellow arrow heads). No YAP1 staining was detected in cells in the tumour mass of Mutant YAP$^{f/f}$ mice. Staining was only found in blood vessels which are not targeted by the NEX-Cre. (red arrow heads). Scale bars = 50 µm.

In this subchapter we could show that dual conditional knockout of *Lats1* and *Lats2* in a subset of NEX expressing cells results in clonal tumour formation. Those tumours are adjacent to the ependymal layer and express high levels of YAP1 which can be found in nuclear localisation. Furthermore, the tumours show stem cell like characteristics and parallels to human ependymoma can be found. YAP1 was demonstrated to play a central role in the generation of those tumours as its deregulation is sufficient to cause tumourigenesis. Additionally, we could show the dependence of the development of these tumours on YAP1 and TAZ.

Chapter 5. Murine tumours are ependymoma like

The animal model with the conditional knockout of LATS1 and LATS2 under the control of the NEX promoter was found to develop cell clusters in the brain in 100% of the mutant mice (LATS1/2 cKO) older than one week. Initial examinations showed first indications of similarity between those lesions and ependymoma, a type of brain cancer.

5.1 Detected murine tumours recapitulate morphological and expression features of human ependymoma.

5.1.1 Tumours in LATS1/2 cKO animals show morphological characteristics of human ependymoma

We hypothesized, that the dysplasia arising in the mice are ependymoma-like. To test this, we investigated the pathological characteristics of the LATS1/2 cKO tumours, in serial sections of paraffin embedded P20 brains and compared to known characteristics of ependymoma. Therefore, a neuropathologist Dr. Federico Roncaroli at the University of Manchester specialised in brain tumours was consulted and a collaboration initiated. Based on his expertise he concluded that the cell mass showed clear histological features of ependymoma. Serial sections of paraffin embedded H&E stained P20 LATS1/2 cKO mouse brains, showed periventricular multifocal tumours in continuity with the ependymal layer (Figure 5.1.A). Under closer histological analysis, the tumours appear as moderately cellular lesions with compressive margin (Figure 5.1.B). They were composed of uniform cells with slightly hyperchromatic nucleus and scanty or fibrillary cytoplasm (Figure 5.1.C). A few tubules and perivascular arrangement of tumour cells reminiscent of perivascular pseudo-rosettes were present (Figure 5.1.E). Some cells contained intra-cytoplasmic vacuoles (Figure 5.1.D). Mitoses could not be observed. Lesion surrounding tissue shows reactive astrocytosis and microglial response.

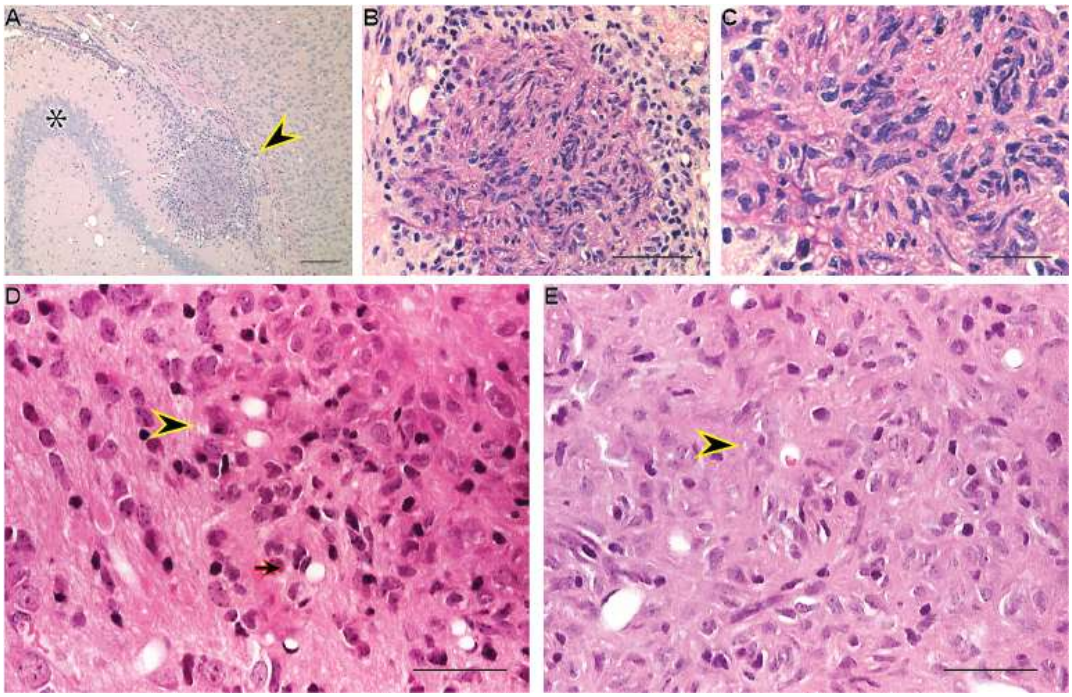

Figure 5.1. Tumours in LATS1/2 KO mice recapitulate features of human ependymoma.

A-E. H&E, **A**. The cell mass (arrowhead) seems to grow out from the ependymal layer of the anterior temporal horn of the lateral ventricle at the level of hippocampus (* CA3). Scale bar = 500 µm. The dysplasia has a compressive margin (**B**, scale bar = 500 µm) and is composed of fascicles of spindle cells with focal nuclear clustering (**C**, scale bar = 200 µm). **D-E**. The tumour shows tubules (yellow arrowhead) and paranuclear vacuoles (red arrow) (**D**, scale bar =50 µm) and perivascular arrangement of tumour cells that is reminiscent of perivascular pseudo-rosettes (yellow arrowhead) (**E**, scale bar = 50 µm).

No clear perivascular pseudorosettes were identified, which can be found in a majority of human patients, but also have been reported absent in a number of ependymoma mouse models (Ozawa et al 2018) (Pajtler et al 2019). A potential reason could be that the examined mouse tumours were too recent and small.

To try to address that, a small cohort of LATS1/2 cKO animals was aged to 2 months under strict daily monitoring with regular weighing (All animals were housed with at least one non-mutant animal in the same cage. Mice losing more than 10% of bodyweight (taken from the highest they have been recorded) or showed signs of suffering were sacrificed prior to the experimental endpoint. Ten LATS1/2 cKO animals entered the aging study (from two breeding pairs and four litters in total)).

As expected first signs of neurological deficiency started arising around the age of P14 in double conditional knockout animals. Those symptoms intensified over the

next couple of days and all animals developed a strong head tilt and head flics. Five mice did not make it past P23 due to too much weight loss and showing first signs of distress, besides the expected symptoms (Figure 5.2.A). One further animal was scarified prematurely due to a sudden weight loss by the age of P40. Four animals made it to two months of age. Those animals had vivid eyes, a shiny fur and no lack of hydration nor hunched posture was observed at any point.

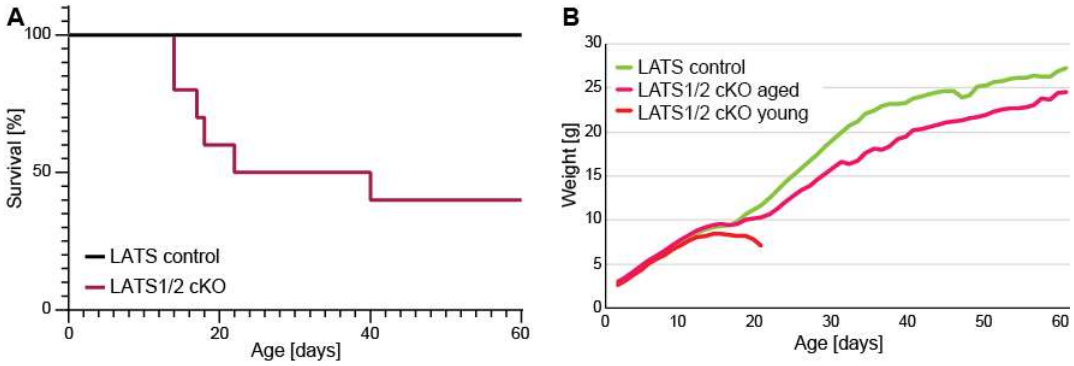

Figure 5.2. LATS1/2 cKO animals demonstrate reduced survival and lower weight.

A. LATS1/2 cKO animals (n = 10) part of the two-month aging cohort showed again a reduced survival rate of double mutant animals compared to control mice (n = 6). **B**. Double floxed animals showed a reduced weight compared to litter mate controls (n = 6) and could be split into two groups differentiated by early weight drop (LATS1/2 cKO young, n = 5) and those able to be kept beyond three weeks of age (LATS1/2 cKO aged, n = 5). Trend line of weight progression is shown.

As a result of the continued weighing regime described above, the LATS1/2 cKO animals could be grouped into two cohorts: One group of mutant animals lost too much body weight by the age of three weeks and had to be collected prematurely (Figure 5.2.B). The second cohort was able to gain weight and consistently stayed at a lower weight when compared to their non-mutant littermates. Besides the expected symptoms of spinning and/or balance issues, we did not observe any signs of distress. The difference could be due to the size and exact location of the tumours as this has been noted before in this study, when focusing on the P20 animals.

Three brains of the two-month LATS1/2 cKO were examined after processing and H&E staining, but no pseudorosettes could be found at this time point. All had tumours in the lateral ventricles, which were morphologically very similar to the tumours at P20, apart from being a bit bigger in two out of the three mice observed when compared to the P20 brains. One animal showed a bilateral mass in the IV

ventricle going through the Luschka foramen, looking very similar to a human ependymoma. From this experiment we concluded that the lack of pseudorosettes is unlikely to be due to the tumours being very recent. It is more likely that the difference arises from species differences.

5.1.2 Tumours in LATS1/2 cKO animals are positive for markers found in human ependymoma

In addition to the H&E stainings done on the P20 brain sections, we performed further stainings to draw a better comparison with human patients (Figure 5.3). Cells within the tumour showed clear nuclear and at lesser extent cytoplasmic YAP1 expression. They weakly express MUC1 (EMA) and exhibit focal positivity for GFAP. Furthermore, cytokeratin 18, Nestin and Vimentin which are present in radial glial cells are also found in the tumour as seen before with immunofluorescence staining. The neuronal marker NeuN is yet again consistently negative in the tumour mass. The proliferative marker Ki67 was found expressed in the tumour indicating active cell division. In collaboration with Dr Federico Roncaroli it was concluded that the light microscopic features and the immunoprofile of the LATS1/2 cKO tumours showed strong parallels to human ependymoma (CRUZ–SANCHEZ et al 1988) (Vege et al 2000) (Hasselblatt & Paulus 2003). The histological presentation of the tumours, such as distinct location and compressive margin taken together with the stainings, in particular cytokeratin 18 and MUC1 lead to this interpretation.

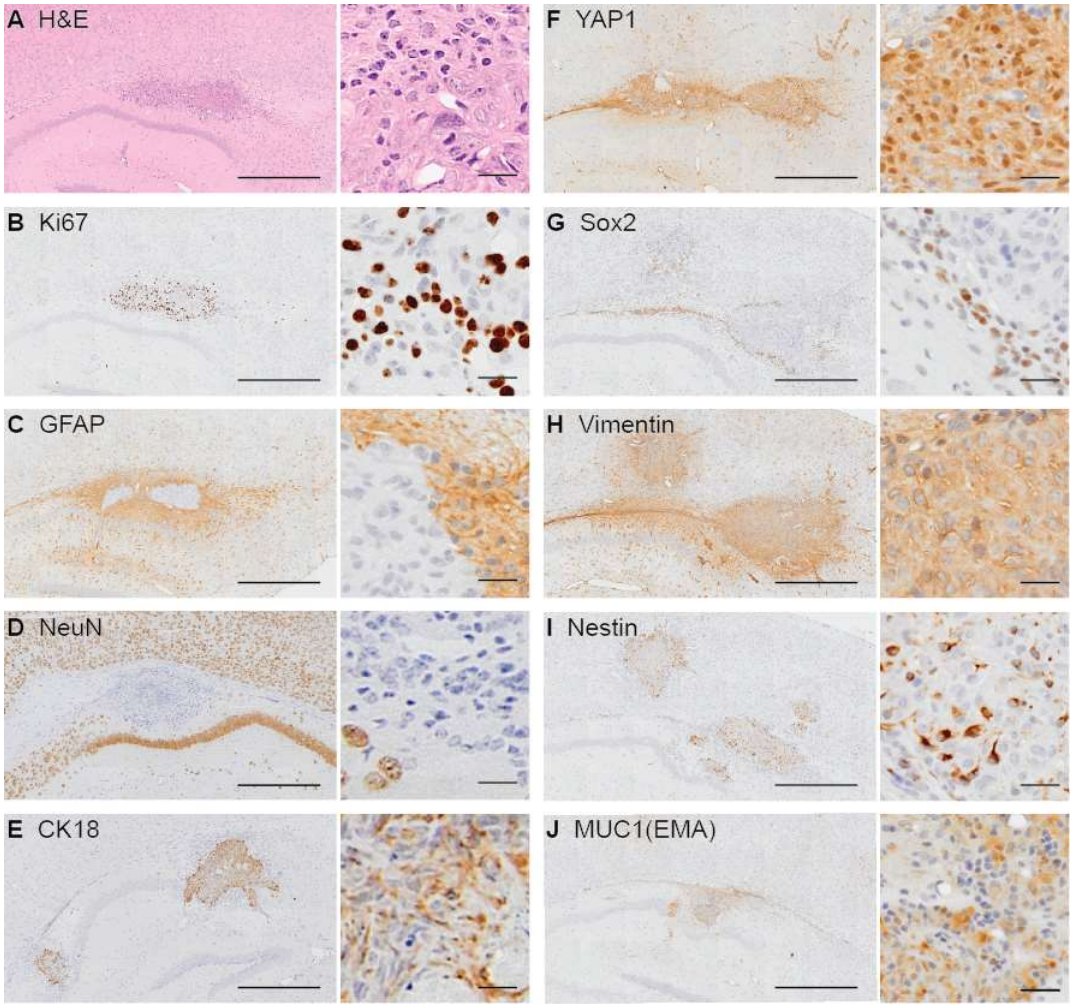

Figure 5.3. LATS1/2 cKO immunohistochemistry profile.

A-C & **F-J** are serial sections through the same brain tumour while **D** and **E** are taken from different brains. Actively dividing cells are present (Ki67, **B**). Tumours are focally positive for GFAP (**C**) and reactive astrocytes surrounding the lesion are also GFAP-positive. NeuN (**D**) is absent from the tumour while cytokeratin 18 (CK18, **E**) shows strong positive expression. YAP1 (**F**) can be found to be nuclear and cytoplasmic in the tumour and SOX2 (**G**) showed to present in the boarder of the tumour. Vimentin (**H**) and Nestin (**I**) show strong positive staining while weak cytoplasmic expression of MUC1 (EMA, **J**) could be found in the dysplasia. GFAP, CK18, YAP1, SOX2, Vimentin, Nestin and MUC1 showed expression to similar levels as in the ependymal layer of those animals. Scale bars, overview = 500 µm, detail = 30 µm.

Notably, the ependymal layer in the murine brain also showed clear positive staining for cytokeratin 18 as previously shown (Figure 5.4) (Miettinen et al 1986).

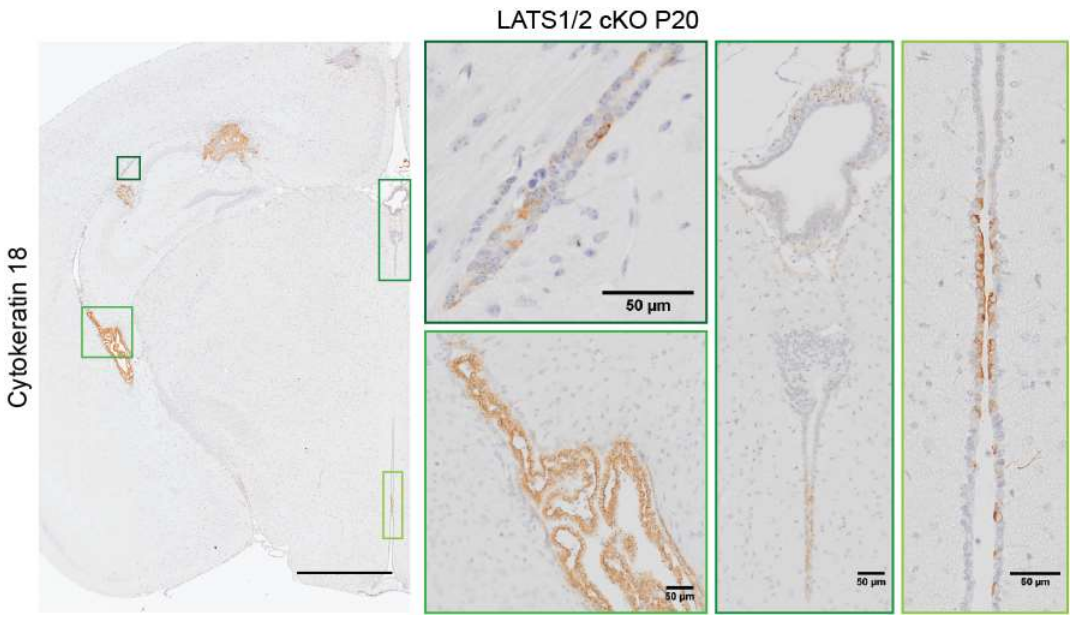

Figure 5.4. Cytokeratin 18 expressed in the normal ependymal layer.

IHC stained P20 LATS1/2 cKO brain with cytokeratin 18 demonstrating positive staining in various ependymal layer across the brain. Scale bars overview = 1 mm, close ups = 50 µm

5.1.3 Ultrastructure pathology of LATS1/2 deleted tumours shows microvilli and tight junctions which are diagnostic features in human ependymoma

To further test the hypotheses that the murine tumours resemble human ependymoma, the tissue was investigated in its ultrastructure. Electron microscopy is an important diagnostic method to identify fine structures and differentiate tumours in particular when light microscopy shows atypical features (Baloyannis & Baloyannis 2014).

Therefore, the murine tumours were further characterised by 3D electron microscopy. The electron microscopic images were taken by Marie-Charlotte Dolmart. We focused on two relatively small tumours adjacent to the ependymal region to be able to capture the whole tumour with the maximum scan space on the instrument. First the areas of the tumours were identified using micro-computed tomography (micro-CT) by comparing to the DAPI fluorescent image of the consecutive section of the brain (Figure 5.5.A, B). Next, we inspected multiple regions of the tumours using serial blockface scanning electron microscopy (SBF

SEM). It could be observed that both tumours exhibit a clear boarder defined by darker contrast of the tumour cells compared to the surrounding cells (Figure 5.5.C).

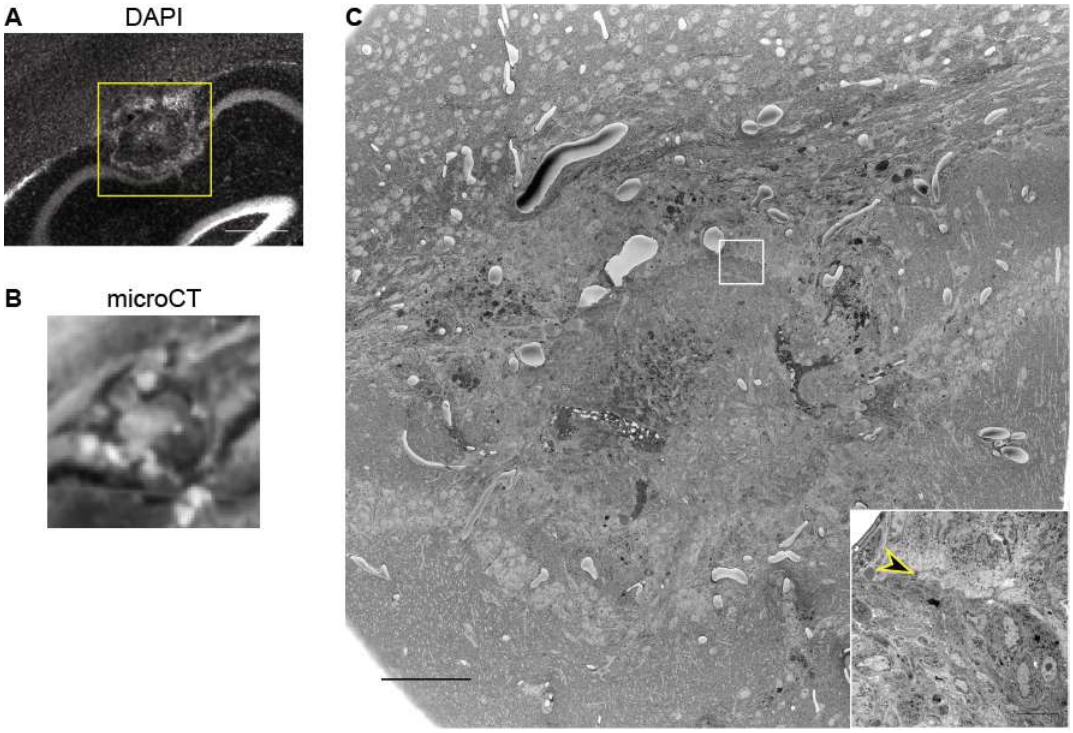

Figure 5.5. EM on murine tumour overview and boarder.

A. DAPI stained vibratome section and consecutive section used for ultrastructural analysis shown in MicroCT (**B**). Yellow square containing tumour indicates area taken for SEM. Scale bar = 500 µm. **C**. Overview of tumour are using SEM. Close-up shows contrast difference at boarder of tumour it it`s surrounding. Scale bar = 100 µm.

One of investigated tumours was at the boarder of a normal appearing ependymal lining of the lateral ventricle (Figure 5.6). This area was examined further as a reference to normal ependymal. As expected for ependymal cells, the cells showed tight junctions, cilia and microvilli.

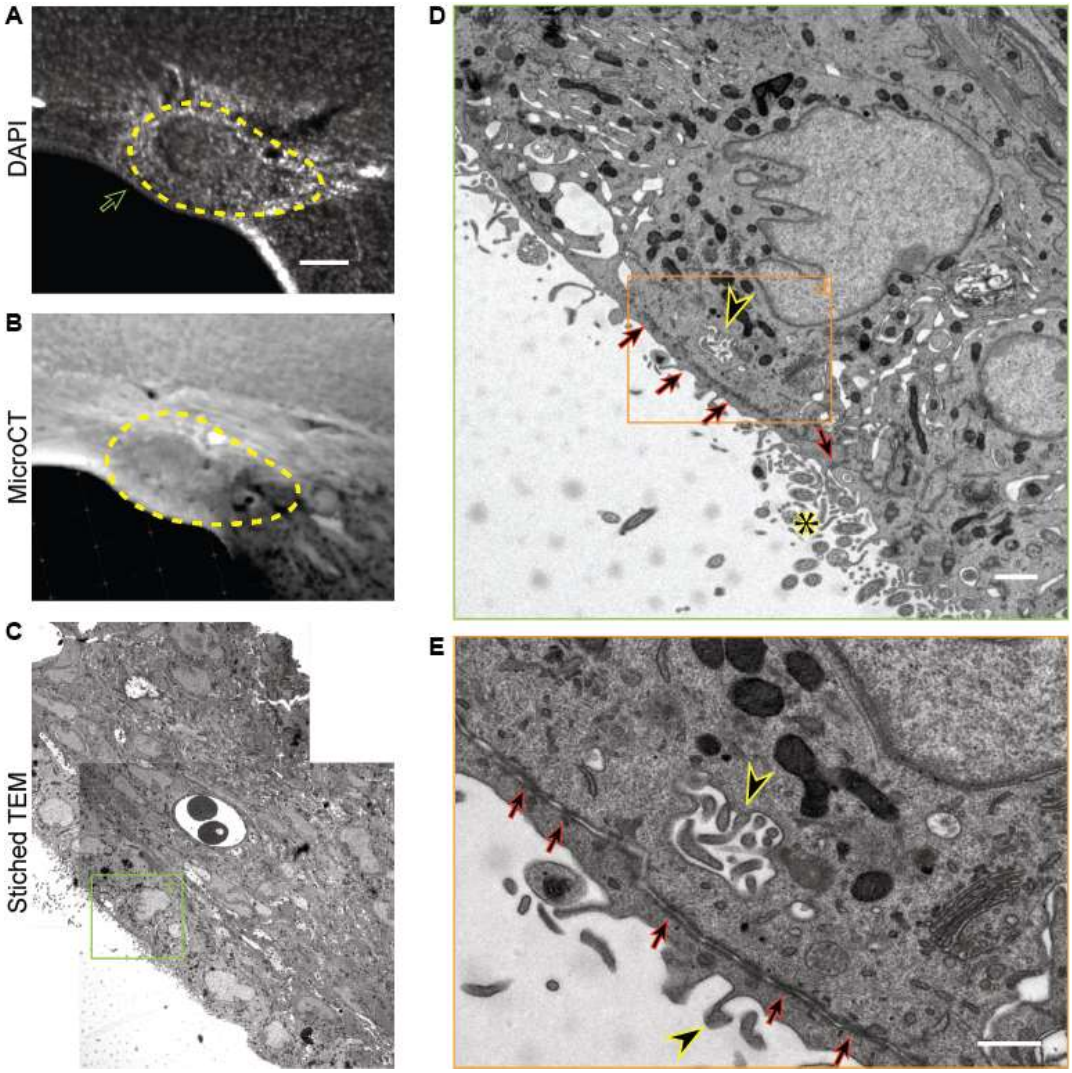

Figure 5.6. EM of normal murine ependymal layer neighbouring LATS1/2 cKO tumour.

A. DAPI stained vibratome section and consecutive section used for TEM shown in MicroCT (**B**). Yellow dashed line circling LATS1/2 cKO tumour, green arrow pointing at location of zoom in of following images. Scale bar = 500 µm. **C**. Stitched overview of tumour neighbouring ependymal layer appearing normal. Indication imaged region of interest shown in **D**. TEM 6000x of ependymal layer. Red arrows = tight junctions, yellow arrowhead = microvilli. Yellow asterisk = cilia; scale bar = 1 µm. **E**. TEM 26500x, higher magnification of microvilli (yellow arrowhead) which appear intracytoplasmatic due to membrane fold. Red arrow = tight junctions; scale bar = 0.5 µm.

Inside the tumours, in a selection of 13 regions of interest throughout the 3D volume of both tumours, microvilli and tight junctions could be found throughout (Figure 5.7). Their presence was confirmed by transmission electron microscopy (TEM). Such tight junctions and microvilli are well-known characteristics of the ependymal cells, and examples of these can be seen in unaffected areas of the ventricles (Figure 5.6).

Microvilli and tight junctions are common features associated with ependymoma (Soriano-Navarro et al 2015), a distinguishing property from other brain tumours. These findings strongly suggest that YAP1 miss-regulation and activation causes mouse brain tumours with striking characteristics of a human ependymoma.

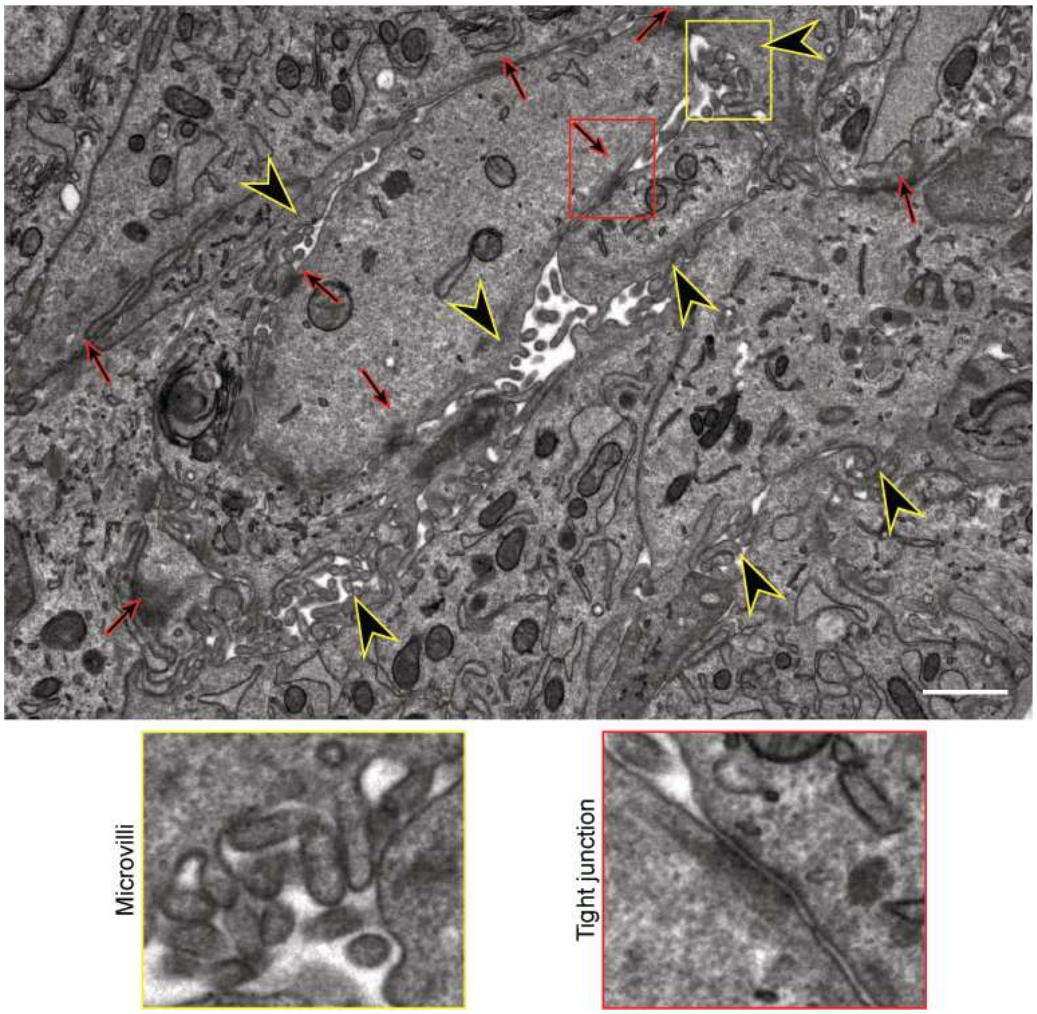

Figure 5.7. EM on murine LATS1/2 cKO tumour showing ependymoma features.

TEM 9900x, red arrow = tight junctions, yellow arrowhead = microvilli. Close up to two areas containing microvilli (yellow square) and tight junction (red square). Scale bar = 1 μm.

5.2 Multi-omic analysis of murine tumours

To get a better understating of the network of changes within tumours, taking a more discovery approach, the total levels and changes of RNA and protein were investigated. Five nlsYAP5SA mice (*Nex$^{Cre/+}$; Yap1$^{nlsYAP5SA/+}$*) and five unaffected littermates (*Nex$^{+/+}$; Yap1$^{nlsYAP5SA/+}$*) were used. Additionally, three non-littermate C57BL/6 control mice were included for RNA sequencing, but not the Mass spectrometry screen (Figure 5.8).

This mouse model was chosen for multiple reasons. One major factor was, that the isolation of LATS1/2 cKO clonal tumours would have been technical challenging, but more importantly there would be difficulty of obtaining control tissue as ideally this would be ependymal cells. Moreover, running the risk of not obtaining sufficient material for the assays, which would have been to be compensated with increasing the animal number. Not isolating those tumours would have most likely lead to altered levels disappearing in the background noise. The nlsYAP5SA provided the advantage of simplifying the tissue harvest procedure which additionally reduced the tissue handling prior to stabilisation to a minimum and consequently reduced potential degradation and risk of loss of material substantially. Furthermore, it allowed to take a global view on the changes happening in the brain and resolved the issue of obtaining appropriate control tissue.

The brains of the mice were divided into three parts excluding the olfactory bubs and most of the brain stem. The right hemispheres and the cerebellums were subject to sequencing, while the left hemispheres were processed for proteomics analysis. The library preparation and the RNA Sequencing on the Illumina HiSeq 4000 was performed by the Advanced Sequencing Facility at the Francis Crick Institute. The workflow is shown in figure and explained further in the material and methods section (page 40).

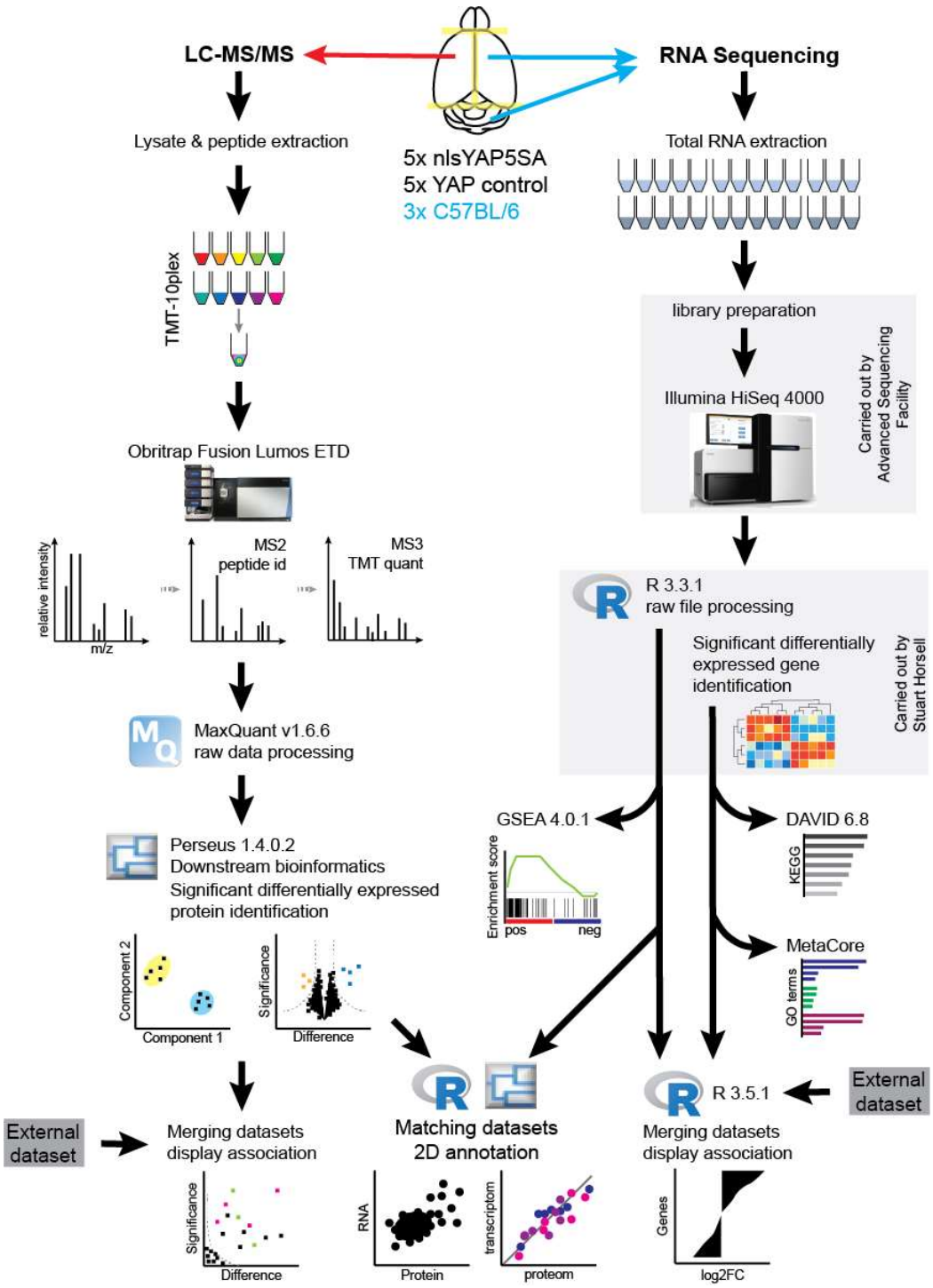

Figure 5.8. Proteomics and sequencing workflow of nlsYAP5SA and YAP control brain tissue samples.

5.2.1 Total RNA sequencing of nlsYAP5Sanls brains demonstrate parallels to human YAP1-fusion supratentorial ependymoma

The right hemisphere samples and the cerebellum samples were processed in parallel and analysed separately. In both regions the C57BL/6 controls clustered as expected with the YAP controls. Of the total 48,795 identifiable genes, 30,280 were detected in the hemisphere samples and 30,960 in the cerebellum. Comparing the YAP controls with the nlsYAP5SA brain regions showed a high number in significantly differentially expressed genes (DEGs) of 2,035 for the hemisphere and 8,253 for the cerebellum (Figure 5.9.A,C). The significantly DEGs lists were generated by Stuart Horswell using the DESeq2 R package applying the Wald significance test with a threshold of 0.05 for significance. Additionally, comparing the YAP control with the C57BL/6 samples led to a far smaller list in significantly DEGs, 57 and 152 in the hemisphere and the cerebellum samples (Figure 5.9.B,D), respectively. This showed that the YAP control animals were not much different to their original background line.

Since the hemisphere is a collection of multiple brain region with an array of different specialised cells, the subtle expression changes in the tumours might be diluted leading to the reduced number of significantly changed mRNA levels detected. The two gene lists from the two different brain areas overlapped in a total of 1,664 being significantly differentially expressed in both (Figure 5.9.E). For further analysis, the right hemisphere gene list was taken forward as most comparable to the samples taken for proteomics screening.

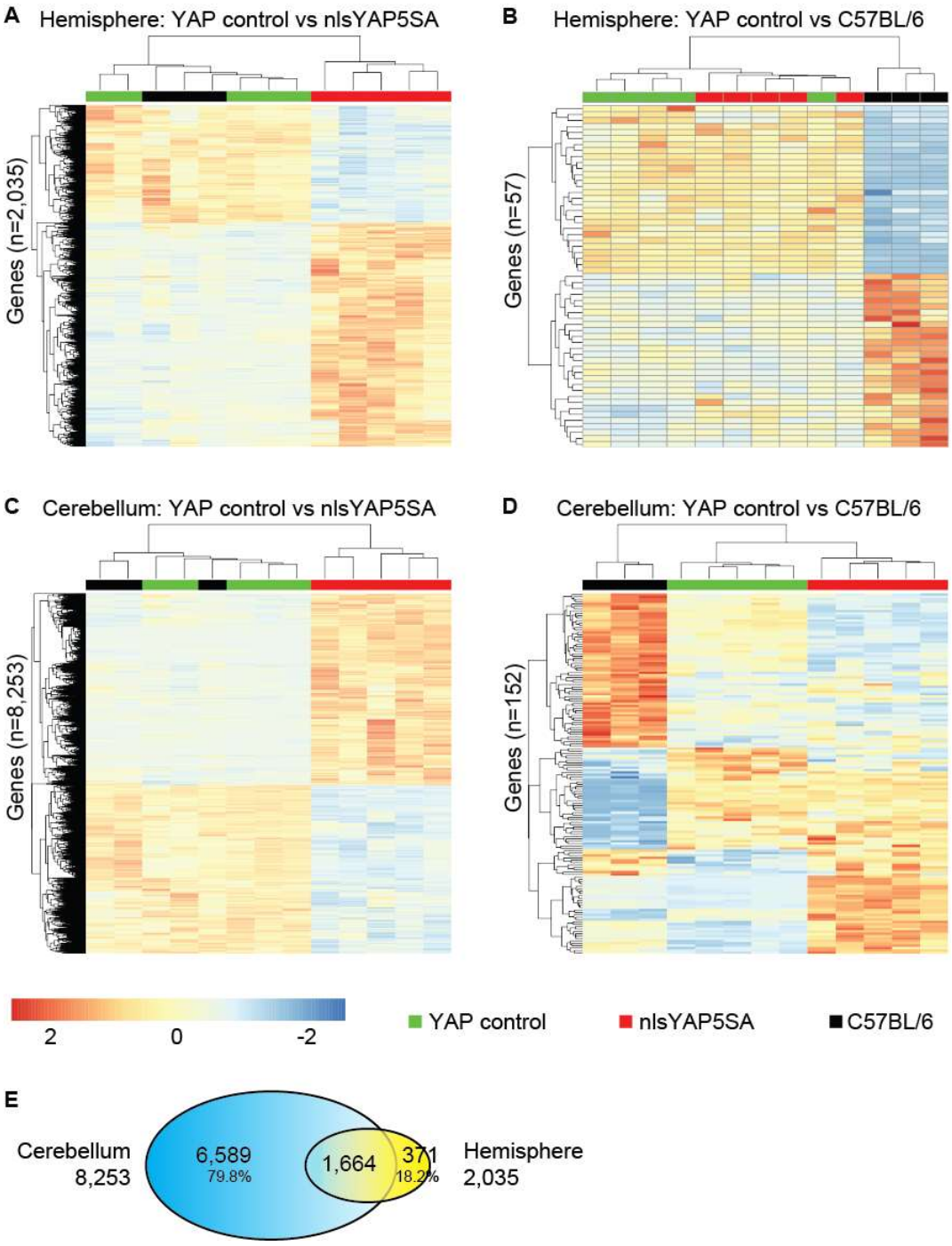

Figure 5.9. YAP control animals and nlsYAP5SA samples build two distinct gene expression clusters.

Gene expression analysis for YAP controls versus nlsYAP5SA in which 13 animals (5x YAP control = *NEX*$^{+/+}$ *YAP1*$^{nlsYAP5SA/+}$; 5x nlsYAP5SA = *NEX*$^{Cre/+}$ *YAP1*$^{nlsYAP5SA/+}$ and three C57BL/6) were analysed utilising the Illumina HiSeq 4000. **A-D**. heat maps displaying significantly differentially expressed genes when two groups are compared and the third group is displayed, but not part of the individual comparison to display clustering. **A** & **C**. Per brain region comparison

of YAP control versus nlsYAP5SA brains resulting in 2,035 and 8,253 significantly differentially expressed genes (DEGs) in the hemisphere and the cerebellum samples respectively. C57BL/6 gene expression profile of those genes fits within the YAP control cluster in both cases. **B** & **D**. A comparison of YAP control versus C57BL/6 samples lead to a low number in significantly DEGs. **E**. Overlapping the significantly DEGs lists of YAP controls vs nlsYAP5SA shows 1,664 genes are significantly altered in their expression in both investigated brain areas.

Based on their differential measured levels in nlsYAP5SA and littermate control animals in the hemisphere samples all 30,280 identified RNAs were ranked. Subsequently, we performed a gene enrichment analysis (GSEA) with the Kyoto Encyclopedia of Genes and Genomes (KEGG) database to detect gene sets that are overrepresented at either end of the ranked list. The top 10 upregulated gene groups found in nlsYAP5SA include “Pathways in Cancer”, “Cytokine Receptor Interaction” and “Focal Adhesion” (Figure 5.10.A). Those are in line with YAP1`s ability for cancer induction and resulting immune response. One of the most down regulated KEGG annotation in nlsYAP5SA showed to be “Oxidative Phosphorylation” (Figure 5.10.B), which could indicate changes in the energy metabolism of the tumours.

A

KEGG Name (positive Top10)	NES	Size
Pathways in Cancer	4.996	311
Cytokine Receptor Interaction	4.813	207
Toll Like Receptor Signaling Pathway	4.508	87
Focal Adhesion	4.356	196
Ecm Receptor Interaction	4.221	83
Tgf Beta Signaling Pathway	4.183	84
Lysosome	4.077	118
Jak Stat Signaling Pathway	3.897	124
Leishmania Infection	3.672	52
Leukocyte Transendothelial Migration	3.409	111

B

KEGG Name (negative Top10)	NES	Size
Parkinsons Disease	-7.169	107
Oxidative Phosphorylation	-7.133	109
Huntingtons Disease	-5.818	154
Alzheimers Disease	-5.724	145
Ribosome	-4.540	82
Citrate Cycle Tca Cycle	-3.353	28
Cardiac Muscle Contraction	-2.905	74
Steroid Biosynthesis	-2.820	16
Axon Guidance	-2.704	127
Proteasome	-2.672	43

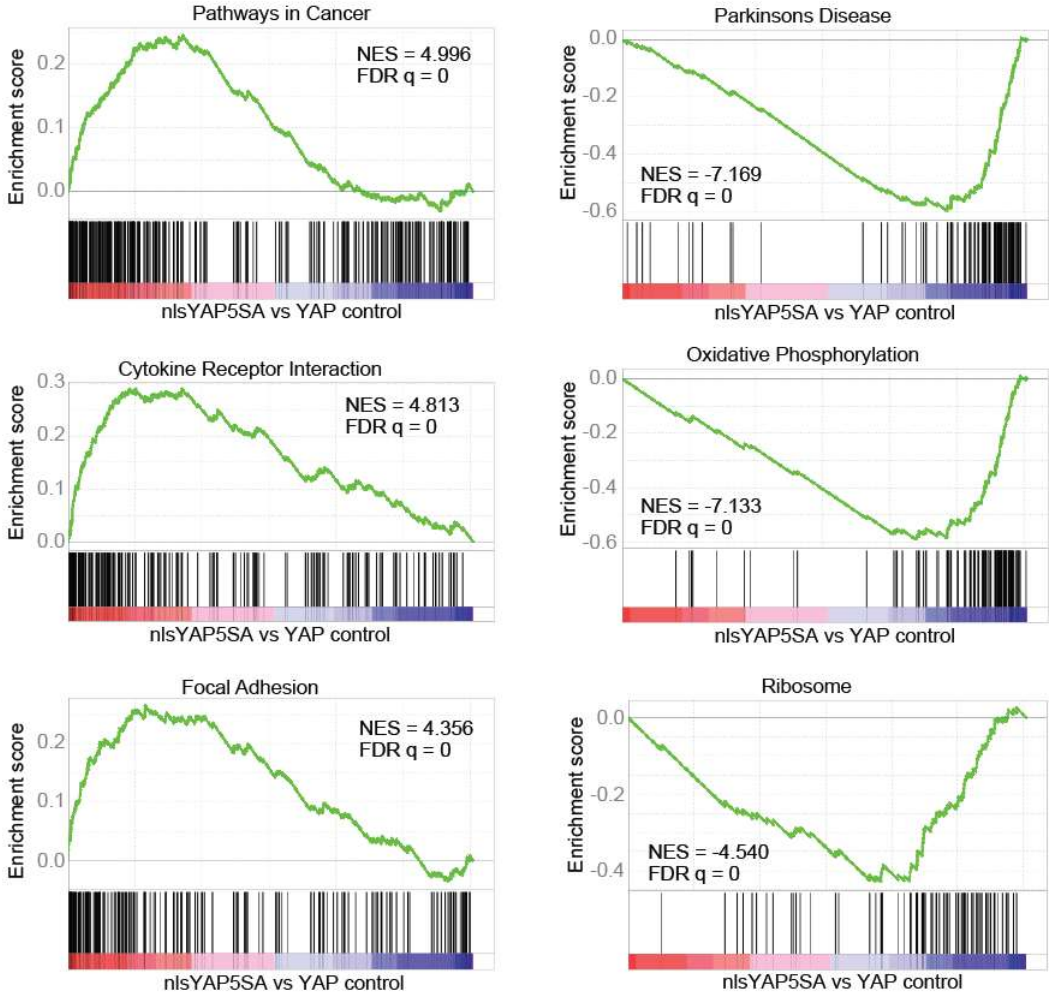

Figure 5.10. Gene enrichment analysis (GSEA) of YAP control vs nlsYAP5SA hemisphere samples.

A. The 10 most enriched gene groups ranked by NES (normalised enrichment score) and amount of associated genes found in the dataset (Size) are shown. **B**. The 10 most reduced gene groups ranked by NES and amount of associated genes found in the dataset (Size) are shown Three example blots are shown each

In a complementary analysis, the 2,035 significantly DEGs (1,335 up and 700 down regulated) in the right hemisphere between the two genotypes were evaluated using the online tool DAVID (v6.8). Focusing on the KEGG defined gene sets one of the most significantly differentially regulated found gene sets was “Hippo Signalling Pathway” (Figure 5.11.A). Additionally, multiple gene groups concerning immune and infection related genes came up. Moreover, looking at an individual gene level several known YAP1 downstream targets (Wang et al 2018) were found to be significantly increase in nlsYAP5SA animals at mRNA level, including AMOTL2, CTGF, CYR61, ANKRD1 and AXL. Neurod6 (NEX) was found to be amongst the most downregulated genes.

Another online tool, MetaCore (version 19.3.69800), was used for Gene Ontology (GO) term enrichment. Again the significantly DEGs list was uploaded. Across the three GO categories (Biological Process, Molecular Function, Cellular Component) all included terms associated with neuronal/brain activity and development being amongst the most down regulated, such as “modulation of chemical synaptic transmission”, “nervous system development”, “neuron projection” and multiple channel activities (Figure 5.11.B). On the upregulated side, we could found again immune related terms “immune system process” and multiple extracellular referring terms.

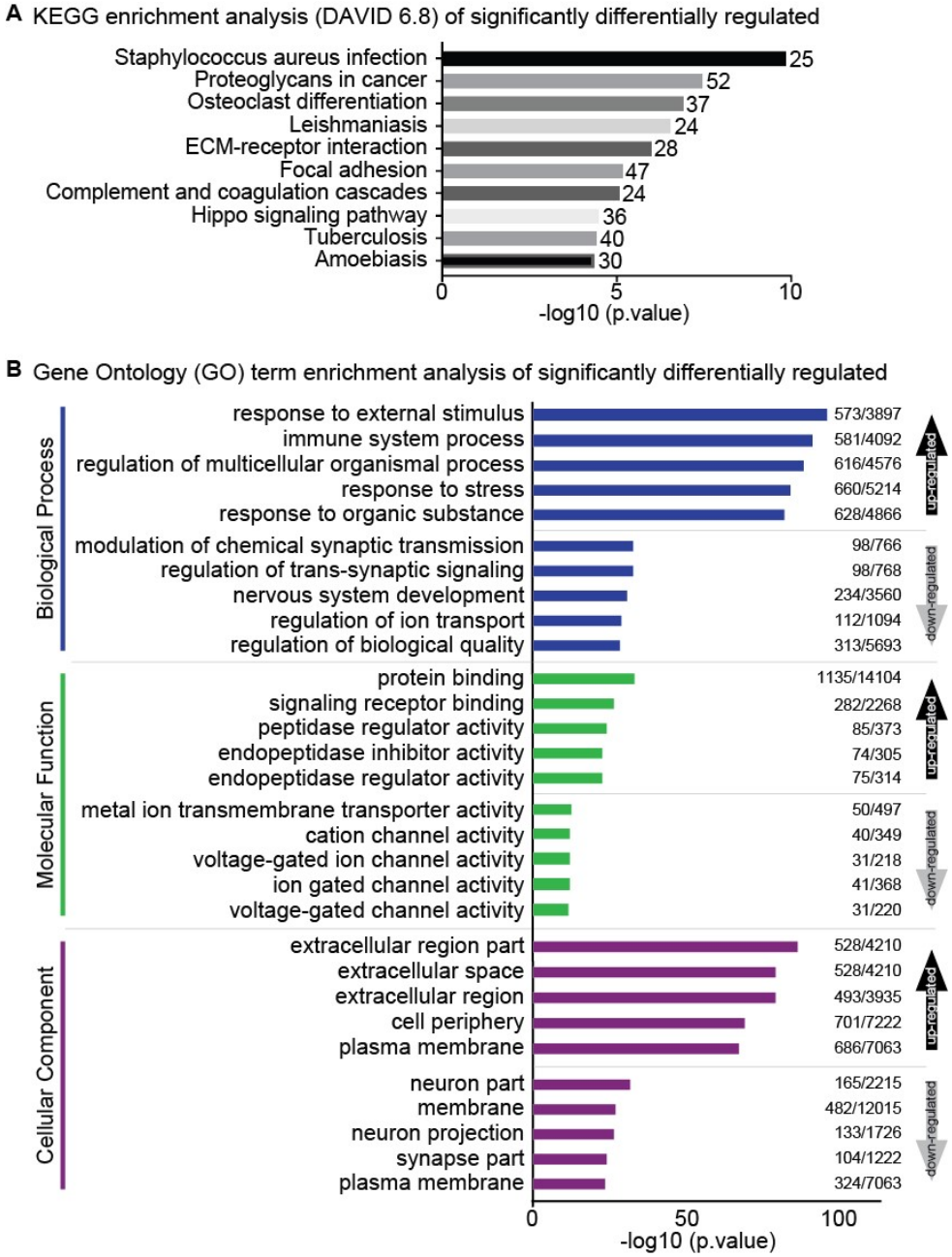

Figure 5.11. Annotation enrichment analysis on significantly DEGs.

A. KEGG enrichment analysis utilizing online tool DAVID 6.8 uploading significantly DEGs in hemisphere samples (1,979 of the 2,035 submitted genes were ID`ed). Top ten KEGG annotations, sorted by significance, are displayed including count of genes associated with each category within the submitted gene list. **B**. Gene Ontology (GO) enrichment analysis performed with the online tool MetaCore (version 19.3.69800) uploading significantly DEGs of hemisphere samples. Top five up- and down-regulated GO annotations terms are shown for Biological Process, Molecular Function and Cellular Component, ranked by p-value. Numbers indicate how many genes have been found in the submitted gene list compared to the total number of genes associated with this GO term within MetaCore.

Subsequently, we investigated how the gene expression profile found in the nlsYAP5SA mouse model compared to available published gene expression data from human ependymoma subtypes. A recent published study generated molecular signature list of genes associated with either the ST-EPN-YAP1 or the ST-EPN-RELA subtype (Pajtler et al 2019). To do so, they performed a comparative transcriptome profile analysis between the two subtypes including samples from both human patients and a mouse model (YAP1-MAMLD1 fusion and C11orf95-RELA driven) per subtype (Pajtler et al 2015) (Pajtler et al 2019). This list includes 354 unique genes of which 151 had a YAP1 association tag and the remaining 203 have been associated with the RELA subtype. 350 of those genes were present in our full nlsYAP15SA transcriptome dataset when matched by gene name. Those genes were ranked according to the fold change in nlsYAP15SA compared to YAP control mice. It could be shown that RELA fusion associated genes are almost equally distributed across the up and down regulated genes in the nlsYAP5SA model (Figure 5.12.B) (46% up and 54% down of total RELA fusion associated genes). However, genes that have been marked to be specific for the YAP1 fusion subtype showed to be clearly overrepresented in the upregulated side of the fold change (Figure 5.12.A) (78% up and 33% down of total YAP1 fusion associated genes).

We performed a second, further restricted, analysis only accepting genes that are significantly differentially expressed in the nlsYAP5SA model. Out of the 354 reported genes, 89 were found in the nlsYAP5SA significantly DEG list when matched by gene name. The pattern in this analysis was even more striking with 98% (45/46) YAP1 fusion specific genes upregulated in nlsYAP5SA animals (Figure 5.12.D). In comparison 20 out of the 43 (46%) RELA fusion associated genes were increased and 23 showed to be reduced in nlsYAP5SA animals. In both analysis YAP1-fusion associated genes dominated the top of the list as measured with higher log2 fold changes (Figure 5.12.C).

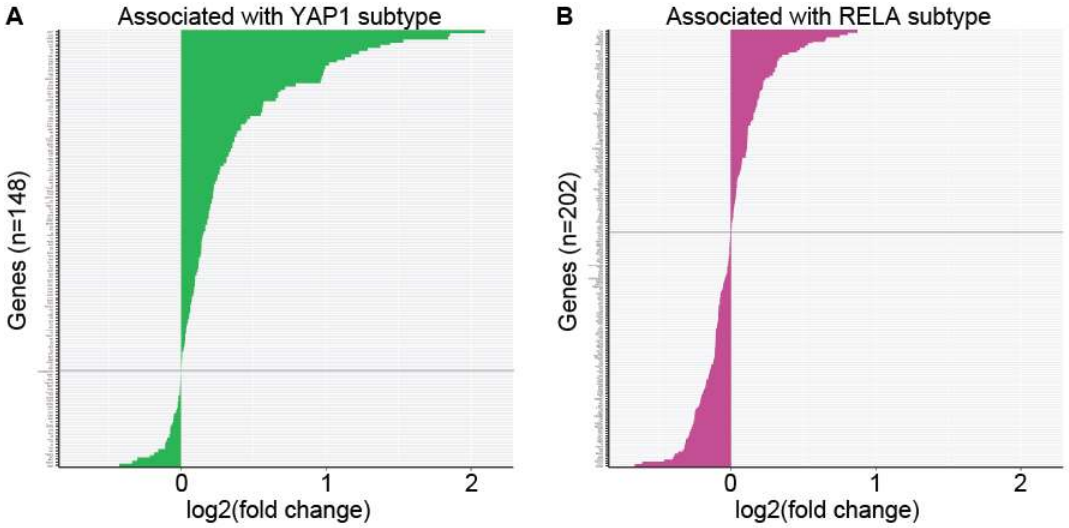

C

rank	Gene	log2 FC	Status
1	Ankrd1	2.10	YAP1 specific
2	Cyr61	1.86	YAP1 specific
3	Prss23	1.84	YAP1 specific
4	Col8a2	1.53	YAP1 specific
5	Ajuba	1.44	YAP1 specific
6	Npr3	1.38	YAP1 specific
7	Ctgf	1.29	YAP1 specific
8	Krt7	1.23	YAP1 specific
9	C5ar1	1.17	YAP1 specific
10	Krt18	1.13	YAP1 specific

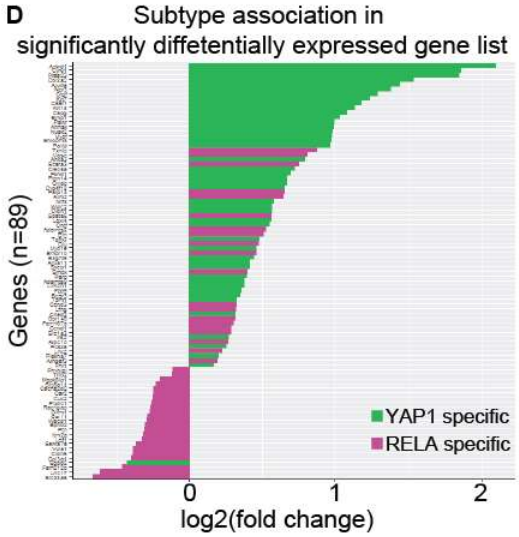

Figure 5.12. Dataset shows enrichment for YAP1-fusion ependymoma associated genes.

A published gene list of YAP1 and RELA association by Pajtler *et al* (Pajtler et al 2019) was used to assign specificity to detected genes in the RNA expression data from the nlsYAP5SA sequencing screen. **A-C**. 350 genes of the 354 in reference list were present in the full gene list of the hemisphere samples. Log2 fold change measured in YAP control vs. nlsYAP5SA were ranked from highest to lowest. **A**. Of the 148 YAP1-fusion ependymoma associated genes, 115 were increased in the nlsYAP5SA mice. **B**. Whereas, RELA-fusion specific genes were almost equally distributed. **C**. The 10 highest ranked genes all show to be associated with the YAP1-fusion ependymoma subtype. **D**. If the significantly DEG list was taken, 89 out of the 354 in the reference list could be matched, of which 46 showed YAP1 and 43 RELA association. All but one YAP1 fusion specified gene (green) were significantly upregulated in the nlsYAP5SA mice. RELA association (purple) showed again an equal distribution of genes being either up (20) or down (23) regulated.

These figures demonstrate that the proportion of YAP1 associated genes that are found increased in the nlsYAP5SA mice are much higher than the proportion of RELA fusion specific genes ($p < 0.0001$, Chi squared test). This shows that the YAP1-MAMLD1 fusion gene associated signature is present in the nlsYAP5SA mouse model. Among the 18 genes with the highest expression changes in nlsYAP5SA are numerous known YAP1 downstream targets such as *Ankrd1, Cyr61* and *Ctgf* (Wang et al 2018). Notably, cytokeratin 18 which was found expressed in the ependymal layer and in the LATS1/2 cKO tumours, was among the top 10 increased YAP1 associated genes in the nlsYAP5SA brains. These results support that the expression of nlsYAP5SA in neuronal precursor cells leads to a gene expression profile resembling human YAP1-MAMLD1 fusion ependymoma.

5.2.2 Full proteome analysis of nlsYAP5Sanls brains exhibits good correlation with transcriptomic analysis

To investigate further which changes observed in the total mRNA screen translate into protein level changes, a full proteome screen was performed. From the same five nlsYAP5SA mice and the five control litter mates brains the transcriptomic screen was performed on, the proteomics analysis was done on their left hemisphere (Figure 5.8). Therefore, the samples were labelled with a TMT (Tandem Mass Tag) 10-plex kit enabling relative quantitative analysis. A total of 6,643 proteins was identified and the principal component analysis (PCA), in particular component 1, showed two clearly separated clusters of the samples representing the two different genotypes (Figure 5.13).

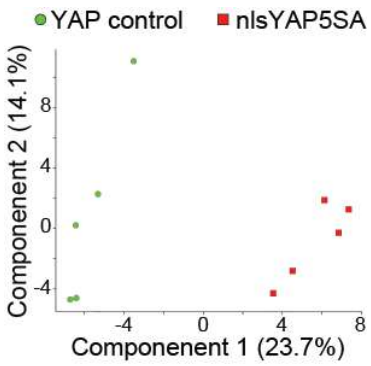

Figure 5.13. PCA of full proteome shows clear separation according to genotype.
Principal component analysis (PCA) was performed on proteomics dataset acquired from a 10plex TMT Mass spectrometry analysis including five nlsYAP5SA and five YAP control animals. A clear clustering of the two different genotypes can be seen.

To get a global view on changes we investigated if the identified proteins can be associated with particular cell types in the brain. For this, the proteomics dataset was overlaid with an existing full proteomics dataset on central nervous system cell types (Sharma et al 2015). The dataset from Sharma *et al* included the full proteome of four CNS cell types (astrocytes, microglia, neurons and oligodendrocytes) directly isolated from the mouse brain and analysed as well as a dataset of cells cultured before proteomic analysis. Cell type association of a protein to a particular cell type was defined by the expression value (reported by Sharma K. *et al*) being a minimum of 3 in one of the four isolated cell types and the value with at least double in one of the cell types compared to any of the other three. Within the nlsYAP5SA compared to control littermates dataset an increase in microglia and astrocyte associated proteins could be observed indicating a microglial response (Figure 5.14). Among the upregulated proteins C1qa, C1qb, C1qc and C4b, complement cascade proteins, could be found (Figure 5.15) which is in agreement with the KEGG enrichment analysis performed on the transcriptome dataset pointing towards increased immune response components (Figure 5.11.A). Simultaneously, significantly decreased proteins in tumour bearing mice were associated more with neurons and oligodendrocytes.

Also YAP1, GFAP and Vimentin, which been identified via immunofluorescence to be highly enriched in the tumours could be found significantly upregulated in the proteomics dataset (Figure 5.15). Significantly differentially measured protein levels

were determined by Welch difference test (two sided t-test) in the software Perseus with threshold set to FDR = 0.05 and s0 = 0.1.

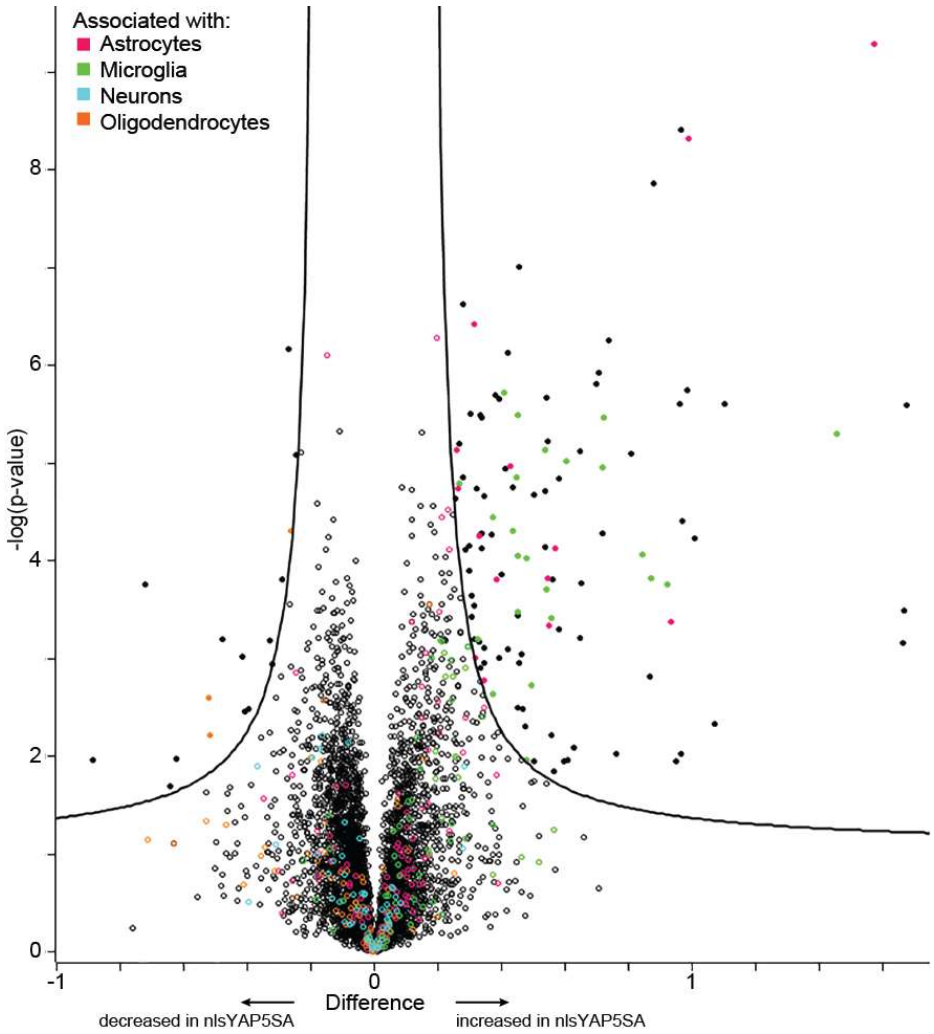

Figure 5.14. Volcano plot of proteomics dataset shows significant enrichment of astrocyte and microglia associated proteins.

Protein expression in nlsYAP5SA mouse brains compared to YAP control animals. Cell type enriched proteins for astrocytes (magenta), microglia (green), neurons (cyan) or oligodendrocytes (orange). CNS cell type association was defined by incorporating data published by Sharma *et al* (Sharma et al 2015). In short, association of a protein was defined by the expression value reported of at least 3 in one of the four cell types and the maximum value had to be at least double in one compared to the other three cell types. Each circle represents one protein and significantly different measured proteins are shown in filled circles. Significance is displayed by the black line defined by a two sided Welch t-test (FDR = 0.05, s0 = 0.1). The X-axis, showing log2 transformed fold change, has been locked to [-1,1.75] excluding the display of one protein, eliminating Eif2s3y, a Y-linked protein, enriched due to the mixed gender of experimental animals.

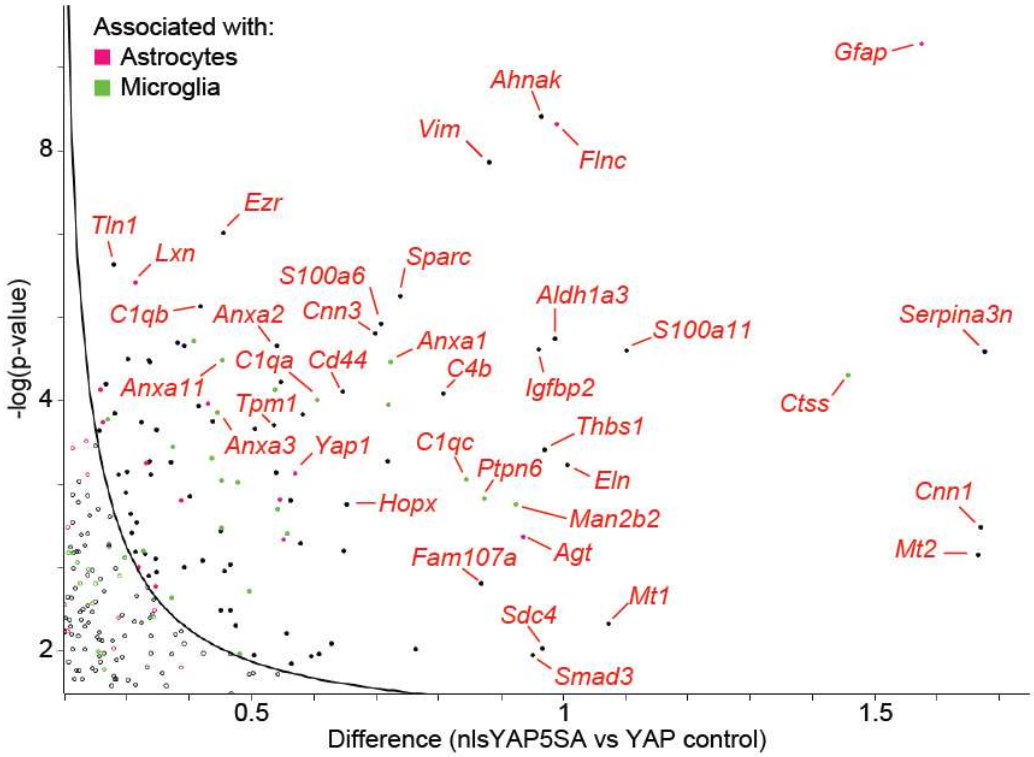

Figure 5.15. Significantly upregulated proteins in nlsYAP5SA confirm previous found enriched proteins.

Enlarged area of the volcano plot shown in Figure 5.14 to display and name significantly upregulated proteins identified in the nlsYAP5Sa brains.

Ependymal cells were not part of the screened CNS cells in the dataset provided by Sharma *et al*, we next investigated if proteins without cell type association can be associated with the tumours. Of the 129 significantly differentially expressed proteins in the nlsYAP5SA animals 113 were increased and 16 were decreased in nlsYAP5SA brains (Figure 5.16). In this analysis a slightly less stringent cell type association cut-off was chosen: The expression value had to be at least double in one cell type compared to the others, but the minimum value was dismissed. This resulted in 31 proteins linked to astrocytes, 40 with microglia, 12 with neurons and 7 with oligodendrocytes. Again, demonstrating an increase in microglial and astrocytic response seen in the global approach. In the next step the cultured CNS dataset provided by Sharma *et al* was taken into account for cell type association (same less stringed cut offs as used before) to further filter the remaining 23 proteins. This led to a total of 10 unassociated proteins which remained not associated to any particular

CNS cell type or even detected in the other dataset. Seven of those proteins could be, after literature review, associated with extra cellular matrix. This could be a reason that they were not detected in the Sharma *et al* dataset, as their isolated or cultured cell types have been analysed, stripped of the extra cellular matrix. The three remaining proteins were HOPX, IFITM2 and TPM1. Upon closer inspection, TPM1 showed to be expressed in all CNS cell types, just not specific for one and therefore less of an interest. The other two were not detected in the CNS dataset. IFITM2 was found to have only a MS/MS count of 1, a Score of 2.3923 and 1 unique peptide with 12.5% sequence coverage. In comparison HOPX had better overall scores (MS/MS count = 8, Score = 146.15, 3 unique peptides with 74% sequence coverage), making it the first choice candidate to follow up on.

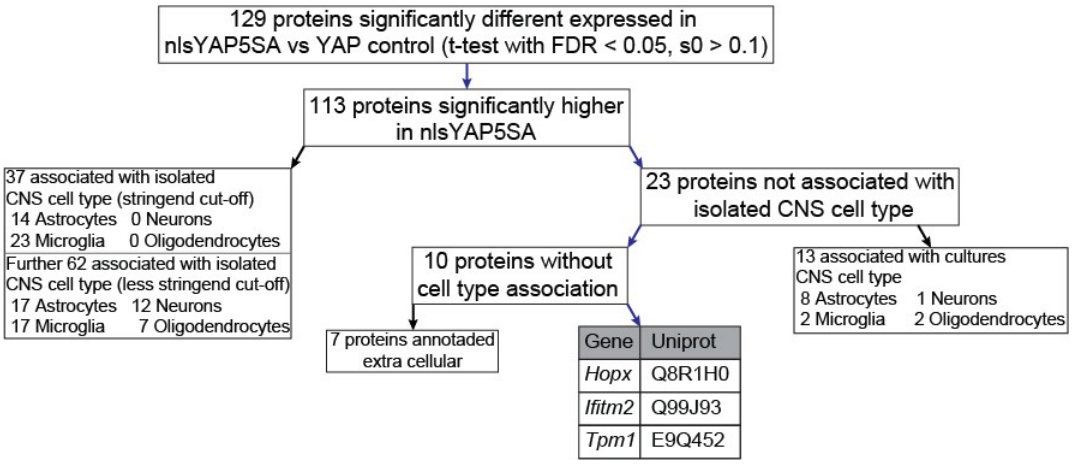

Figure 5.16. Candidate identification in proteomics dataset.

By implementing published CNS cell type proteomics data, the nlsYAP5SA full proteome dataset was filtered. First, significance was determined with Welch t-test (FDR = 0.05, s0 = 0.1) comparing the five nlsYAP5SA versus the five YAP control samples. Of the 129 significantly differentially expressed proteins, 113 were upregulated. Of those 90 were associated to a cell type taken from the Sharma *et al* dataset (Sharma et al 2015) (less stringed cut off was chosen, but results of more stringed are shown as well). The remaining 23 proteins were filtered against the cultured CNS cells screen resulting in 10 proteins without cell type association. Most of them were found to be secreted extracellular proteins, therefore potentially missing in the CNS datasets resulting in a final three proteins, HOPX, IFIRM2 and TMP1.

A goal from the beginning was to join the transcriptome and proteome datasets to not only see changes confined to one of them but to get a better understanding of the dynamics between the two fields in the nlsYAP5SA animals. When overlaying the proteomics dataset with the transcriptomic analysis matching the by gene names,

21.3% of genes found expressed in the total RNA were also found represented in the protein dataset (Figure 5.17.A). Furthermore, for 85 genes both the mRNA and the protein levels were identified to be significantly increased in the nlsYAP5SA brains compared to the control littermates.

When plotting the overlapped dataset (6,439 genes represented in both mRNA and protein), a positive correlation with a Pearson`s correlation coefficient was 0.5 could be observed between the transcript (Stat value) and the protein (Welch difference) level (Figure 5.17.B). Genes previously described to be associated with ependymoma, such as *Gfap*, *Vim* and *Anxa1* could be shown to be increased in mRNA as well as in protein level. *Yap1* and *Hopx*, both co-transcription factors, were found upregulated in both datasets. Also the complement cascade factors linked to inflammation were again amongst the significantly upregulated. Among the genes downregulated in both datasets *Nefl*, *Nefm* and *Nefh* were found which are neurofilaments important for the maintenance of neuronal calibre. Interestingly, also some none correlating genes can be found, such as *Ctgf*, which shows an increase in mRNA which does not appear to be translated into a change in protein level suggesting posttranscriptional control which was later confirmed by Western blot (Figure 5.19).

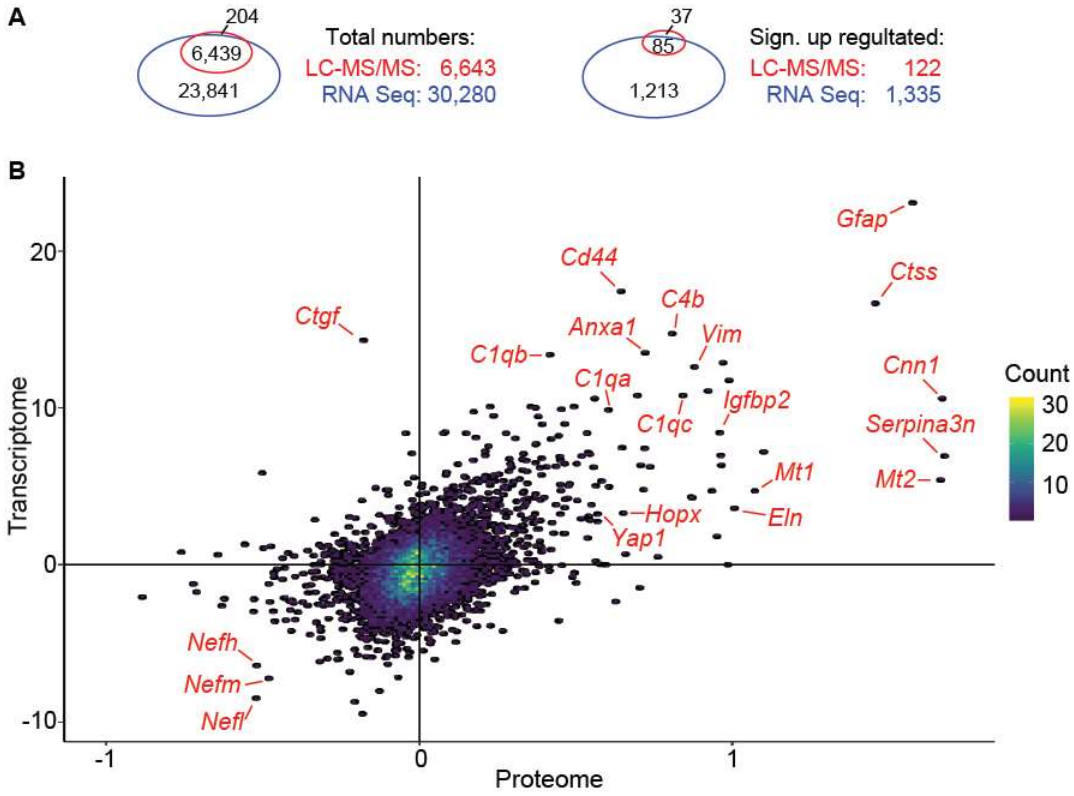

Figure 5.17. Correlation between proteome and transcriptome dataset.

A. VENN diagrams illustrating the overlap between the proteome (LC-MS/MS, red) and the transcriptome (RNA Sequencing, blue) datasets. Left = total numbers, right = significantly upregulated genes in nlsYAP5SA. **B**. Density scatter plot of all 6,439 genes represented in both datasets plotted by expression difference between YAP control vs nlsYAP5SA (proteome = Welch difference, transcriptome = stat value). Datasets show a correlation coefficient of 0.5. Each point represents one gene and a selection is labelled with name.

Next, the categorical enrichment in two dimensions was calculated as described previously (Cox & Mann 2012). The overlapped dataset was annotated using gene ontology (Biological Process, Molecular Function and Cellular Compartment) and KEGG annotations embedded within the Perseus software. Plotting the annotations, a good correlation between transcriptome and proteome with a Person`s correlation coefficient of 0.844 (correlation 2D enrichment scores) could be demonstrated (Figure 5.18.A). Annotations which were found in the transcriptome dataset using other software, were found also in the overlap such as “Staphylococcus aureus infection” and “Complement and coagulation cascade” being the most upregulated shared annotations. “Parkinsons`s disease” and “Oxidative phosphorylation” were found amongst the most down regulated KEGG terms. A subset of annotations was found upregulated in the proteome which did not appear to be reflected in the transcriptome containing multiple terms associated to RNA processing (Figure 5.18.B). This showed that changes found in the tumours not only arise from transcriptional differences to normal expression, but also downstream regulation playing a role. Therefore, having a bigger picture including multiple “-omic” approaches is beneficial in understanding the regulation within tumours.

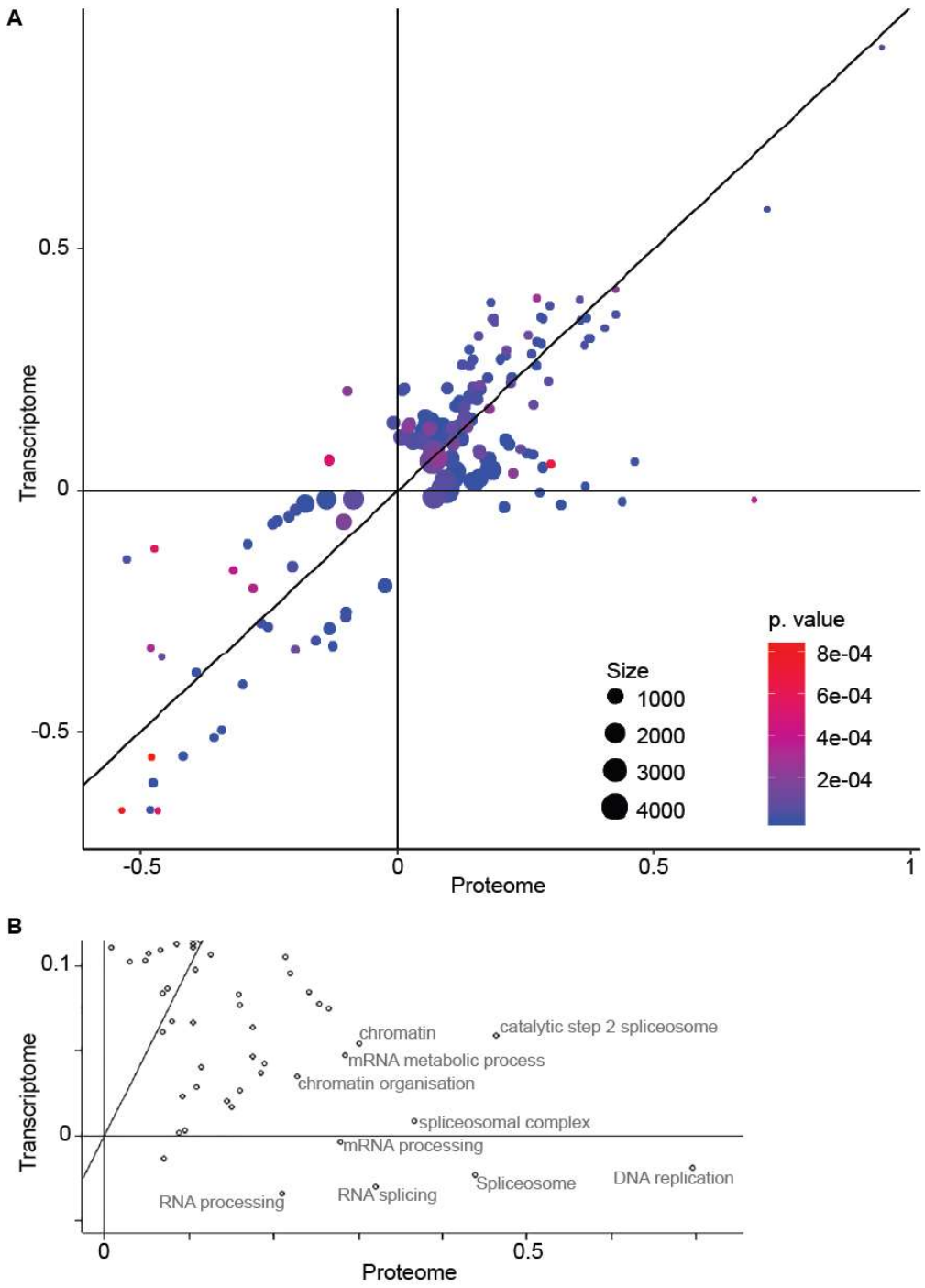

Figure 5.18. Gene annotation of merged proteome and transcriptome shows good correlation.

A. Proteins and corresponding mRNAs were matched by gene name. 2D annotation enrichment with Gene Ontology (BP, MF, CC) and KEGG was done in Perseus v1.4.0.2. Each dot represents one annotation, the colour indicated the corresponding p-value and the size matches the associated number of genes found within the dataset. **B**. Enlarged area of plot shown in A on annotations upregulated rather in the proteome dataset then the transcriptome.

5.3 Validating findings from RNA sequencing and Mass spectrometry *in vivo*

5.3.1 YAP1 effectors and upregulated genes identified in the transcriptomic and proteomic screens are highly expressed in LATS1/2 cKO tumours

Findings made in the RNA sequencing and the Mass spectrometry screens were taken forward to be tested and validated on an individual level. First, we confirmed with Western blot that Vimentin, GFAP and HOPX are significantly increased in nlsYAP5SA brains where also YAP1 is overexpressed (Figure 5.19). As seen already in the proteomics screen, CTGF which has been found to have higher mRNA levels in tumour bearing mice, does not show increased protein levels. Additionally, LATS1/2 and TAZ expression levels as well as their overall protein levels did not show a difference. Samples were lysed and Western blots were done by Andre Lopes.

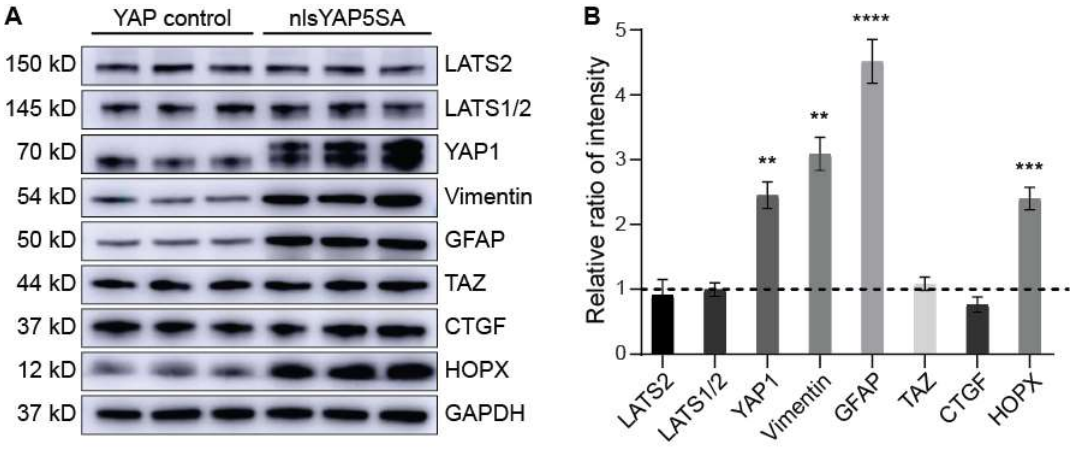

Figure 5.19. Western blots confirm findings in proteomics screen.

A. Right hemispheres of three YAP control and three nlsYAP5SA animals were lysed and analysed via western blot. **B**. Quantifications (normalised to loading control GAPDH and relative to averaged YAP control) shows significant increase in YAP1 ($p = 0.004$), Vimentin ($p = 0.002$), GFAP ($p < 0.0001$) and HOPX ($p = 0.0002$). Student`s t-test was performed. Error bars = SEM.

Further, we tested if identified upregulated proteins in nlsYAP5SA mice could also be found increased in LATS1/2 cKO tumours. YAP1 downstream effectors ANKRD1, AMOTL2 and AXL showed some of the highest upregulation in the transcriptomic screen and could also be found increased in expression in LATS1/2 cKO tumours (Figure 5.20). ANKDR1 was abundant in the centre of the tumour, whereas AMOTL2 and AXL showed stronger staining at the border. Also a positive staining of C3, which plays a role in the activation of the complement system, was observed increased at the periphery of the tumours. *Anxa1*, which was found significantly upregulate in both screens and has been associated with ependymoma (de Bont et al 2007) could also be found highly increase throughout the LATS1/2 cKO tumours (Figure 5.21). Therefore, in both of the preclinical mouse models the canonical YAP1 signalling effectors appear to be relevant in the tumour development of ependymoma-like tumours.

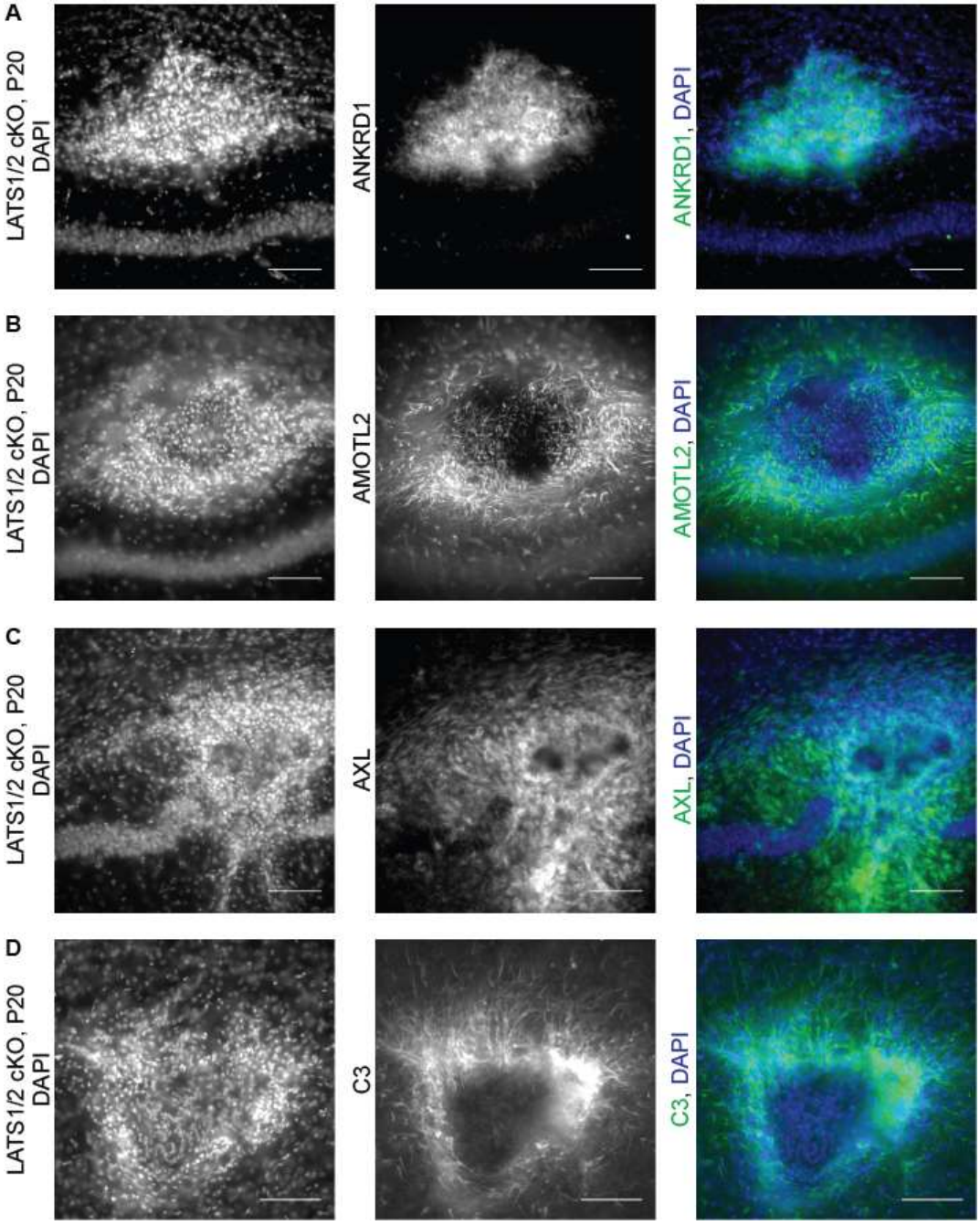

Figure 5.20. Proteins identified upregulated in nlsYAP5SA confirmed in LATS1/2 cKO tumours.

A-D. Representative immunofluorescence stainings in coronal vibratome sections of tumours in P20 LATS1/2 cKO brains. **A-C**. YAP1 target genes show strong staining. ANKRD1 (**A**) is uniformly upregulated throughout the tumour AMOTL2 (**B**) and AXL (**C**) show expression in the tumour mass and further increase towards its boarders. **D**. C3, part of the complement cascade, was found positive in particular increase towards the periphery of the tumour. Scale bars = 100 µm.

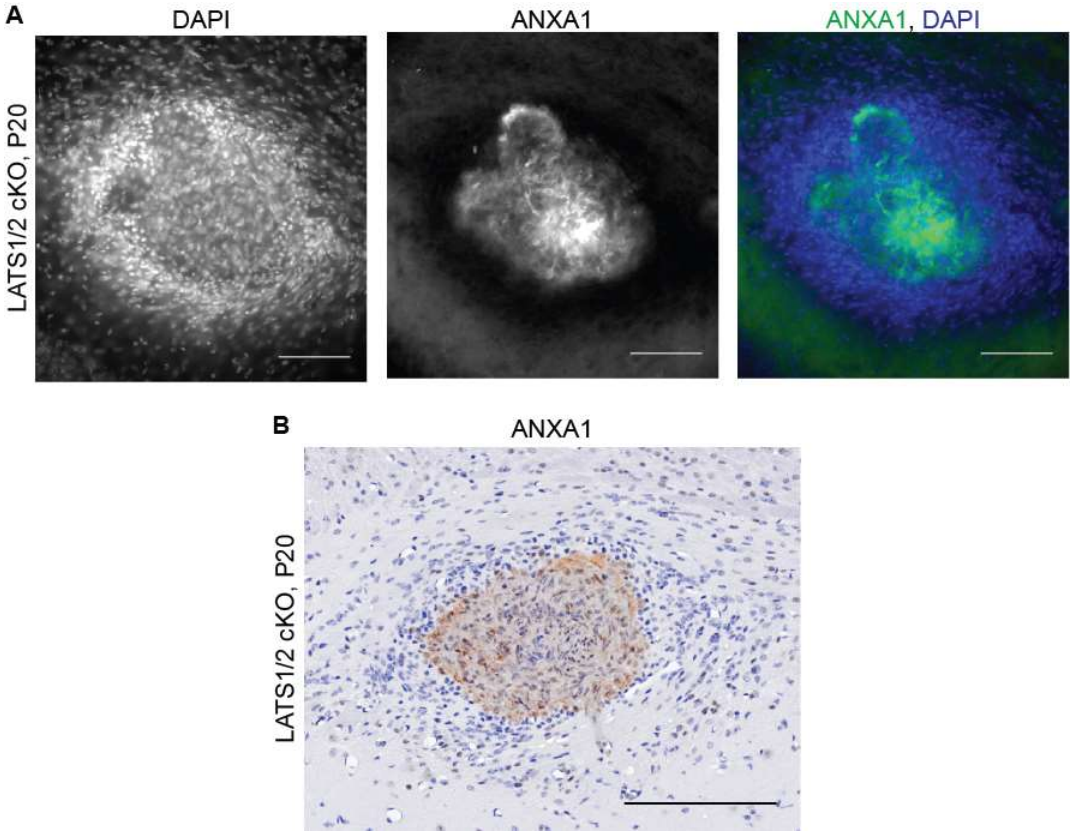

Figure 5.21. ANXA1 is found enriched in the murine tumour.

ANXA1 was found increased throughout the cell mass, in nuclear as well as in cytoplasmic location. The used antibody worked for both techniques immunofluorescence (**A**, scale bar = 100 µm) and immunohistochemistry (**B**, Scale bar = 200 µm).

Homeodomain-only protein (HOPX) was found increased in both screens and more importantly identified as the most promising candidate in the cell type filtering approach. It has been reported to be expressed in many tissues including neuronal stem cells with astrocytic fate (Mariotto et al 2016) (Zweifel et al 2018). Taking a closer look, we found the transcriptional co-activator to be present both the nucleus and the cytoplasm. Particularly high expression levels could be observed in the cerebellum and the dentate gyrus in control animals (Figure 5.22, Figure 5.23.B), which was documented before (Li et al 2015). In mutant animals, HOPX was upregulated in both tumour bearing mouse model systems in particular the boarders (Figure 5.22, Figure 5.23.A,C). It showed high expression in the deformed hippocampus area in the nlsYAP5SA brains (Figure 5.22). Furthermore, HOPX was present in cells exhibiting YAP1 nuclear localisation in LATS1/2 cKO tumours (Figure 5.23.A). Those results suggest a close relationship between HOPX and deregulated

YAP1 and HOPX being robustly induced in tumour cells with YAP1 activity. HOPX can be found nuclear located and therefore most likely active in its transcriptional co-activator role in the LATS1/2 cKO tumours.

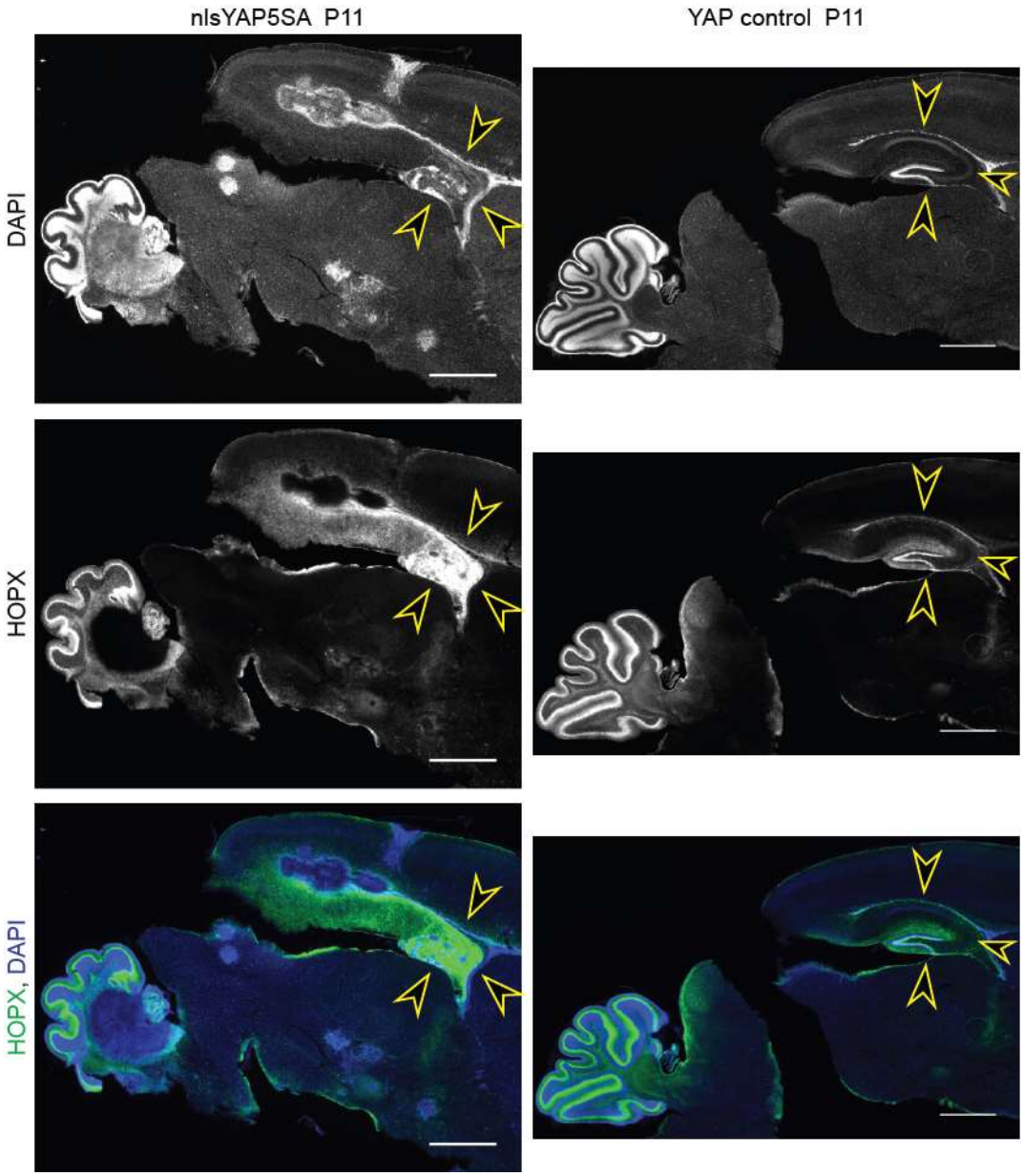

Figure 5.22. HOPX upregulated in nlsYAP5SA animal.

Immunofluorescence staining of HOPX in sagittal vibratome section of nlsYAP5SA and YAP control at P11. Expected positive staining is observed in dentate gyrus and cerebellum. Increased staining is found in nlsYAP5SA brains at the edges of the tumours and the hippocampal area (yellow arrowheads). Scale bars = 1 mm

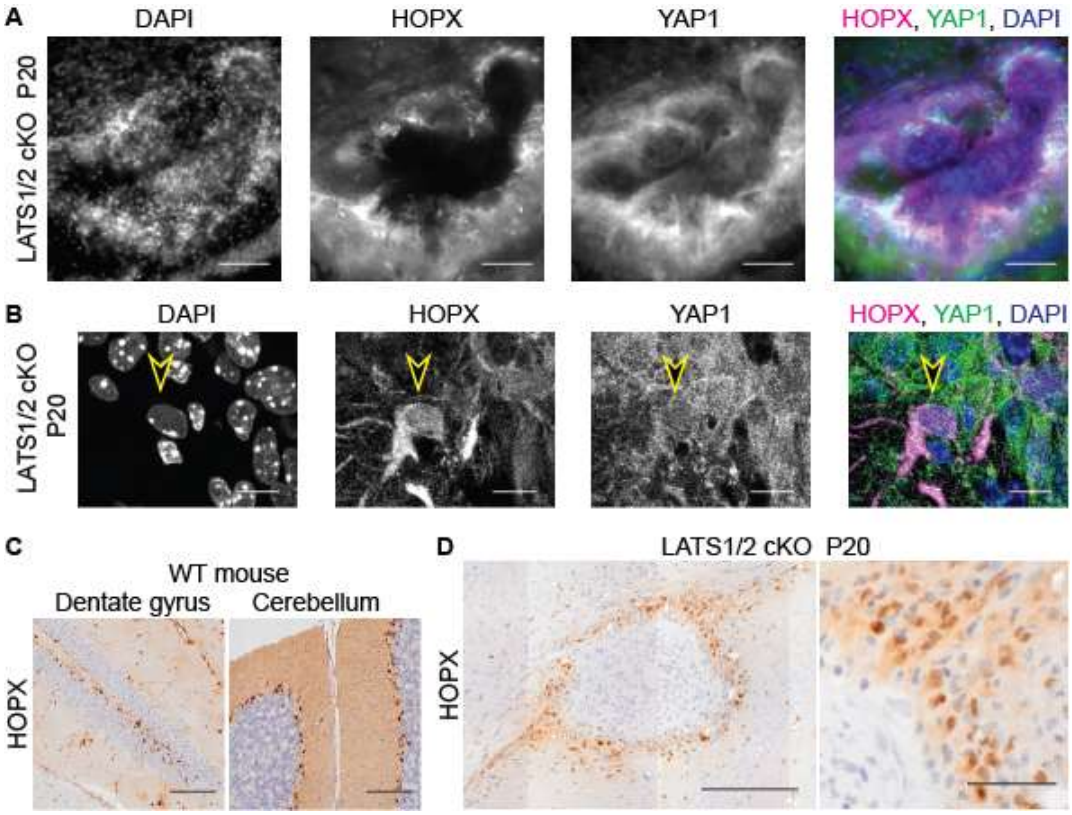

Figure 5.23. HOPX is increase in LATS1/2 cKO tumours.

A-B. Immunofluorescence of HOPX and YAP1 in a LATS1/2 cKO tumour at P20, showing higher staining at tumour edge, HOPX co-localizes with YAP1 in this area (white shows co-localisation, Scale bar = 100 μm). Example cell shown from a different LATS1/2 cKO tumour shows co expression of HOPX and YAP1 in one cell (**B**) (yellow arrowhead, Scale bar = 10 μm). **C-D**. Immunohistochemistry staining of HOPX. **C**. Positive staining found in the dentate gyrus the cerebellum in a wild type (WT). Scale bars = 100 μm. **D**. Tumours in LATS1/2 cKO P20 exhibit strong positive and also nuclear localised staining along the borders. Scale bar overview = 100 μm, close up = 10 μm.

5.3.2 HOPX us increased in human YAP1-fusion ependymoma patients

In the next step, the potential markers identified in the proteomics screen were confirmed by immunostainings in LATS1/2 cKO tumours and were further tested in human patient ependymoma tumour samples. Our goal was to see if from our screens, we could identify novel molecular signatures specific for YAP1-fusion ependymoma.

In spite of successful immunofluorescence stainings in mice, some antibodies did not show specific immunohistochemistry staining such as AMOTL2, ANKRD1 and

AXL. HOPX a very promising candidate and ANXA1 worked in the mouse brain IHC, so we tested them in human samples.

Human samples of two different ependymoma subtypes YAP1-MAMLD1 and C11orf95-RELA fusion (n = 3 patients each, provided by Dr Felipe Andreiuolo) were tested. First, one section per patient was tested for YAP1 and a second one for NFkB p65 expression. In YAP1-MAMLD1 tumours nuclear YAP1 could be observed (Figure 5.24, Figure 7.1), as previously described (Pagès et al 2019). Also in line with current literature, p65 was only found localised in the nucleus in C11orf95-RELA ependymoma patients (Figure 5.24, Figure 7.2) (Gessi et al 2019) (Pagès et al 2019). ANXA1 was expressed in all three YAP1-fusion cases but could also be found in RELA driven patients (Figure 5.24, Figure 7.4).

Remarkably, HOPX (homeodomain-only protein homeobox) was expressed in all three tested YAP1-MAMLD1 fusion ependymoma patients and was largely negative in the three C11orf95-RELA fusion tumours (Figure 5.24, Figure 7.3). It has been reported that HOPX is suppressed or absent in malignancies (Mariotto et al 2016) (Asanoma et al 2003). Interestingly, HOPX has been listed as a subtype specific enhancer in YAP1-fusion ependymomas (Mack et al 2017). HOPX is unable to bind DNA and can be found expressed in various tissues and has been linked with balancing proliferation and differentiation (Mariotto et al 2016). Furthermore, it has been reported that a population of basal radial glial cells is dependent on HOPX during development (Vaid et al 2018).

It can be speculated that increased HOPX expression might be associated with a more favourable outcome for YAP1-fusion ependymoma. Nevertheless, these initial results have to be followed up by a larger study including more patients and subtypes.

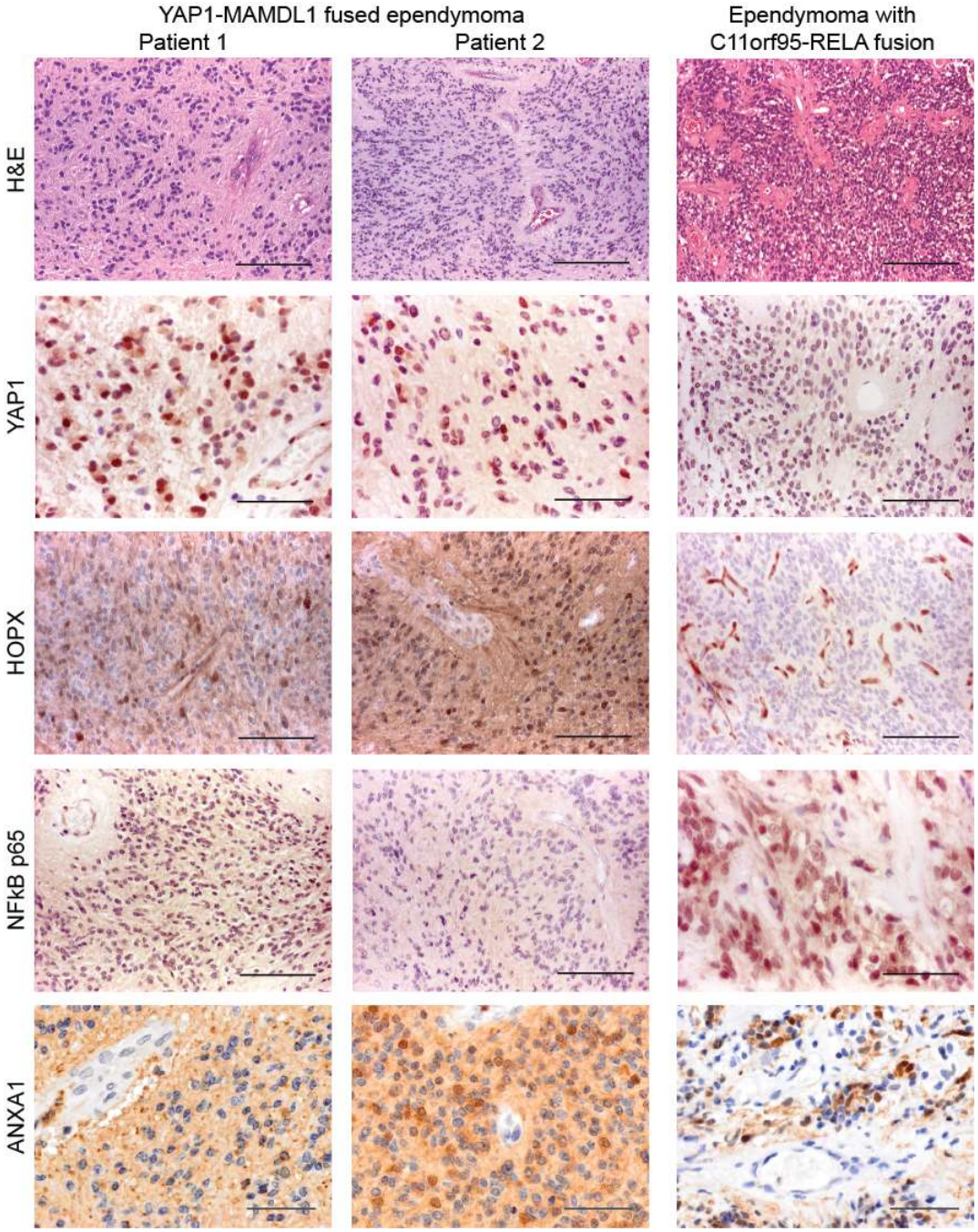

Figure 5.24. Human YAP1- and RELA- fusion ependymoma patients.

The two shown YAP1-MAMLD1 fused ependymoma characterised by uniform cells forming pseudo-rosettes in a fibrillary background (H&E, scale bars; Patient 1 = 100 µm, Patient 2 = 200 µm). The tumour cells demonstrate nuclear expression of YAP1 (immunoperoxidase, scale bar = 50 µm) and there is cytoplasmic and nuclear expression of HOPX (immunoperoxidase, scale bar = 100 µm). NFkB p65 is negative in tumour cells (immunoperoxidase, scale bar = 100 µm) while ANXA1 presents positive (immunoperoxidase, scale bar = 50 µm). The shown case of ependymoma with C11orf95-RELA fusion shows densely cellular sheets of tumour cells

with hyperchromatic nucleus; perivascular pseudo-rosettes are present (H&E, scale bar = 200 μm). No YAP1 expression is found in the tumour cells (immunoperoxidase, scale bar = 100 μm). HOPX in only found in endothelial cells while absent in tumour cells (immunoperoxidase, scale bar = 100 μm). Tumour cells show nuclear and cytoplasmic p65 expression (immunoperoxidase, scale bar = 50 μm). Tumour cells can also be found positive for ANXA1 (immunoperoxidase, scale bar = 50 μm).

In this subchapter we showed that the described mouse models, LATS1/2 cKO and nlsYAP5SA, recapitulate features of human ependymoma. Besides showing morphological similarities, also ultrastructural features commonly seen in ependymoma were found. RNA sequencing enabled us to show that the nlsYAP5SA brains showed a higher enrichment in YAP1-fusion ependymoma associated genes them RELA associated ones. The proteomics analysis revealed an enrichment in microglial and astrocytic response confirming our preceding IF observations. Furthermore, we identified HOPX to be selectively increased in the tested YAP1-MAMLD1 fusion and absent in RELA-fusion patients.

Chapter 6. Discussion

6.1 Function of LATS2 in post-mitotic neurons and the developing brain

The initial aim of this project was to study the post mitotic roles and functions of LATS2 in mammalian neurons. The first results we obtained from primary neuron cultures were compliant with findings in drosophila (Emoto et al 2006), that LATS2 (Warts in flies) does not appear to play a role in the development of the dendritic arbour. However, we could see effects on the dendritic spine density and maturation upon manipulation of normal LATS2 function. The period of time the neurons can be kept healthy in culture is limiting and is probably not long enough to study the mechanism of maintenance in this system sufficiently and reliably. Consequently, we decided to study the kinase function *in vivo* and soon realised that the conditional knockout in the NEX-Cre expressing model we chose was showing a clear phenotype. However, unexpectedly this was, at least not primarily, due to the alteration of neuronal function. The phenotypical abnormalities such as balance loss and lack of weight gain are most likely secondary effects of the rapidly growing cell mass and not called forth directly by the conditional lack of LATS1/2. The variety of the symptoms can be caused by the exact location of the cell clusters in each individual animal. As previously described LATS1 and LATS2 have overlapping functions, able to compensate when one is lost (Furth & Aylon 2017). This can also be seen here as the knockout of both is necessary to give rise to this neoplasia.

It has to be noted that the received constructs to study dendritic arbour phenotypes have not been checked for functionality in the neuronal system. Consequently, there is the possibility that the lack of striking phenotypes is due to a reduced or lack of activity of the expressed LATS2 constructs.

In the canonical Hippo Pathway LATS1/2 act as tumour suppressors controlling the activity of YAP1 (Zhao et al 2010). Unphosphorylated YAP localises to the nucleus promoting proliferation and cell survival. Overexpression and/or failure of proper regulation of YAP1 can be found in a wide range of tumours (Harvey et al 2013). Therefore, tumorigenesis due to knockdown of LATS1/2 is not very surprising. While the NEX-Cre driver is extensively used to study excitatory pyramidal neurons of the cortex and hippocampus, it has been reported that a small number of NEX

expressing cells in VZ can be found to counterstain with proliferation markers (Wu et al 2005). This indicates that *Nex* is expressed in a subset of committed neuronal progenitor cells.
As result the focus of the work was changed to investigate the origin of those cell clusters and explore its characteristics and potential links to human diseases.

6.2 Characterisation of LATS1/2 knockout induced dysplasia in the brain

The lesions we found in LATS1/2 cKO animals are negative for neuronal markers such as NeuN and Tuj1, showing that they are not post mitotic neurons. In this study it was observed that NEX-Cre triggers Ai14 reporter expression in ependymal cells positive for YAP1, Nestin and Ki67. It is widely believed that ependymal cells are derived from radial glial cells at E14-16 (Spassky et al 2005) (Kriegstein & Alvarez-Buylla 2009). Besides exhibiting stem cell like characteristics, shown by the expression of Nestin and the ability to proliferate (Ki67) the cell clusters are positive for ependymal markers such as Vimentin and MUC1 (EMA). The findings indicate that either the *Nex* promoter is turned on in a common precursor of ependymal cells and pyramidal neurons or that NEX is expressed independently in both pyramidal neuron precursors and ependymal cell or its precursors. It is known that NEX is expressed by pyramidal neurons throughout life and it appears that in the ependymal lineage or a subset of ependymal cells, NEX could be expressed in a transient manner. Alternatively, it is possible that the mutated cells are not directly subject to the knockout of Lats1/2 and rather a by-standard effect is seen. As it could be that the dual knockout creates a tumour promoting microenvironment (Lorger 2012). For an instance, the knockout targeted cells could lead to an inflammatory response in the brain and thus negatively affect neighbouring cells. However, inflammatory markers used showed predominantly absence in immunofluorescence staining.

This study further demonstrated that the control of the activity of YAP1 and its close homolog TAZ is crucial for limiting the proliferation in neuronal precursor cells. In particular, the neurons of the hippocampus are severely affected, as expression of hyperactive YAP1 (nlsYAP5SA) lead to a severely malformed hippocampus, lacking

differentiation. These findings are in agreement with earlier reports that miss-regulation of NF2, a positive regulator of the Hippo pathway, can alter hippocampal formation by limiting progenitor number and enabling hippocampal neuron differentiation, effects that were found to be mediated by YAP1 (Lavado et al 2013) (Lavado et al 2018). Data obtained from the LATS1/2 cKO mouse model indicates that LATS kinases play a part in supressing and controlling YAP1 activity in progenitors, limiting their proliferation.

Besides showing that uncontrollable YAP1 is sufficient for tumourigenesis, it was found that the tumour development is dependent on YAP1/TAZ. Depletion of those co-transcription factors in the LATS1/2 cKO mouse model lead to a dosage dependent decrease of average tumour size at the age of P20 and also resulted in reduction of observed number of cell clusters. No tumours could be found in P20 animals depleted of both *Yap1* and one *Taz* alleles. It remains to be tested if at later stages those animals might develop tumours.

6.3 Murine tumours are ependymoma like

Model systems for ependymoma are important for studying disease development, identifying driving processes and investigating therapeutic interventions. In particular, understanding the underlying biology of histologically similar, however molecular distinct subtypes is crucial. Patient derived xenografts have been successfully developed (Milde et al 2011) (Barszczyk et al 2014), recapitulating features of their donor and are beneficial in studying potential treatments. The development of mouse models mimicking the genetic origins are valuable to get a better understanding of the cells of origin and the roots of the disease (Johnson et al 2010) (Ozawa et al 2018) (Pajtler et al 2019). As an example, cerebral embryonic neural stem cells were isolated from Ink4a/Arf depleted mice, a recurrently mutated locus in human supratentorial ependymoma (Taylor et al 2005). Those cells were infected with Ephb2 expressing viruses and re-implanted into immunocompromised mice (Johnson et al 2010) leading to tumours with high similarities to ependymoma. These were then used in a high-throughput screen identifying 5-fluoroucil as a potential treatment (Atkinson et al 2011), which is under clinical evaluation (Wright

et al 2015). In another mouse model, RELA^{FUS1}, Nestin expressing stem cells were transduced with a c11ORF95-RELA fusion protein (Ozawa et al 2018), resulting in ependymoma like tumours.

A histological feature found commonly in human ependymoma are pseudorosettes, which similarly to other mouse models (Ozawa et al 2018) (Pajtler et al 2019) could not be found in LATS1/2 cKO, but were described in the mEPEphb2 mouse model system (Johnson et al 2010). Multiple factors could influence the absence in the LATS1/2 cKO model, such as species difference, tumour size and maturity.

The LATS1/2 cKO mouse model recapitulates histological and ultrastructural features found in human patients and presents positive for markers commonly used in ependymoma characterisation such as MUC1 (EMA) and cytokeratin. Furthermore, as for the nlsYAP5SA, the tumours located in the periventricular region, which is where also human YAP1-MAMDL1 fusion ependymoma is found (Andreiuolo et al 2019). On the other hand, RELA-fused ependymoma are more commonly observed in cortical centred location (Pagès et al 2019). A recently published study demonstrated that expression of YAP1-MAMDL1 fusion in nestin expressing NSC induce ependymoma like tumours in mice (Pajtler et al 2019). It was described that due to MAMLD1, YAP1 was increased nuclear and resulted in YAP1 dependent gene regulation. The LATS1/2 cKO and in particular the nlsYAP5SA model could show that increased YAP1 activity alone is sufficient to drive tumourigenesis. This supports the notion in YAP1 subtype ependymoma that the fusion protein, such as MAMDL1, are potential important for the nuclear localisation and activation of YAP1 and consequently leading to tumour development. Furthermore, by utilising RNA Sequencing, we could demonstrate that nlsYAP5SA mouse brains show a higher enrichment for YAP1-MAMDL1 fused human ependymoma as well as induced mouse model associated genes then with RELA-fusion.

Combining transcriptome and proteomics analysis, proved to be quite informative and showed that not all RNA level changes are translated into altered protein levels. As transcription and translation are highly regulated multi-step processes, it is not surprising to observe non-correlative behaviour between mRNA and protein level changes. Of all proteins detected 97% had their matched mRNA detected in the transcriptomic screen. The most highly upregulated protein hits are of potential use

as markers and were subsequently tested further. One of them, HOPX showed to be selectively highly increased in YAP1-MAMLD1 fusion ependymoma in the tested cases. A larger study including additional ependymoma subtypes besides YAP1-fusion and RELA-fusion, but also other brain tumours are needed to investigate the specificity of this marker. If such a marker holds true, it would simplify the patient stratification and instead of sequencing the patient genome, a simple staining could be performed, at least as first indication. Also, it could be investigated how this could be used as advantage to develop a targeted and subtype specific therapy.

By integrating cell type association, the proteomics analysis demonstrated an increase of microglia and astrocytic proteins, such as GFAP, ANXA1 and complement factors. Overall, the data collected from the multi-omics approach combining with other previously published datasets supported the notion of nlsYAP5SA and LATS1/2 cKO mice being useful ependymoma models. This is further supported by the histological characterisation and the ultrastructural features observed in the LATS1/2 cKO brains, demonstrating clear parallels to human ependymoma. Due to the observations, both mouse models could play a valuable role in understanding the biology of YAP1-fusion ependymoma and be used for pre-clinical research. There might be limitations due to the small tumour sizes and increase lethality. Nevertheless, using those genetically defined mouse models complemented with xenografts studies could aid a more comprehensive understanding of this understudied ependymoma subtype.

6.4 Future outlook

It would be very interesting to repeat the transcriptomic and proteomics screens with human YAP1-fusion ependymoma patient samples and subsequently combine the obtained data with the results gained from the nlsYAP5SA mouse model. This would aid to shed more light on the usefulness of this mouse model and the comparability to human patients. Moreover, the same analysis done on the mouse data could be applied to the human patient samples using the advantage of getting insights in protein and mRNA level changes. As patient material is limited, getting a versatile and combined dataset for others to build upon would be a further advantage. Upscaling of this approach is also easily possible as thus is not limiting the amount

of samples that can be processed. In a follow up step even other tumour types could be included, to further investigate ependymoma specific traits, distinguishing it from other tumour types. However, this could also be attempted on a data analysis level, by incorporating already published high quality data.

Another next step would include the further investigation of HOPX as a marker. As for now we only used three RELA-fusion and three YAP1-fusion patient samples. Consequently, the question remains if the increased HOPX level is specific for the YAP1-fusion type or if it can also be found increased in other subtypes. In general, the presented data is a promising indication, but requires to be validated using more patient samples of RELA- and YAP1-fusion patients. Therefore, a bigger patient cohort including multiple ependymoma subtypes would be needed. Ideally, this would also include samples of other brain tumours like glioblastoma to further investigate tumour specificity.
The obtained data can be further analysed and combined with available data sets to discover more potential markers. Furthermore, the proteins identified in our screen should be investigated further. As for some, the tested antibodies did not show specific staining in IHC. More antibodies from different vendors could be tested and potentially leading to more targets to take forward.

Chapter 7. Appendix

Stainings of human samples of the two different ependymoma subtypes YAP1-MAMLD1 and C11orf95-RELA fusion (n = 3 patients each, provided by Dr Felipe Andreiuolo). The following figures show the full set of all six patient samples stained for YAP1, RELA, HOPX and ANXA1, in extension of Figure 5.24.

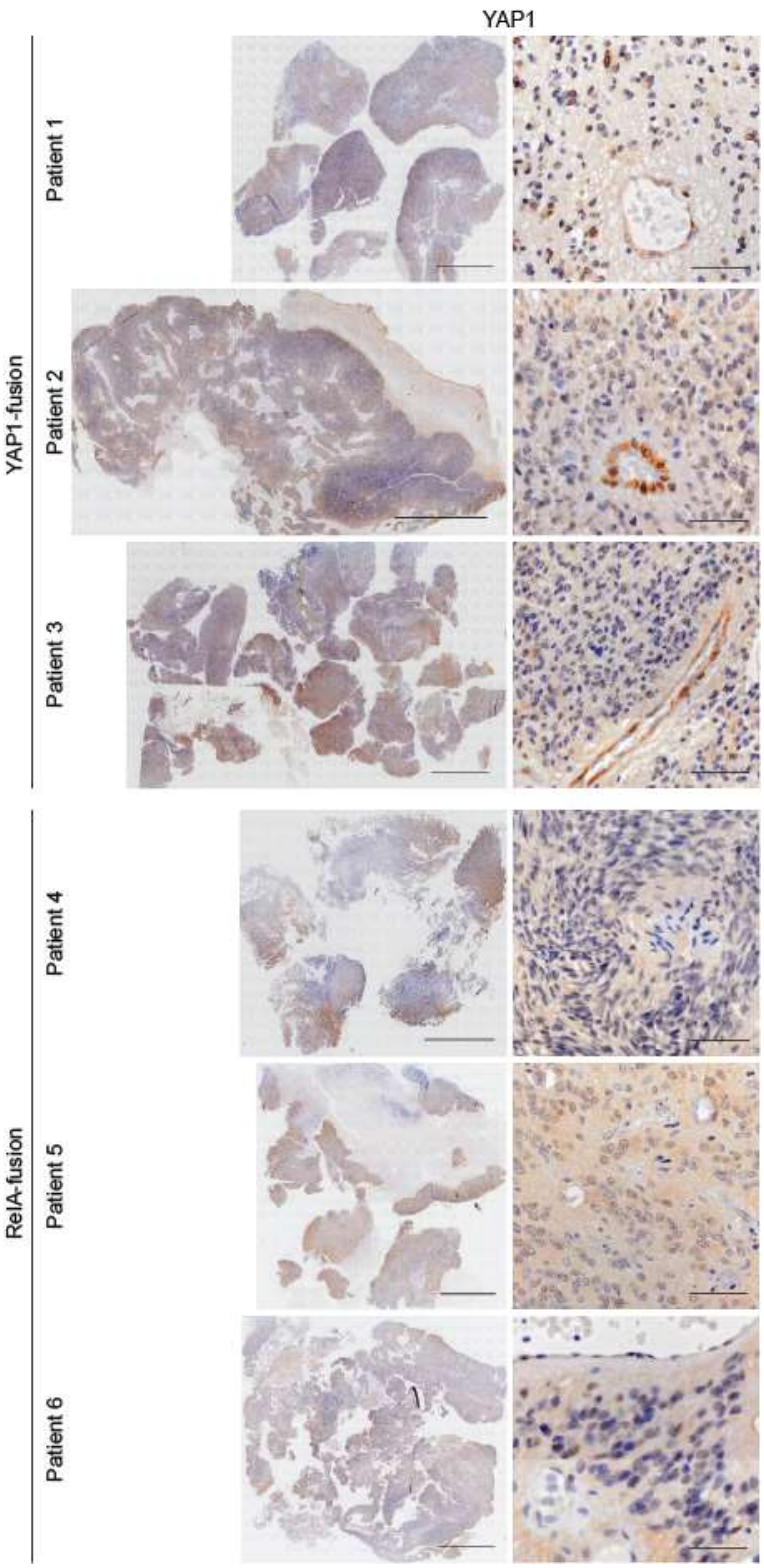

Figure 7.1. YAP1 IHC in human ependymoma patients.

Overview of all patient tissue stained and one representative highly zoomed area shown each. Scale bar overview = 5 mm, zoom = 50 µm.

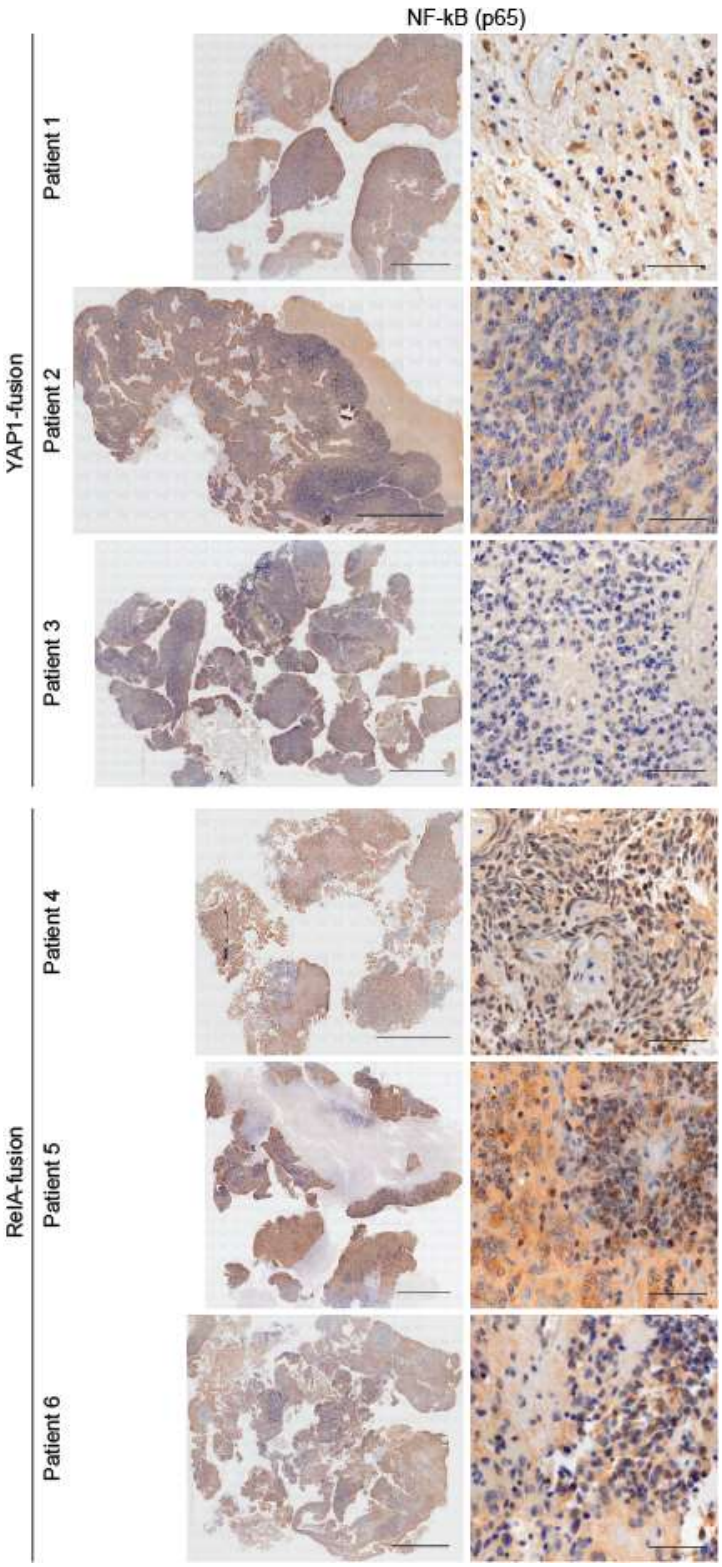

Figure 7.2. RELA IHC in human ependymoma patients.

Overview of all patient tissue stained and one representative highly zoomed area shown each. Scale bar overview = 5 mm, zoom = 50 µm.

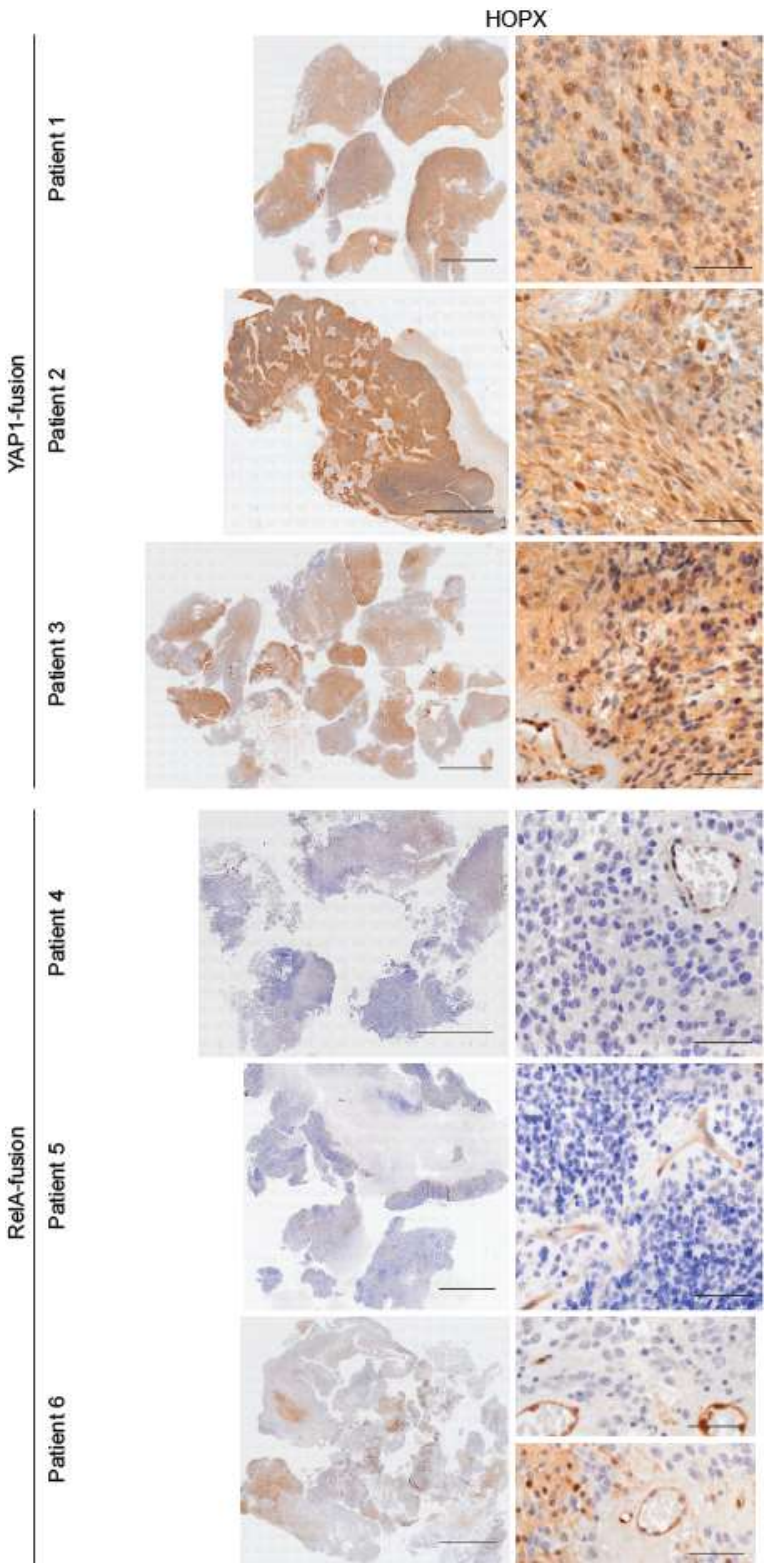

Figure 7.3. HOPX IHC in human ependymoma patients.

Overview of all patient tissue stained and one representative highly zoomed area shown each. Scale bar overview = 5 mm, zoom = 50 µm.

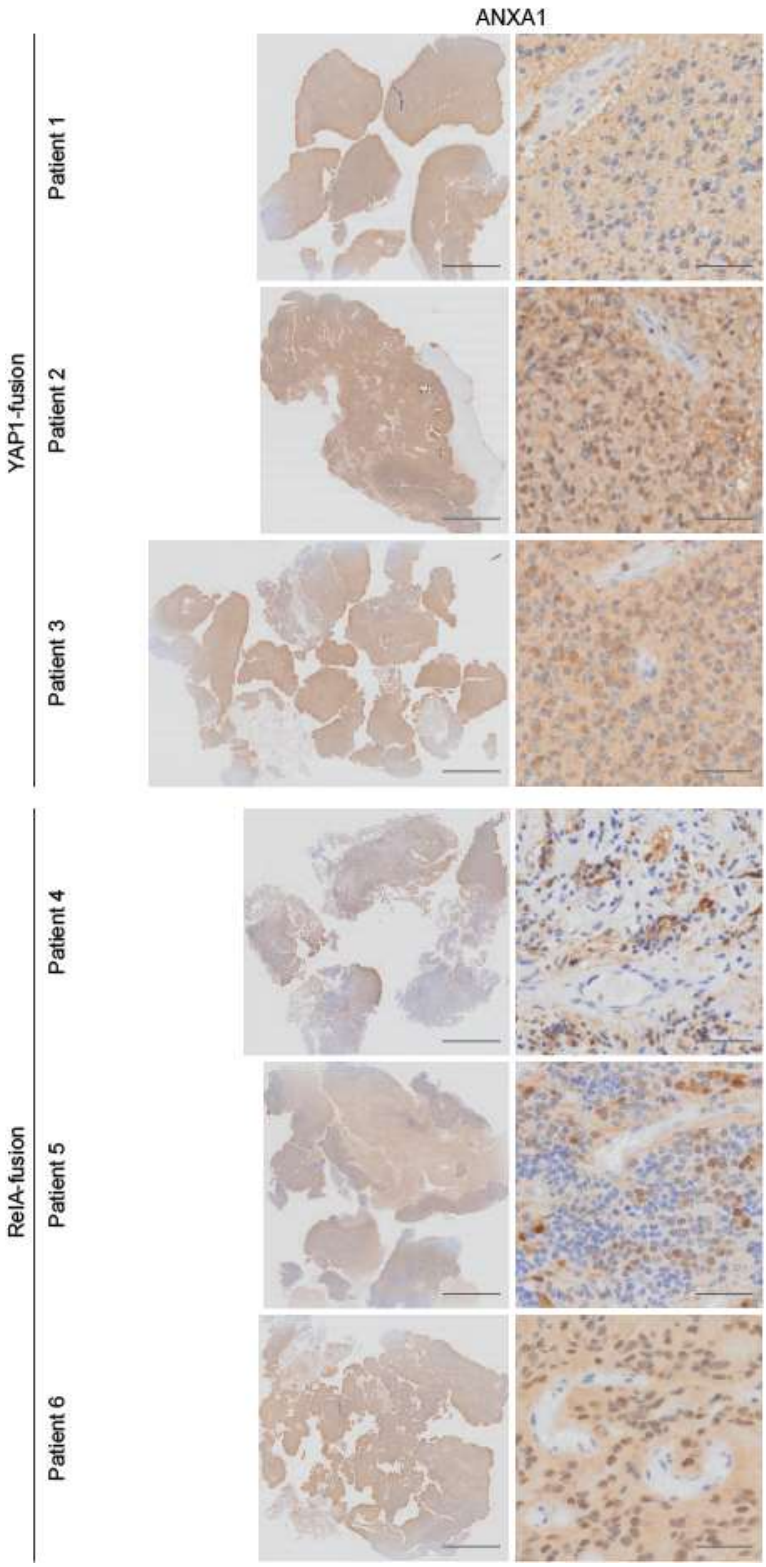

Figure 7.4. ANXA1 IHC in human ependymoma patient.

Overview of all patient tissue stained and one representative highly zoomed area shown each. Scale bar overview = 5 mm, zoom = 50 µm.

Reference List

The core of this work has been published (Eder et al 2020).

Agarwal A, Dibaj P, Kassmann CM, Goebbels S, Nave K-A, Schwab MH. 2012. In Vivo Imaging and Noninvasive Ablation of Pyramidal Neurons in Adult NEX-CreERT2 Mice. *Cereb. Cortex* 22: 1473-86

Ahmed AA, Mohamed AD, Gener M, Li W, Taboada E. 2017. YAP and the Hippo pathway in pediatric cancer. *Molecular & Cellular Oncology* 4: e1295127

Aldape K, Brindle KM, Chesler L, Chopra R, Gajjar A, et al. 2019. Challenges to curing primary brain tumours. *Nat Rev Clin Oncol* 16: 509-20

Andreiuolo F, Varlet P, Tauziède-Espariat A, Jünger ST, Dörner E, et al. 2019. Childhood supratentorial ependymomas with YAP1-MAMLD1 fusion: an entity with characteristic clinical, radiological, cytogenetic and histopathological features. *Brain Pathol.* 29: 205-16

Asanoma K, Matsuda T, Kondo H, Kato K, Kishino T, et al. 2003. NECC1, a candidate choriocarcinoma suppressor gene that encodes a homeodomain consensus motif☆☆Sequence data from this article have been deposited with the DDBJ/EMBL/GenBank Data Libraries under Accession No. AB059410. *Genomics* 81: 15-25

Atkinson Jennifer M, Shelat Anang A, Carcaboso Angel M, Kranenburg Tanya A, Arnold LA, et al. 2011. An Integrated In Vitro and In Vivo High-Throughput Screen Identifies Treatment Leads for Ependymoma. *Cancer Cell* 20: 384-99

Bai H, Gayyed MF, Lam-Himlin DM, Klein AP, Nayar SK, et al. 2012. Expression of Yes-associated protein modulates Survivin expression in primary liver malignancies. *Human Pathology* 43: 1376-85

Baloyannis SJ, Baloyannis IS. 2014. The fine structure of ependymomas. *CNS Oncology* 3: 49-59

Barszczyk M, Buczkowicz P, Castelo-Branco P, Mack SC, Ramaswamy V, et al. 2014. Telomerase inhibition abolishes the tumorigenicity of pediatric ependymoma tumor-initiating cells. *Acta Neuropathol.* 128: 863-77

Basu-Roy U, Bayin NS, Rattanakorn K, Han E, Placantonakis DG, et al. 2015. Sox2 antagonizes the Hippo pathway to maintain stemness in cancer cells. *Nat. Commun.* 6: 6411-11

Benson R, Mallick S, Julka P, Rath G. 2016. Molecular predictive and prognostic factors in ependymoma. *Neurology India* 64: 279-86

Bertrand N, Castro DS, Guillemot F. 2002. Proneural genes and the specification of neural cell types. *Nat. Rev. Neurosci.* 3: 517-30

Bigio MR. 2010. Ependymal cells: biology and pathology. *Acta Neuropathol.* 119

Boin A, Couvelard A, Couderc C, Brito I, Filipescu D, et al. 2014. Proteomic screening identifies a YAP-driven signaling network linked to tumor cell proliferation in human schwannomas. *Neuro-Oncology* 16: 1196-209

Buccoliero AM, Castiglione F, Degl'Innocenti DR, Sardi I, Genitori L, Taddei GL. 2010. MERLIN EXPRESSION IN PEDIATRIC ANAPLASTIC EPENDYMOMAS REAL TIME PCR STUDY. *Fetal and Pediatric Pathology* 29: 245-54

Cardona A, Saalfeld S, Schindelin J, Arganda-Carreras I, Preibisch S, et al. 2012. TrakEM2 Software for Neural Circuit Reconstruction. *PLoS ONE* 7: e38011

Chen Y, Han H, Seo G, Vargas RE, Yang B, et al. 2020. Systematic analysis of the Hippo pathway organization and oncogenic alteration in evolution. *Sci. Rep.* 10: 3173

Cornils H, Stegert MR, Hergovich A, Hynx D, Schmitz D, et al. 2010. Ablation of the Kinase NDR1 Predisposes Mice to the Development of T Cell Lymphoma. *Sci. Signal.* 3: ra47-ra47

Cotton JL, Li Q, Ma L, Park J-S, Wang J, et al. 2017. YAP/TAZ and Hedgehog Coordinate Growth and Patterning in Gastrointestinal Mesenchyme. *Dev. Cell* 43: 35-47.e4

Cox J, Mann M. 2012. 1D and 2D annotation enrichment: a statistical method integrating quantitative proteomics with complementary high-throughput data. *BMC Bioinformatics* 13: S12

CRUZ–SANCHEZ FF, ROSSI ML, ESIRI MM, READING M. 1988. EPITHELIAL MEMBRANE ANTIGEN EXPRESSION IN EPENDYMOMAS. *Neuropathol. Appl. Neurobiol.* 14: 197-205

Davis JR, Tapon N. 2019. Hippo signalling during development. *Development* 146: dev167106

de Bont JM, den Boer ML, Kros JM, Passier MMCJ, Reddingius RE, et al. 2007. Identification of Novel Biomarkers in Pediatric Primitive Neuroectodermal Tumors and Ependymomas by Proteome-Wide Analysis. *Journal of Neuropathology & Experimental Neurology* 66: 505-16

DeRan M, Yang J, Shen C-H, Peters Eric C, Fitamant J, et al. 2014. Energy Stress Regulates Hippo-YAP Signaling Involving AMPK-Mediated Regulation of Angiomotin-like 1 Protein. *Cell Rep.* 9: 495-503

Dobin A, Davis CA, Schlesinger F, Drenkow J, Zaleski C, et al. 2012. STAR: ultrafast universal RNA-seq aligner. *Bioinformatics* 29: 15-21

Dong J, Feldmann G, Huang J, Wu S, Zhang N, et al. 2007. Elucidation of a Universal Size-Control Mechanism in Drosophila and Mammals. *Cell* 130: 1120-33

Dupont S, Morsut L, Aragona M, Enzo E, Giulitti S, et al. 2011. Role of YAP/TAZ in mechanotransduction. *Nature* 474: 179-83

Eder N, Roncaroli F, Dolmart M-C, Horswell S, Andreiuolo F, et al. 2020. YAP1/TAZ drives ependymoma-like tumour formation in mice. *Nat. Commun.* 11: 2380

Elbediwy A, Vincent-Mistiaen ZI, Spencer-Dene B, Stone RK, Boeing S, et al. 2016. Integrin signalling regulates YAP and TAZ to control skin homeostasis. *Development* 143: 1674-87

Emoto K, Parrish JZ, Jan LY, Jan YN. 2006. The tumour suppressor Hippo acts with the NDR kinases in dendritic tiling and maintenance. *Nature* 443: 210-13

Fernandez-L A, Northcott PA, Dalton J, Fraga C, Ellison D, et al. 2009. YAP1 is amplified and up-regulated in hedgehog-associated medulloblastomas and mediates Sonic hedgehog-driven neural precursor proliferation. *Genes Dev.* 23: 2729-41

Furth N, Aylon Y. 2017. The LATS1 and LATS2 tumor suppressors: beyond the Hippo pathway. *Cell Death Differ.*

Gerstung M, Jolly C, Leshchiner I, Dentro SC, Gonzalez S, et al. 2020. The evolutionary history of 2,658 cancers. *Nature* 578: 122-28

Gessi M, Giagnacovo M, Modena P, Elefante G, Gianno F, et al. 2019. Role of Immunohistochemistry in the Identification of Supratentorial C11ORF95-RELA Fused Ependymoma in Routine Neuropathology. *The American Journal of Surgical Pathology* 43: 56-63

Goebbels S, Bormuth I, Bode U, Hermanson O, Schwab MH, Nave K-A. 2006. Genetic targeting of principal neurons in neocortex and hippocampus of NEX-Cre mice. *Genesis* 44: 611-21

Gotz M, Huttner WB. 2005. The cell biology of neurogenesis. *Nat. Rev. Mol. Cell Biol.* 6: 777-88

Guan S, Shen R, Lafortune T, Tiao N, Houghton P, et al. 2011. Establishment and characterization of clinically relevant models of ependymoma: a true challenge for targeted therapy. *Neuro-Oncology* 13: 748-58

Gumbiner BM, Kim N-G. 2014. The Hippo-YAP signaling pathway and contact inhibition of growth. *J. Cell Sci.* 127: 709-17

Guo X, Zhao Y, Yan H, Yang Y, Shen S, et al. 2017. Single tumor-initiating cells evade immune clearance by recruiting type II macrophages. *Genes Dev.* 31: 247-59

Han Y. 2019. Analysis of the role of the Hippo pathway in cancer. *J. Transl. Med.* 17: 116

Hao Y, Chun A, Cheung K, Rashidi B, Yang X. 2008. Tumor Suppressor LATS1 Is a Negative Regulator of Oncogene YAP. *J. Biol. Chem.* 283: 5496-509

Harvey KF, Zhang X, Thomas DM. 2013. The Hippo pathway and human cancer. *Nat. Rev. Cancer* 13: 246-57

Hasselblatt M, Paulus W. 2003. Sensitivity and specificity of epithelial membrane antigen staining patterns in ependymomas. *Acta Neuropathol.* 106: 385-88

Hergovich A. 2012. Mammalian Hippo signalling: a kinase network regulated by protein–protein interactions. *Biochem. Soc. Trans.* 40: 124-28

Hergovich A. 2016. The Roles of NDR Protein Kinases in Hippo Signalling. *Genes* 7: 16

Hermans E, Hulleman E. 2020. Patient-Derived Orthotopic Xenograft Models of Pediatric Brain Tumors: In a Mature Phase or Still in Its Infancy? *Front. Oncol.* 9

Huang DW, Sherman BT, Lempicki RA. 2008. Bioinformatics enrichment tools: paths toward the comprehensive functional analysis of large gene lists. *Nucleic Acids Res.* 37: 1-13

Huang DW, Sherman BT, Lempicki RA. 2009. Systematic and integrative analysis of large gene lists using DAVID bioinformatics resources. *Nat. Protoc.* 4: 44-57

Johnson RA, Wright KD, Poppleton H, Mohankumar KM, Finkelstein D, et al. 2010. Cross-species genomics matches driver mutations and cell compartments to model ependymoma. *Nature* 466: 632-36

Jones DTW, Banito A, Grünewald TGP, Haber M, Jäger N, et al. 2019. Molecular characteristics and therapeutic vulnerabilities across paediatric solid tumours. *Nat. Rev. Cancer* 19: 420-38

Kim C-L, Choi S-H, Mo J-S. 2019. Role of the Hippo Pathway in Fibrosis and Cancer. *Cells* 8: 468

Kriegstein A, Alvarez-Buylla A. 2009. The Glial Nature of Embryonic and Adult Neural Stem Cells In *Annu. Rev. Neurosci.*, pp. 149-84. Palo Alto: Annual Reviews

Kyrousi C, Lygerou Z, Taraviras S. 2017. How a radial glial cell decides to become a multiciliated ependymal cell. *Glia* 65: 1032-42

Lapointe S, Perry A, Butowski NA. 2018. Primary brain tumours in adults. *The Lancet* 392: 432-46

Lavado A, He Y, Paré J, Neale G, Olson EN, et al. 2013. Tumor suppressor Nf2 limits expansion of the neural progenitor pool by inhibiting Yap/Taz transcriptional coactivators. *Development* 140: 3323-34

Lavado A, Park JY, Paré J, Finkelstein D, Pan H, et al. 2018. The Hippo Pathway Prevents YAP/TAZ-Driven Hypertranscription and Controls Neural Progenitor Number. *Dev. Cell* 47: 576-91.e8

Li B, Dewey CN. 2011. RSEM: accurate transcript quantification from RNA-Seq data with or without a reference genome. *BMC Bioinformatics* 12: 323

Li D, Takeda N, Jain R, Manderfield LJ, Liu F, et al. 2015. Hopx distinguishes hippocampal from lateral ventricle neural stem cells. *Stem Cell Res.* 15: 522-29

Li H, Handsaker B, Wysoker A, Fennell T, Ruan J, et al. 2009. The Sequence Alignment/Map format and SAMtools. *Bioinformatics* 25: 2078-79

Li W, Cooper J, Zhou L, Yang C, Erdjument-Bromage H, et al. 2014. Merlin/NF2 Loss-Driven Tumorigenesis Linked to CRL4DCAF1-Mediated Inhibition of the Hippo Pathway Kinases Lats1 and 2 in the Nucleus. *Cancer Cell* 26: 48-60

Loeb KR, Loeb LA. 2000. Significance of multiple mutations in cancer. *Carcinogenesis* 21: 379-85

Lorger M. 2012. Tumor microenvironment in the brain. *Cancers* 4: 218-43

Louis DN, Perry A, Reifenberger G, von Deimling A, Figarella-Branger D, et al. 2016. The 2016 World Health Organization Classification of Tumors of the Central Nervous System: a summary. *Acta Neuropathol.* 131: 803-20

Love MI, Huber W, Anders S. 2014. Moderated estimation of fold change and dispersion for RNA-seq data with DESeq2. *Genome Biol.* 15: 550

Lu L, Li Y, Kim SM, Bossuyt W, Liu P, et al. 2010. Hippo signaling is a potent in vivo growth and tumor suppressor pathway in the mammalian liver. *Proceedings of the National Academy of Sciences* 107: 1437-42

Ma S, Meng Z, Chen R, Guan K-L. 2019. The Hippo Pathway: Biology and Pathophysiology. *Annu. Rev. Biochem.* 88: 577-604

Mack SC, Pajtler KW, Chavez L, Okonechnikov K, Bertrand KC, et al. 2017. Therapeutic targeting of ependymoma as informed by oncogenic enhancer profiling. *Nature* 553: 101

Madisen L, Zwingman TA, Sunkin SM, Oh SW, Zariwala HA, et al. 2010. A robust and high-throughput Cre reporting and characterization system for the whole mouse brain. *Nat. Neurosci.* 13: 133-40

Malbari F, Lindsay H. 2020. Genetics of Common Pediatric Brain Tumors. *Pediatric Neurology* 104: 3-12

Manning SA, Dent LG, Kondo S, Zhao ZW, Plachta N, Harvey KF. 2018. Dynamic Fluctuations in Subcellular Localization of the Hippo Pathway Effector Yorkie In Vivo. *Curr. Biol.* 28: 1651-60.e4

Mariotto A, Pavlova O, Park H-S, Huber M, Hohl D. 2016. HOPX: The Unusual Homeodomain-Containing Protein. *J. Invest. Dermatol.* 136: 905-11

McFaline-Figueroa JR, Lee EQ. 2018. Brain Tumors. *The American Journal of Medicine* 131: 874-82

Mclendon RE, Fung K-M, Bentley RC, Rasheed BKA, Trojanowski JQ, et al. 1996. Production and Characterization of Two Ependymoma Xenografts. *Journal of Neuropathology & Experimental Neurology* 55: 540-48

McPherson JP, Tamblyn L, Elia A. 2004a. Lats2/Kpm is required for embryonic development, proliferation control and genomic integrity. *EMBO J.* 23

McPherson JP, Tamblyn L, Elia A, Migon E, Shehabeldin A, et al. 2004b. Lats2/Kpm is required for embryonic development, proliferation control and genomic integrity. *EMBO J.* 23: 3677-88

Meng Z, Moroishi T, Guan K-L. 2016. Mechanisms of Hippo pathway regulation. *Genes Dev.* 30: 1-17

Miettinen M, Clark R, Virtanen I. 1986. Intermediate filament proteins in choroid plexus and ependyma and their tumors. *The American journal of pathology* 123: 231-40

Milde T, Kleber S, Korshunov A, Witt H, Hielscher T, et al. 2011. A novel human high-risk ependymoma stem cell model reveals the differentiation-inducing potential of the histone deacetylase inhibitor Vorinostat. *Acta Neuropathol.* 122: 637

Moroishi T, Hansen CG, Guan K-L. 2015. The emerging roles of YAP and TAZ in cancer. *Nat. Rev. Cancer* 15: 73

Moroishi T, Hayashi T, Pan W-W, Fujita Y, Holt MV, et al. 2016. The Hippo Pathway Kinases LATS1/2 Suppress Cancer Immunity. *Cell* 167: 1525-39.e17

Muzumdar MD, Tasic B, Miyamichi K, Li L, Luo L. 2007. A global double-fluorescent Cre reporter mouse. *Genesis* 45: 593-605

Nishioka N, Inoue K-i, Adachi K, Kiyonari H, Ota M, et al. 2009. The Hippo Signaling Pathway Components Lats and Yap Pattern Tead4 Activity to Distinguish Mouse Trophectoderm from Inner Cell Mass. *Dev. Cell* 16: 398-410

Orr BA, Bai HB, Odia Y, Jain D, Anders RA, Eberhart CG. 2011. Yes-Associated Protein 1 Is Widely Expressed in Human Brain Tumors and Promotes Glioblastoma Growth. *Journal of Neuropathology and Experimental Neurology* 70: 568-77

Ostrom QT, Gittleman H, Xu J, Kromer C, Wolinsky Y, et al. 2016. CBTRUS Statistical Report: Primary Brain and Other Central Nervous System Tumors Diagnosed in the United States in 2009-2013. *Neuro-Oncology* 18: v1-v75

Ozawa T, Arora S, Szulzewsky F, Juric-Sekhar G, Miyajima Y, et al. 2018. A De Novo Mouse Model of C11orf95-RELA Fusion-Driven Ependymoma Identifies Driver Functions in Addition to NF-κB. *Cell Rep.* 23: 3787-97

Pagès M, Pajtler KW, Puget S, Castel D, Boddaert N, et al. 2019. Diagnostics of pediatric supratentorial RELA ependymomas: integration of information from histopathology, genetics, DNA methylation and imaging. *Brain Pathol.* 29: 325-35

Pajtler KW, Wei Y, Okonechnikov K, Silva PBG, Vouri M, et al. 2019. YAP1 subgroup supratentorial ependymoma requires TEAD and nuclear factor I-mediated transcriptional programmes for tumorigenesis. *Nat. Commun.* 10: 3914

Pajtler KW, Witt H, Sill M, Jones DTW, Hovestadt V, et al. 2015. Molecular Classification of Ependymal Tumors across All CNS Compartments, Histopathological Grades, and Age Groups. *Cancer Cell* 27: 728-43

Panciera T, Azzolin L, Fujimura A, Di Biagio D, Frasson C, et al. 2016. Induction of Expandable Tissue-Specific Stem/Progenitor Cells through Transient Expression of YAP/TAZ. *Cell Stem Cell* 19: 725-37

Parker M, Mohankumar KM, Punchihewa C, Weinlich R, Dalton JD, et al. 2014. C11orf95–RELA fusions drive oncogenic NF-κB signalling in ependymoma. *Nature* 506: 451

Pearce LR, Komander D, Alessi DR. 2010. The nuts and bolts of AGC protein kinases. *Nat. Rev. Mol. Cell Biol.* 11: 9-22

Piccolo S, Dupont S, Cordenonsi M. 2014. The Biology of YAP/TAZ: Hippo Signaling and Beyond. *Physiol. Rev.* 94: 1287-312

Pocaterra A, Romani P, Dupont S. 2020. YAP/TAZ functions and their regulation at a glance. *J. Cell Sci.* 133: jcs230425

Pollack IF, Agnihotri S, Broniscer A. 2019. Childhood brain tumors: current management, biological insights, and future directions. 23: 261

Poon CLC, Mitchell KA, Kondo S, Cheng LY, Harvey KF. 2016. The Hippo Pathway Regulates Neuroblasts and Brain Size in Drosophila melanogaster. *Curr. Biol.* 26: 1034-42

Royer LA, Weigert M, Günther U, Maghelli N, Jug F, et al. 2015. ClearVolume: open-source live 3D visualization for light-sheet microscopy. *Nat. Methods* 12: 480-81

Schnitzer J, Franke W, Schachner M. 1981. Immunocytochemical demonstration of vimentin in astrocytes and ependymal cells of developing and adult mouse nervous system. *The Journal of Cell Biology* 90: 435-47

Sharma K, Schmitt S, Bergner CG, Tyanova S, Kannaiyan N, et al. 2015. Cell type- and brain region-resolved mouse brain proteome. *Nat. Neurosci.* 18: 1819-31

Soriano-Navarro M, Ramírez M, Bernet L, Martinez Banaclocha M, Cano R, et al. 2015. Ultrastructural Pathology of Anaplastic and Grade II Ependymomas reveals Distinctive Ciliary Structures – Electron Microscopy Redux AU - Alfaro-Cervelló, Clara. *Ultrastructural Pathology* 39: 23-29

Spassky N, Merkle FT, Flames N, Tramontin AD, García-Verdugo JM, Alvarez-Buylla A. 2005. Adult Ependymal Cells Are Postmitotic and Are Derived from Radial Glial Cells during Embryogenesis. *The Journal of Neuroscience* 25: 10

St John MAR, Tao W, Fei X, Fukumoto R, Carcangiu ML, et al. 1999. Mice deficient of Lats1 develop soft-tissue sarcomas, ovarian tumours and pituitary dysfunction. *Nat. Genet.* 21: 182-86

Subramanian A, Tamayo P, Mootha VK, Mukherjee S, Ebert BL, et al. 2005. Gene set enrichment analysis: A knowledge-based approach for interpreting genome-wide expression profiles. *Proceedings of the National Academy of Sciences* 102: 15545-50

Supèr H, Soriano E, Uylings HBM. 1998. The functions of the preplate in development and evolution of the neocortex and hippocampus. *Brain Research Reviews* 27: 40-64

Taylor MD, Poppleton H, Fuller C, Su X, Liu Y, et al. 2005. Radial glia cells are candidate stem cells of ependymoma. *Cancer Cell* 8: 323-35

Thorp N, Gandola L. 2019. Management of Ependymoma in Children, Adolescents and Young Adults. *Clinical Oncology* 31: 162-70

Totaro A, Panciera T, Piccolo S. 2018. YAP/TAZ upstream signals and downstream responses. *Nat. Cell Biol.* 20: 888-99

Vaid S, Camp JG, Hersemann L, Eugster Oegema C, Heninger A-K, et al. 2018. A novel population of Hopx-dependent basal radial glial cells in the developing mouse neocortex. *Development* 145: dev169276

Vege KDS, Giannini C, Scheithauer BW. 2000. The immunophenotype of ependymomas. *Applied Immunohistochemistry & Molecular Morphology* 8: 25-31

Wang Y, Xu X, Maglic D, Dill MT, Mojumdar K, et al. 2018. Comprehensive Molecular Characterization of the Hippo Signaling Pathway in Cancer. *Cell Rep.* 25: 1304-17.e5

Wesseling P, Capper D. 2018. WHO 2016 Classification of gliomas. *Neuropathol. Appl. Neurobiol.* 44: 139-50

Wright KD, Daryani VM, Turner DC, Onar-Thomas A, Boulos N, et al. 2015. Phase I study of 5-fluorouracil in children and young adults with recurrent ependymoma. *Neuro-Oncology* 17: 1620-27

Wu S-X, Goebbels S, Nakamura K, Nakamura K, Kometani K, et al. 2005. Pyramidal neurons of upper cortical layers generated by NEX-positive progenitor cells in the subventricular zone. *Proc. Natl. Acad. Sci. U. S. A.* 102: 17172-77

Xia Y, Shen S, Verma IM. 2014. NF-κB, an Active Player in Human Cancers. *Cancer Immunology Research* 2: 823-30

Yan F, Qian M, He Q, Zhu H, Yang B. 2020. The posttranslational modifications of Hippo-YAP pathway in cancer. *Biochimica et Biophysica Acta (BBA) - General Subjects* 1864: 129397

Yao Y, Mack SC, Taylor MD. 2011. Molecular genetics of ependymoma. *Chinese Journal of Cancer* 30: 669-81

Yi J, Lu L, Yanger K, Wang W, Sohn BH, et al. 2016. Large tumor suppressor homologs 1 and 2 regulate mouse liver progenitor cell proliferation and maturation through antagonism of the coactivators YAP and TAZ. *Hepatology* 64: 1757-72

Yin F, Yu J, Zheng Y, Chen Q, Zhang N, Pan D. 2013. Spatial Organization of Hippo Signaling at the Plasma Membrane Mediated by the Tumor Suppressor Merlin/NF2. *Cell* 154: 1342-55

Yu F-X, Zhao B, Panupinthu N, Jewell Jenna L, Lian I, et al. 2012. Regulation of the Hippo-YAP Pathway by G-Protein-Coupled Receptor Signaling. *Cell* 150: 780-91

Yu T, Bachman J, Lai ZC. 2015. Mutation analysis of large tumor suppressor genes LATS1 and LATS2 supports a tumor suppressor role in human cancer. *Protein Cell* 6: 6-11

Zanconato F, Cordenonsi M, Piccolo S. 2016. YAP/TAZ at the Roots of Cancer. *Cancer Cell* 29: 783-803

Zanconato F, Forcato M, Battilana G, Azzolin L, Quaranta E, et al. 2015. Genome-wide association between YAP/TAZ/TEAD and AP-1 at enhancers drives oncogenic growth. *Nat. Cell Biol.* 17: 1218-27

Zhang L, Tang F, Terracciano L, Hynx D, Kohler R, et al. 2015. NDR Functions as a Physiological YAP1 Kinase in the Intestinal Epithelium. *Curr. Biol.* 25: 296-305

Zhao B, Li L, Lei Q, Guan K-L. 2010. The Hippo–YAP pathway in organ size control and tumorigenesis: an updated version. *Genes Dev.* 24: 862-74

Zhao B, Tumaneng K, Guan K-L. 2011. The Hippo pathway in organ size control, tissue regeneration and stem cell self-renewal. *Nat. Cell Biol.* 13: 877-83

Zhao B, Wei X, Li W, Udan RS, Yang Q, et al. 2007. Inactivation of YAP oncoprotein by the Hippo pathway is involved in cell contact inhibition and tissue growth control. *Genes Dev.* 21: 2747-61

Zhao B, Ye X, Yu J, Li L, Li W, et al. 2008. TEAD mediates YAP-dependent gene induction and growth control. *Genes Dev.* 22: 1962-71

Zheng Y, Wang W, Liu B, Deng H, Uster E, Pan D. 2015. Identification of Happyhour/MAP4K as Alternative Hpo/Mst-like Kinases in the Hippo Kinase Cascade. *Dev. Cell* 34: 642-55

Zweifel S, Marcy G, Lo Guidice Q, Li D, Heinrich C, et al. 2018. HOPX Defines Heterogeneity of Postnatal Subventricular Zone Neural Stem Cells. *Stem Cell Reports* 11: 770-83